APTD 0613

PB 199 412

THREE RADIOMETRIC DATA ANALYSIS TECHNIQUES FOR MEASURING AIR TEMPERATURE PROFILES

by

W. D. Mount, B. R. Fow,
C. V. Wick and C. M. Maloy

FINAL REPORT
Contract No. CPA 22-69-116

Period Covered: 1969 June 23 to 1970 October 23
Contract Monitor: T. Lemmons

Prepared for

DIVISION OF METEOROLOGY
AIR POLLUTION CONTROL OFFICE*
ENVIRONMENTAL PROTECTION AGENCY
DURHAM, NORTH CAROLINA 22701

*Formerly National Air Pollution Control Administration

SPERRY RAND RESEARCH CENTER
SUDBURY, MASSACHUSETTS 01776

Reproduced by
NATIONAL TECHNICAL
INFORMATION SERVICE
Springfield, Va. 22151

111

SRRC–CR–70–27

THREE RADIOMETRIC DATA ANALYSIS TECHNIQUES FOR MEASURING AIR TEMPERATURE PROFILES

by

W. D. Mount, B. R. Fow,
C. V. Wick and C. M. Maloy

FINAL REPORT
Contract No. CPA 22–69–116

Period Covered: 1969 June 23 to 1970 October 23
Contract Monitor: T. Lemmons

Prepared for

DIVISION OF METEOROLOGY
AIR POLLUTION CONTROL OFFICE*
ENVIRONMENTAL PROTECTION AGENCY
DURHAM, NORTH CAROLINA 22701

*Formerly National Air Pollution Control Administration

SPERRY RAND RESEARCH CENTER
SUDBURY, MASSACHUSETTS 01776

PB 199 412

BIBLIOGRAPHIC DATA SHEET

1. Report No. APTD-0673

2.

3. Recipient's Accession No.

4. Title and Subtitle

Three Radiometric Data Analysis Techniques for Measuring Air Temperature Profiles

5. Report Date October 23, 1970

6.

7. Author(s) W. D. Mount, B. R. Fow, C. V. Wick and C. M. Maloy

8. Performing Organization Rept. No.

9. Performing Organization Name and Address

Sperry Rand Research Center
Sudbury, Massachusetts 01776

10. Project/Task/Work Unit No.

11. Contract/Grant No. CPA 22-69-116

12. Sponsoring Organization Name and Address

Division of Meteorology
Air Pollution Control Office
Environmental Protection Agency
411 W. Chapel Hill Street
Durham, North Carolina 22701

13. Type of Report & Period Covered Final

14.

15. Supplementary Notes

16. Abstracts

The problem of determining the height of the base, the intensity and the thickness of an elevated inversion layer from radiometric THERMASONDE data is discussed. Three advanced radiometric data analysis techniques emphasizing the detection and measurement of these salient features of elevated inversions are proposed. The techniques include: 1. a statistical procedure for finding the best three-straight-line representation of the true profile from the radiometric data--called the gradient altitude model, 2. a relaxation procedure for finding the ambient temperature at sixteen preselected heights from the surface to 2.54 km, and 3. several analog and empirical techniques for detecting the presence and determing the base heights and other features of an elevated inversion directly from the recorder outputs of THERMASONDE data. The initial development and evaluation of these techniques using simulated and real data are presented. The results show that the problem of determining the features of an elevated inversion becomes more difficult as the height of its base increases, its intensity decreases, and its thickness decreases. The relaxation technique appears to be capable of providing accurate descriptions of the temperature profile in the case of elevated inversions of up to 5.

17. Key Words and Document Analysis. 17a. Descriptors

Radiation measuring instruments
Thermal measuring instruments
Meteorological instruments
Temperature inversions

17b. Identifiers/Open-Ended Terms

Radiometric thermasonde

17c. COSATI Field/Group 4/B, 13/B

18. Availability Statement Unlimited

19. Security Class (This Report) UNCLASSIFIED

20. Security Class (This Page) UNCLASSIFIED

21. No. of Pages 113

22. Price

FORM NTIS-35 (10-70)

USCOMM-DC 40329-P71

ABSTRACT

The problem of determining the height of the base, the intensity, and thickness of an elevated inversion layer from radiometric THERMASONDE™ data is discussed. Three advanced radiometric data analysis techniques emphasizing the detection and measurement of these salient features of elevated inversions are proposed. The techniques include: (1) a statistical procedure for finding the best three-straight-line representation of the true profile from the radiometric data--called the gradient altitude model, (2) a relaxation procedure for finding the ambient temperature at sixteen preselected heights from the surface to 2.54 km, and (3) several analog and empirical techniques for detecting the presence and determining the base heights and other features of an elevated inversion directly (without the use of computers) from the recorder outputs of THERMASONDE™ data. The initial development and evaluation of these techniques using simulated and real data are presented. The results show that the problem of determining the features of an elevated inversion becomes more difficult as the height of its base increases, its intensity decreases, and its thickness decreases. The relaxation technique appears to be capable of providing accurate descriptions of the temperature profile in the case of elevated inversions of up to .5 km base height. The analog library and gradient model determine the base heights of inversions up to 1.5 km to within an average of 13.9 percent of their absolute value. The average absolute height difference between THERMASONDE™ and helicopter observations of the mixing layer is 0.08 km. Because of the natural variability of this parameter, this difference is equivalent to using a helicopter sounding which is less than one hour old.

TABLE OF CONTENTS

Section		Page
1	INTRODUCTION AND GENERAL SUMMARY	1
2	GRADIENT ALTITUDE MODEL	5
3	LIMITED RANGE RELAXATION TECHNIQUE	45
4	ANALOG AND EMPIRICAL TECHNIQUES	67
5	CONCLUSIONS	99
	REFERENCES	101

LIST OF ILLUSTRATIONS

Figure	Description	Page
1	An observed temperature profile and representations thereof by a model temperature profile consisting of three truncated straight-line segments and by a best fit low-order polynomial. The observed profile was obtained at Raleigh, N. C. by a helicopter sounding on 1969 October 15.	8
2	Comparison of the exact value of the atmosphere absorption coefficient and the approximation expression $\tilde{\gamma}_\nu(z) = \exp \{b_\nu - a_\nu z\}$. The temperature profile from which the exact values were obtained is also shown.	10
3	Presumed nature of the $F(\underline{P})$ surface illustrating the difficulty of finding the best fitting combination of parameters by certain analytical methods such as those employing gradients of $F(\underline{P})$.	22
4	Results of using GRID inversion scheme on simulated radiometric data from four model temperature profiles.	27, 28
5	Results of Tests A1 and E1.	33
6	Results of Tests A2 and E2.	34
7	Results of Tests A3 and E3.	35
8	Results of Tests A4 and E4.	36
9	Comparison of measured and calculated brightness temperatures.	38
10	Results of using GRID inversion scheme on actual and simulated radiometric data from Cincinnati, Ohio, Gest St., 1969 Feb. 26.	40
11	Results of using GRID inversion scheme on actual radiometric data from Raleigh, N. C., 1969 Oct. 15.	41
12	Results of using GRID inversion scheme on actual radiometric data from Vandenberg AFB 1969 Dec. 5, 1547-1609 PST.	43
13	Sum of the residuals, the sum of the squares of the residuals, and the sum of the absolute values of the residuals due to the relaxation of three 5 C elevated inversions of .25 km thickness where the bases of the inversions are at .5 km, 1.0 km, and 1.5 km, respectively.	55
14	Comparison of the initially guessed profile $\hat{T}(z)_0$ and the resulting predicted profiles after the 1st and 9th iterations with the true temperature profile $T(z)$ having a 0.5 km elevated inversion.	57

LIST OF ILLUSTRATIONS - Cont'd

Figure	Description	Page
15	Comparison of the initially guessed profile $\hat{T}(z)_o$ and the resulting predicted profiles after the 1st and 9th iterations with the true temperature profile $T(z)$ having a 1.0 km elevated inversion.	59
16	Comparison of the initially guessed profile $\hat{T}(z)_o$ and the resulting predicted profiles after the 1st and 9th iterations with the true temperature profile $T(z)$ having a 1.5 km elevated inversion.	61
17	Sum of the residuals, the sum of the squares of the residuals, and the sum of the absolute values of the residuals due to the relaxation of three 5 C elevated inversions of .25 km thickness where the bases of the inversions are at .5 km, 1.0 km, and 1.5 km, respectively.	63
18	Comparison of the predicted profile resulting after the 7th iteration with the true temperature profile having a 0.5 km elevated inversion.	64
19	Comparison of the predicted profile resulting after the 8th iteration with the true temperature profile having a 1.5 km elevated inversion.	65
20	Lack of correlation between breakpoint and inversion height.	69
21	Model elevated inversion temperature profiles. In all three sets the profile above the inversion is the U. S. Standard Atmosphere.	71
22	Model scan curves for profiles having elevated inversions of different heights. The curves are displaced an arbitrary 0.5 K at 0 degrees elevation.	76
23	Model scan curves for profiles having elevated inversions of different intensities.	77
24	Model scan curves for profiles having elevated inversions of different thicknesses.	78
25	Actual radiometric scan curve vs. analog model scan curve for Cincinnati and Raleigh.	81
26	Actual radiometric scan curve vs. analog model scan curve for Vandenberg AFB.	82
27	Predicted analog model vs. observed temperature profile for Cincinnati, 1969 Feb. 20, 0806 EST.	84

LIST OF ILLUSTRATIONS - Cont'd

Figure	Description	Page
28	Predicted analog model vs. observed temperature profile for Cincinnati, 1969 Feb. 26, 1405 EST.	85
29	Predicted analog model vs. observed temperature profile for Clearwater, 1969 Feb. 5, 1443 EST.	86
30	Predicted analog model vs. observed temperature profile for Raleigh, 1969 Oct. 15, 1653 EST.	87
31	Predicted analog model vs. observed temperature profile for Vandenberg AFB, 1969 Dec. 4, 1047 PST.	88
32	Predicted analog model vs. observed temperature profile for Vandenberg AFB, 1969 Dec. 4, 1422 PST.	89
33	Predicted analog model vs. observed temperature profile for Vandenberg AFB, 1969 Dec. 5, 1547 PST.	90
34	Predicted analog model vs. observed temperature profile for Vandenberg AFB, 1969 Dec. 6, 0843 PST.	91
35	Predicted analog model vs. observed temperature profile for Vandenberg AFB, 1969 Dec. 6, 1042 PST.	92
36	Predicted analog model vs. observed temperature profile for Vandemberg AFB, 1969 Dec. 6, 1612 PST.	93
37	Predicted analog model vs. observed temperature profile for Vandenberg AFB, 1969 Dec. 7, 1100 PST.	94

LIST OF TABLES

Table	Description	Page
I	EXACT VS. APPROXIMATE BRIGHTNESS TEMPERATURES AND RESIDUAL PROFILE CONTRIBUTION	16
II	EXACT VS. APPROXIMATE BRIGHTNESS TEMPERATURES AND RESIDUAL PROFILE CONTRIBUTION	17
III	EXACT VS. APPROXIMATE BRIGHTNESS TEMPERATURES AND RESIDUAL PROFILE CONTRIBUTION	19
IV	PARAMETERS OF THE MODEL PROFILES	24
V	TRIAL VALUES OF GAM PARAMETERS	25
VI	FIRST AND SECOND CHOICE BEST FITTING PARAMETERS SELECTED BY GRID ACCORDING TO A MINIMUM SUM OF SQUARES CRITERION	26
VII	FIRST AND SECOND CHOICE BEST FITTING PARAMETERS SELECTED BY GRID ACCORDING TO A MINIMUM SUM OF ABSOLUTE VALUES CRITERION	26
VIII	TRIAL VALUES OF THE GAM PARAMETERS USED IN THE SERIES OF TESTS ON THE BISMARCK, N.D., SIMULATED DATA	30
IX	BEST FITTING GAM PARAMETERS SELECTED BY GRID ACCORDING TO MINIMUM SUM OF SQUARES AND MINIMUM SUM OF ABSOLUTE VALUES CRITERIA	31
X	TRIAL VALUES OF GAM PARAMETERS	39
XI	TRIAL VALUES OF GAM PARAMETERS	42
XII	VALUES OF $\beta(\theta)$ FOR THE FOUR MODEL PROFILES	48
XIII	ANGLE-HEIGHT GRID	49
XIV	HELICOPTER VS. RADIOMETRICALLY MEASURED HEIGHT OF MIXING LAYER	96

SECTION I

INTRODUCTION AND GENERAL SUMMARY

Several years ago there was considerable skepticism as to the possibility of deriving any useful information on the vertical temperature structure of the atmosphere using only ground-based, passive probing techniques. At the time there were several analytical studies which showed varying degrees of success, but none looked particularly promising for field application. Part of the problem was attempting to do too much too soon; another part was due to state-of-the-art limitations in the hardware development of radiometric instrumentation. The physics and mathematics of the radiative transfer phenomenon impose an inherent limitation on the atmospheric height to which detailed temperature profile information can be obtained, so it became essential to establish the initial feasibility to justify proceeding in remotely sounding the atmosphere. Thus emphasis was placed on tackling that portion of the problem which was most amenable to solution, namely the lowest layer of the atmosphere. Furthermore, a combined experimental and analytical approach was taken so that neither the signal processing nor hardware techniques imposed unrealistic demands upon the other, thereby allowing the the results from each to aid in understanding and improving the performance of the other.

Computer simulation of the radiational and climatological characteristics of the atmosphere was used to develop the applicable height concept as a tool for establishing the initial feasibility of remote probing. This procedure had the advantage of providing nearly a real time interpretation of observed radiometric data to derive gross features of the vertical temperature profile. It was developed for use on lapse-type profiles and for distinguishing the different types of low-level atmospheric stability conditions. Experimental results verified the capability of being able to remotely observe lapse, ground-based and low-elevated inversion type profiles. It should be recognized that the applicable height concept made no modification to the observed radiometric brightness temperature; all it did was to specify a set of heights above a station at which the actual atmospheric temperatures are assumed to be equal to a set of brightness temperature measurements. For a given station, surface pressure and radiometer frequency, the set of applicable heights corresponds to a set of elevation angles. This approach does well for the different types of lapse conditions because there are no sharp discontinuities in the temperature profile. On the other hand, for ground-based inversions where the temperature first increases with height before decreasing, the maximum observed radiometric temperature is theoretically always less than the maximum ambient temperature. Even so, the applicable height output specifies the existence of a ground inversion, the height of the inversion, and in general provides a measure of the intensity of the inversion which is about half the magnitude of that observed. Thus the applicable height concept helped establish the feasibility of deriving useful information by passively probing the atmosphere with a millimeter wave radiometer. At the same time, a number of deficient areas were identified in the hardware state of the art and it is only fair to state that subsequent advanced developments in this area proceeded more rapidly than in the signal processing and interpretation area.

The problem of extracting details of the air temperature structure becomes increasingly more difficult the higher the height and the smaller the magnitude of the temperature discontinuity. This is the case with elevated inversions, and efforts to solve this problem were not undertaken to any great extent until this past year when significant advances in hardware and computer simulation technology, coupled with experimental evidence of the utility of passive probing, warranted proceeding to the more difficult area of elevated inversions.

A four-prong attack was made this year in an effort to derive useful information on elevated inversions within the first 1.5 km of the atmosphere. This region is most critical in trapping air pollutants. Two techniques (relaxation and a priori statistical) attempt to invert the radiometric data and derive the actual temperature profile. In effect, these two methods are attempting to solve the entire problem, whereas the other two techniques (gradient altitude model and analog) are geared to resolving the most important operational parameter, the height of the elevated inversions, that in turn, defines the mixing layer of the atmosphere where pollutants are trapped. The foregoing techniques are listed in decreasing order of sophistication.

Work on the a priori statistical approach is being conducted by E. Westwater at the Research Laboratories of the National Oceanic and Atmospheric Administration and they will submit their own separate report. This Final Report will cover the three areas of activity at the Sperry Rand Research Center, namely, the gradient altitude model, relaxation, and analog techniques.

The underlying assumption of the gradient altitude model is that the essence of an actual temperature profile can be represented by a model profile consisting of several straight-line segments. In the present work, attention was focused on a three-line segment model defined by the surface temperature and the following parameters: temperature lapse rate or temperature gradient in the first layer, altitude of the top of the first layer, temperature gradient in the second layer, altitude of the top of the second layer and, finally, the temperature gradient in the third layer. In its application to the analysis of radiometric data, the particular values of the model parameters which result in a best representation of the actual profile are determined statistically on the basis of the closeness between measured brightness temperature distributions and calculated distributions using the model temperature profile. Several methods of implementing this technique were considered. The particular method selected involved comparing and ranking the closeness of the measured and computed brightness temperature distributions corresponding to a finite number of model profiles. The number of model temperature profiles used is limited only by the computer time the user allots for the analysis. The technique was developed using simulated radiometric data. Preliminary results of its use on actual data observed during elevated inversion conditions show it to be very good in specifying the mixing layer depth. With respect to both the model and the method of selecting the parameters this technique is similar to the analog technique that has been developed.

The mathematical relaxation technique starts with an initial guess of the actual temperature profile and computes radiometric brightness temperatures from such a profile. The computed brightness temperatures are compared with the actual for each elevation angle increment and the differences are used to correct the initial guess profile. The modified profile becomes the new initial guess and the process is iterated until convergence is attained. This procedure places no restrictions on the type and shape of the air temperature profile and, as such, has the greatest potential. Presently, however, this technique suffers the most from numerical analysis problems and the usual difficulties of extracting meaningful data from small differences between large numbers.

Of the four different methods, only the analog technique does not require access to a computer for field application. It has been observed that an experienced THERMASONDE™ operator can visually analyze the recorder tracing of the radiometric brightness temperature versus elevation angle and specify the type of temperature distribution in the atmosphere. A more quantitative approach is provided by the analog method. Here the computer simulates the radiometric trace that corresponds to many different types of model profiles. In practice, the observed radiometric trace is visually matched to a library of computer-simulated brightness temperature versus elevation angle records and the profile providing the best fit is selected as representative of the actual. This technique was developed and tried on actual data to derive the mixing layer associated with elevated inversions. Good results were obtained from field observations taken at four different locations: California, Ohio, Florida, and North Carolina.

Each of these techniques and results is discussed in detail in the following sections.

SECTION 2

GRADIENT ALTITUDE MODEL

2.1 Introduction

In the initial stages of work on the problem of determining temperature profiles from radiometric data, the inversion* methods (as they are commonly called) sought to infer the maximum structural information inherent in the observations. It soon became apparent, however, that the information content of even ideal, errorless indirect-sensing measurements was limited[1]. The implication of this realization was that a temperature profile obtained by the inversion of radiometric data would not reveal the same degree of detail as one obtained from direct-sensing measurements of the same atmosphere, except of course in the unlikely case where the structure of the true profile was very simple. The presence of errors in the radiometric data, as would be the case in a real situation, indicated that the degree of detail obtainable in an indirectly observed temperature profile would be even further limited. In addition, numerical-simulation experiments had shown that, in many cases, attempts to derive temperature profiles from actual or simulated realistic data using sophisticated inversion schemes failed miserably. The deduced profile would either show almost no resemblence to that observed by direct means, or, if the inversion procedure were iterative in nature, convergence to a particular solution was generally not achieved.

---

* The mathematical procedures for translating or converting radiometric data in the form of brightness temperature or radiative intensity versus angle of observation and/or frequency into kinetic or air temperature versus altitude or pressure have for many years been referred to as inversion methods. The name derives from the early work on this subject in which simplifying yet reasonably tenable assumptions were postulated that resulted in the brightness temperature versus angle or frequency appearing as the Laplace transform of kinetic temperature versus altitude. Hence the desired function (kinetic temperature versus altitude) was the inverse of the measured function (brightness temperature versus angle or frequency) and could be determined by the process of inverting the transform function. Since this report deals with the meteorological phenomenon called inversion, i.e. ground-based or elevated inversions where the air temperature increases with height, the reader will have to be careful to distinguish between uses of the word 'inversion' which refer to the mathematical process and those which refer to the meteorological phenomenon.

The successful data analysis procedures were generally simple linear operator-type algorithms, such as our applicable height inversion algorithm. Although these schemes were capable of dealing with the crude data provided by the first generation radiometers, the information content of the results was limited especially in the case of reasonably low-noise data taken during the presence of elevated temperature inversions. When applied to such data, the results indicated at best only the presence of an elevated inversion--much the same as a polynomial whose coefficients are determined by a least squares best fit to observed direct sensor data would indicate the presence of the elevated inversion without clearly defining its features (see Fig. 1). The smoothed average-type profiles that these methods yielded were not well suited to the problem of determining base altitudes and vertical temperature gradients of elevated inversions.

2.2 Temperature Profile Models Suited to the Elevated Inversion Problem

The elevated inversion problem, or more simply the determination of mixing layer depths (altitude of the elevated inversion's base) and elevated inversion intensities, appears to require different radiometric data analysis methods.

Particularly important to this problem is that the temperature profile model for which the inversion scheme endeavors to find the parameters must be capable of clearly depicting an elevated inversion-type temperature profile. Temperature profile models utilizing continuous functions, such as polynomials of various types, were considered. Their principal disadvantage is that usually a large number of terms is required for the function to depict the sharp changes in the temperature gradients which occur at the base and top of the inversion layer while the usual procedures for deriving the polynomial coefficients of these from real data generally show an increasing tendency to become unstable as the number of terms increases.

A more appealing type of temperature profile model to use in the solution of this problem would be one in which the parameters to be determined are, or are directly related to, the base, intensity, and thickness of an elevated inversion. A simple temperature profile model with these characteristics consists of a series of connected straight-line segments, as shown in Fig. 1. In this model, which we have called the Gradient Altitude Model (GAM), the temperature gradients Γ_i and the altitudes of the transition points Z_i are the quantities determined by the inversion of the radiometric data.

The GAM satisfies the objective of being capable of clearly depicting a simple elevated inversion. In addition, by doing this with as few as five parameters, some of the instability problems that occur in the schemes which attempt to derive a greater number of parameters may be avoided. An obvious shortcoming of the GAM is its inability to represent complicated temperature profiles such as those having more than one elevated inversion when the number of parameters is limited to five. As will be shown later, in such a circumstance the base of the lower of the two elevated inversions is characterized accurately while the other inversions are represented by an average profile. In the present work, the five-parameter model was investigated since it was deemed to have the best chance of success and, if successful, could provide the information required by APCO. The problems of expanding the GAM to six or more parameters should be part of future investigations.

The fundamental precept in the determination of the GAM parameters from measured brightness temperature is that the particular values of Z_1, Z_2, Γ_1, Γ_2, and Γ_3 which produce the best GAM representation of the true temperature profile also result in minimization of the sum square of the difference between measured brightness temperatures and brightness temperatures calculated using the GAM temperature profiles. These particular values of the parameters have been designated as the "best fitting parameters." The function to be minimized, i.e.,

$$F(\underline{P}) = \sum_{k=1}^{N} \left(T_{B_k} - \hat{T}_{B_k}(\underline{P}) \right)^2 \qquad (1)$$

where $\underline{P} = \{Z_1, Z_2, \Gamma_1, \Gamma_2, \Gamma_3\} = \{P_j\}$ $j = 1, 2, 3, 4, 5$

T_{B_k} = measured brightness temperatures at elevation angle θ_k and frequency ν_k

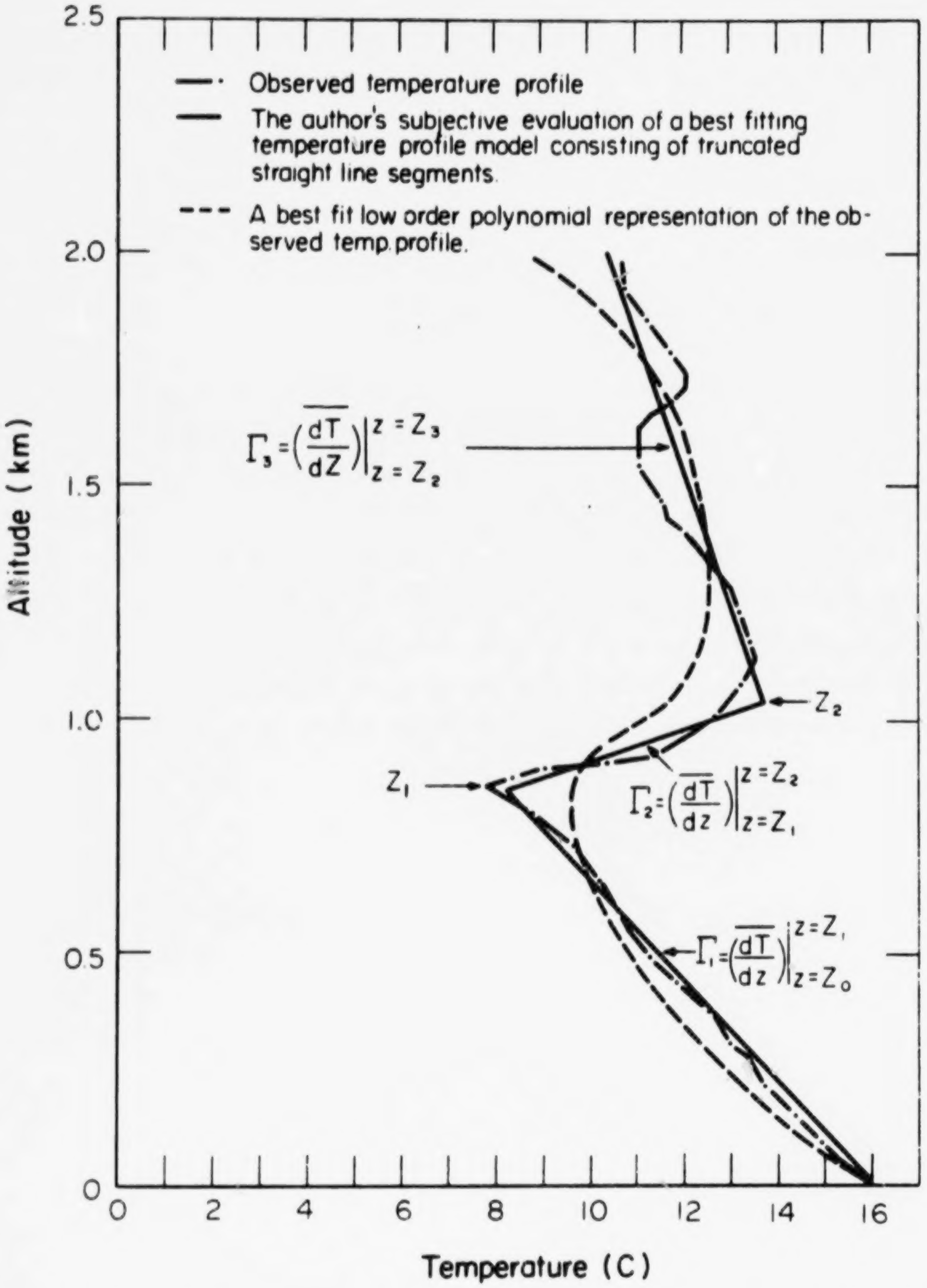

FIG. 1 An observed temperature profile and representations thereof by a model temperature profile consisting of three truncated straight-line segments and by a best fit low-order polynomial. The observed profile was obtained at Raleigh, N. C. by a helicopter sounding on 1969 October 15.

and $\hat{T}_{B_k}$ = calculated brightness temperatures at elevation angle θ_k and frequency ν_k

is nonlinear and the result of applying the necessary conditons for a minimum, i.e.,

$$\frac{\partial F(\underline{P})}{\partial P_j} = 0 \quad j = 1, 2, 3, 4, 5 \tag{2}$$

do not lead to a set of equations from which the value for each of the best fitting parameters can be expressed in terms of the measurements only. There are, however, many numerical procedures for finding the best fitting parameters. A common point among them is that they generate, or are given, a large number of combinations of trial values of the parameters, for which brightness temperatures must be calculated at one or sometimes all of the frequencies and angles of observation. In some cases this may result in a rather large number of brightness temperature calculations which, if done by the usual procedure of numerically evaluating the exact expression for brightness temperature, could be prohibitively costly in terms of computer time. It therefore was necessary to investigate and develop, if possible, a fast-running approximation routine for the calculation of brightness temperature.

2.3 Fast-Running Brightness Temperature Calculations

The principal time-consuming elements in the calculation of brightness temperature from the exact expressions are the complex dependence of the absorption coefficient upon temperature, pressure, humidity, frequency, and the multiplicity of absorption coefficient calculations required for each brightness temperature calculation. Therefore, one effective way to achieve significant time saving in the calculation of brightness temperature is to find a simple but accurate estimation formula for absorption coefficient versus altitude. As shown in Fig. 2, the atmospheric absorption coefficient in the 5 millimeter wavelength region can be approximated with a fair degree of accuracy by the expression

$$\tilde{\gamma}_\nu(z) = e^{b_\nu - a_\nu z} \tag{3}$$

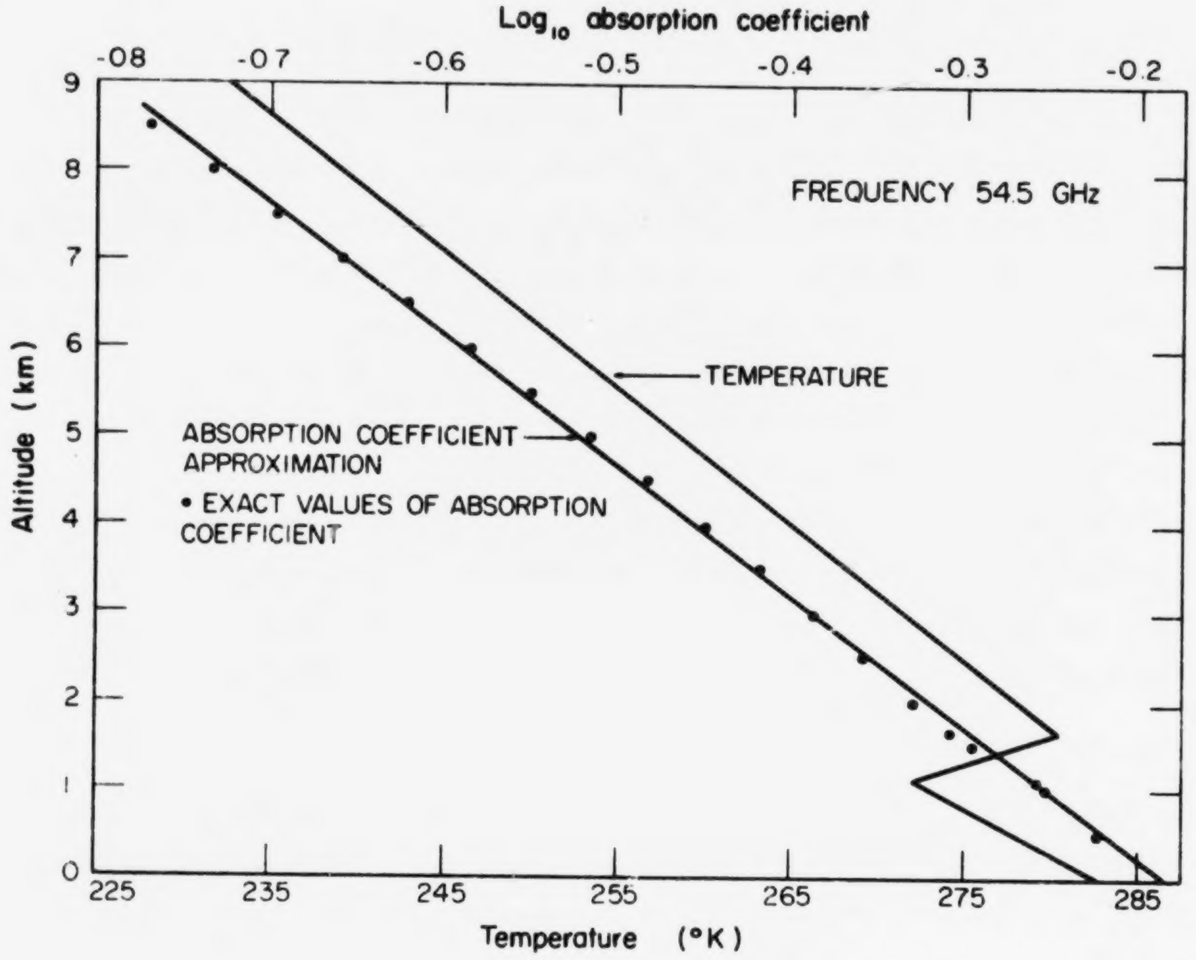

FIG. 2 Comparison of the exact value of the atmosphere absorption coefficient and the approximation expression $\tilde{\gamma}_\nu(z) = \exp\{b_\nu - a_\nu z\}$. The temperature profile from which the exact values were obtained is also shown.

where $\tilde{\gamma}_\nu(z)$ = approximate absorption coefficient at altitude z and frequency ν,

and b_ν, a_ν = frequency-dependent coefficients.

The temperature profile from which the exact values of the absorption coefficient were calculated is also shown in Fig. 2. The relative humidity was assumed to be zero at calculated levels. The pressure profile was determined from the hydrostatic law and the surface pressure. The coefficients a_ν and b_ν are determined by calculating the exact value of the absorption coefficient $\gamma_\nu[T(z), P(z), RH(z)]$ directly from temperature, pressure, and humidity profiles at several altitudes, z_i, $i = 1,2...I$, then by linear regression finding the a_ν and b_ν which minimize the sum

$$\sum_{i=1}^{I}\left(\log_e \gamma_\nu(z_i) - b_\nu + a_\nu z_i\right)^2$$

The exact value of brightness temperature is given by the equation

$$T_{B_k} = \int_0^H T(z)\, \gamma_{\nu_k}(z) \exp\left\{-\int_0^z \gamma_{\nu_k}(z')\, \mu_k\, dz'\right\} \mu_k\, dz + E_k \exp\left\{-\int_0^H \gamma_{\nu_k}(z)\, \mu_k\, dz\right\} \qquad (4)$$

where $\hat{T}_{B_k}$ = brightness temperature

$T(z)$ = temperature profile

$\gamma_{\nu_k}(z)$ = absorption coefficient at frequency ν_k

μ_k = geometric factor at elevation angle θ_k for determining slant path displacement ds from vertical displacement dz.

E_k = equivalent radiative temperature of atmosphere beyond altitude H.

and H = termination altitude.

Note: the index k is used to define both the frequency and angle at which the brightness temperature is calculated.

Letting the temperature profile be defined by

$$T(z) = \begin{cases} T_o + \Gamma_1 z & \text{for } 0 \leq z < Z_1 \\ T_o + \Gamma_1 Z_1 + \Gamma_2(z - Z_1) & Z_1 \leq z < Z_2 \\ T_o + \Gamma_1 Z_1 + \Gamma_2(Z_2 - Z_1) + \Gamma_3(z - Z_2) & Z_2 \leq z < H \end{cases}$$

and using the absorption coefficient approximation (3) in Eq. (4), the brightness temperature for the GAM temperature profile at frequency ν_k and elevation angle θ_k is given by

$$\hat{T}_{B_k} = T_o + (E_k - T_H)e^{-\tau_k(H)} + \Gamma_1 \int_0^{Z_1} e^{-\tau_k(z)}\, dz + \Gamma_2 \int_{Z_1}^{Z_2} e^{-\tau_k(z)}\, dz + \Gamma_3 \int_{Z_2}^{H} e^{-\tau_k(z)}\, dz \qquad (5)$$

where

$$\tau_k(z) = \int_o^z \mu_k \exp\left\{ b_{\nu_k} - a_{\nu_k} z \right\} dz = \bar{\mu}_k \frac{e^{b_k}}{a_k} \left(1 - e^{-a_k z} \right)$$

T_o = surface temperature

and T_H = temperature at altitude H

$\bar{\mu}_k$ = mean value of μ_k over interval $[0, z]$

An accurate and fast running numerical procedure was developed by Mr. Leland A. Gardner of the SRRC Signal Processing Group for evaluating the exponential integrals of the form

$$\int_a^b e^{-\beta e^{-\alpha z}} dz$$

which occur in Eq. (5). The calculation of brightness temperature by Eq. (5) which has been named the fast-running brightness temperature model (FRBTM) appears to be about 2 to 3 times faster than that by the direct numerical integration of Equation (4). The accuracy of the FRBTM in comparison with the exact T_{B_k} is acceptable for the present and will be discussed in more detail later.

The termination altitude H is the maximum height to which information on the temperature profile may be obtained from ground-based brightness temperature measurement. Theoretically, brightness temperature should contain information on the temperature profile up to the limits of the atmosphere. From a practical point of view, however, the exponential decay-like nature of the atmospheric transmittance (Figs. 2 and 3 of Ref. 2) means that the difference between ground-level brightness temperature observations made on two atmospheric temperature profiles identical up to the termination altitude but different beyond this altitude, would, in most cases, be indistinguishable from the measurement uncertainties. Consequently, at and beyond the termination altitude an assumed temperature profile called the residual profile is used to calculate E_k.

The residual profile is specified by the user and is intended to be his best guess of the temperature profile above the termination altitude. In practice this could be the standard atmosphere or a climatological average profile suited to the season and location of the radiometric observations. The underlying assumption here is that the residual profile can be guessed with sufficient accuracy so that its contribution to the calculated brightness temperature, i.e.,

$$(E_k - T_H)e^{-\tau_k H}$$

will be accurate (with respect to the actual value of the brightness temperature contribution of the atmosphere beyond H) to within the uncertainty of the brightness temperature measurement. The realization of this assumption is dependent upon the particular termination altitude chosen, the frequency and angle of the brightness temperature observations, as well as the proximity of the chosen residual profile to the actual profile.

Currently there is no provision for determining the water vapor profile from the radiometric data. Consequently, this too must be estimated or guessed by the user. As in the case of the residual profile, it is felt that a user's guess based upon a surface humidity measurement will, in most cases, result in an indistinguishable difference (in the presence of measurement errors) between calculated brightness temperatures using a guessed vapor profile and those using the actual water vapor profile. The validity of this assumption is, to a large extent, dependent upon frequency of the observations. Observations at the frequencies closest to the center of the 5 mm oxygen absorption band will be least affected by water vapor.

2.4 Evaluation of the Fast-Running Brightness Temperature Model

The accuracy of the FRBTM was evaluated by comparing the approximate brightness temperatures obtained using it with the exact values calculated by direct numerical integration of Equation (4). The comparisons were made using various different combinations of GAM parameter values to determine whether or not the FRBTM yielded better brightness temperature approximations for one type of profile as compared with another. The brightness temperature calculations for each combination of GAM parameters* were made for both 5.0 and 10.0 km termination altitudes to assess the effect of this variable. In all cases, the frequency used was 54.5 GHz, the relative humidity was assumed to be zero at all levels in both the GAM and residual profile regions, and the residual profile used was the U.S. Standard Atmosphere, 1962.

Tables I, II, and III are a sample of the results obtained in the comparison of the FRBTM approximate brightness temperatures and the exact values of brightness temperature. Inspection of the results indicated that each could be classified as belonging in one of the three categories exemplified by each of the tables. The results in Table I, in which the GAM parameters used were those of the temperature profile illustrated in Fig. 2, show that for both 5.0 and 10.0 km termination altitudes there is very good agreement at all elevation angles between the approximate and exact brightness temperatures. The type of result shown in Table I seems to be the general rule for GAM profiles showing an elevated inversion whose thickness $Z_2 - Z_1$ was about 0.5 km. The GAM parameters used to obtain the results shown in Table II are those of a lapse profile with only one temperature gradient change, (indicated by the equality of Z_1 and Z_2), in the GAM region. In this case the FRBTM approximate brightness temperatures were in much closer agreement with the

---

* The value of Γ_3 cannot be chosen or set unlike the other parameters Z_1, Z_2, Γ_1, Γ_2. Γ_3 is instead determined by the temperature at the particular value of Z_2, the termination altitude, and the temperature of the residual profile at the termination altitude. Consequently, only certain particular combinations of surface temperature, GAM parameters, termination altitude and residual profiles will result in the same Γ_3 for profiles with differing termination altitudes but in other respects identical. Therefore in the context of this report profiles referred to as having the same GAM parameters but differing termination altitudes and/or residual profiles are profiles in which the surface temperature, Z_1, Z_2, Γ_1, and Γ_2 are the same.

TABLE I

EXACT VS. APPROXIMATE BRIGHTNESS TEMPERATURES AND RESIDUAL PROFILE CONTRIBUTION FOR Γ_1 = -9.5 C/km, Z_1 = 1.1 km, Γ_2 = 1.5 C/km, Z_2 = 1.65 km

	Γ_3 = -6.9 C/km 5. km Termination				Γ_3 = -6.6 C/km 10. km Termination			
Elevation Angle	T_B Approx. K	T_B Exact K	Diff.* K	Residual Profile Contribution K	T_B Approx. K	T_B Exact K	Diff.* K	Residual Profile Contribution K
0	282.553	282.555	-.002	.000	282.555	282.555	.000	.000
10	280.016	280.015	.001	.000	280.061	280.016	.045	.000
20	270.460	278.459	.001	-.019	278.526	278.480	.046	-.003
30	277.106	277.094	.012	-.264	277.234	277.184	.050	-.097
40	275.301	275.277	.024	-1.065	275.517	275.470	.047	-.541
50	273.068	273.032	.036	-2.429	273.367	273.328	.039	-1.424
60	270.764	270.717	.047	-4.042	271.128	271.098	.030	-2.552
70	268.796	268.742	.054	-5.515	269.207	269.186	.021	-3.623
80	267.488	267.429	.058	-6.527	267.925	267.910	.015	-4.376
90	267.030	266.970	.060	-6.887	267.476	267.463	.013	-4.646

* Diff. = $T_{B_{approx}} - T_{B_{exact}}$

TABLE II

EXACT VS. APPROXIMATE BRIGHTNESS TEMPERATURES AND RESIDUAL PROFILE CONTRIBUTION FOR $\Gamma_1 = -10.5$ C/km, $Z_1 = 1.1$ km, $\Gamma_2 = -4.5$ C/km, $Z_2 = 1.1$ km

Elevation Angle	$\Gamma_3 = -3.8$ C/km 5 km Termination				$\Gamma_3 = -5.3$ C/km 10 km Termination			
	T_B Approx. K	T_B Exact K	Diff.* K	Residual Profile Contribution K	T_B Approx. K	T_B Exact K	Diff.* K	Residual Profile Contribution K
0	282.490	282.554	-.066	.000	282.485	282.554	-.070	.000
10	279.665	279.624	.041	.000	279.732	279.612	.120	.000
20	277.138	277.099	.039	-.019	277.119	276.956	.163	-.003
30	274.928	274.895	.033	-.262	274.725	274.555	.171	-.100
40	272.599	272.573	.026	-1.061	272.226	272.062	.164	-.556
50	270.073	270.054	.019	-2.423	269.572	269.425	.147	-1.455
60	267.610	267.596	.014	-4.035	267.022	266.892	.130	-2.602
70	265.560	265.551	.009	-5.507	264.918	264.803	.115	-3.691
80	264.212	264.207	.005	-6.519	263.541	263.436	.105	-4.451
90	263.743	263.739	.004	-6.879	263.062	262.961	.101	-4.723

* Diff. = $T_{B_{approx}} - T_{B_{exact}}$

exact values for the 5 km termination than for the 10 km termination. The third category of results is exemplified by Table III, in which the GAM parameters depicted a ground layer lapse with a thick isothermal layer above. This category shows the FRBTM approximate brightness temperatures to be in uniformly good agreement with those of the exact expressions at all elevation angles in the case of a 10.0 km termination, while in the case of a 5 km termination the differences between the exact brightness temperatures and those calculated from the FRBTM are markedly greater at the higher elevation angles than at the lower ones. In fact, this particular case exhibited one of the largest observed differences between exact and approximate brightness temperatures.

In general, the agreement between FRBTM and exact brightness temperatures is acceptable for all the parameter value combinations tested when viewed in comparison with the present day absolute accuracy with which brightness temperatures can be measured. The magnitude of the differences between exact and approximate brightness temperatures and the distribution of these differences with respect to elevation angle appears to be dependent upon the particular combination of GAM parameter values for which brightness temperatures are being calculated. There was some indication that parameter value combinations representing elevated inversions of about one-half kilometer thickness tended to give better agreement between the exact and approximate brightness temperatures than other parameter value combinations. The reason for this behavior, which was somewhat unexpected, is not completely understood. Although the principal reason for the differences is undoubtedly the absorption coefficient approximation, a small (but perhaps not insignificant) cause is due to the geometric factor μ_k which is given by the equation

$$\mu_k = \left\{1 - \left(\frac{R_e}{z+R_e}\right)^2 \cos^2 \theta_k\right\}^{-1/2} \qquad (6)$$

where R_e = radius of the earth (See Ref. 2, p11).

In the exact calculation, the variability of μ_k with respect to z is taken into account. However, in the FRBTM it is assumed that since the range

TABLE III

EXACT VS. APPROXIMATE BRIGHTNESS TEMPERATURES AND RESIDUAL PROFILE CONTRIBUTION FOR $\Gamma_1 = -10.5$ C/km, $Z_1 = .9$ km, $\Gamma_2 = 0$ C/km, $Z_2 = 2.5$ km

Elevation Angle	$\Gamma_3 = -5.7$ C/km 5 km Termination				$\Gamma_3 = -6.2$ C/km 10 km Termination			
	T_B Approx. K	T_B Exact K	Diff.* K	Residual Profile Contribution K	T_B Approx. K	T_B Exact K	Diff.* K	Residual Profile Contribution K
0	282.480	282.554	-.075	.000	282.479	282.554	-.075	.000
10	279.742	279.724	.018	.000	279.791	279.723	.068	.000
20	277.779	277.763	.016	-.021	277.835	277.764	.071	-.003
30	276.163	276.128	.035	-.283	276.230	276.158	.072	-.100
40	274.265	274.189	.076	-1.116	274.359	274.285	.074	-.550
50	272.025	271.900	.125	-4.528	272.151	272.074	.077	-1.445
60	269.747	269.575	.172	-4.171	269.902	269.818	.084	-2.586
70	267.811	267.602	.209	-5.673	267.988	267.899	.089	-3.669
80	266.525	266.294	.231	-6.704	266.716	266.622	.094	-4.430
90	266.075	265.836	.239	-7.070	266.270	266.176	.094	-4.703

* Diff. = $T_{B_{approx}} - T_{B_{exact}}$

of z is small (i.e., $0 \le z \le 10$) and therefore $z \ll R_e$, the approximation

$$\bar{\mu}_k \approx \left\{1 - \left(\frac{2R_e}{H+2R_e}\right)^2 \cos^2 \theta_k\right\}^{-\frac{1}{2}} \tag{7}$$

would not introduce significant error in the approximate brightness temperatures but would, of course, remove the complicating effect of the z variability in the geometric factor.

Although approximate brightness temperatures generally showed greater average deviation from the exact values for a 10 km rather than 5 km termination altitude, in many instances, however, they were not significantly larger and, occasionally, smaller. This, in combination with the small reduction in residual profile contribution (a very desirable effect, since it reduces somewhat the accuracy requirements on the residual profile) resulting from the use of a 10 km rather than 5 km termination altitude, would seem to indicate that higher termination altitudes might be preferable in practice. However, as will be shown later, other factors tend to negate this conclusion.

2.5 Methods of Determining the Best Fitting GAM Parameters from Radiometric Data

Originally we had intended to test three methods of determining the best fitting GAM parameters from radiometric data. Two of the methods were techniques in which the user was required to make an initial guess of the parameter values, an estimate of the interval in which the best fitting values of the parameters would be found and other statistical factors relating to the accuracy of the data and the user's confidence in his parameter estimates. With this information as a starting point, deterministic and random methods are used to generate successive sets of values for the GAM parameters which are then used to calculate the sum square of differences between measured and calculated brightness temperatures (Eq. (1)). This process continues until a set of parameter values is found that produces a minimum sum square.

The nature of the function whose minimum is being sought is, however, one in which the surface generated by the sum square of differences appears to have several minima. The problem is to find the parameter values giving rise to the smallest minimum. This particular set of parameter values is assumed to be the ones which best represent the true temperature profile. Figure 3 is an illustration of the nature of the $F(\underline{P})$ surface. Point B represents the minimum that is sought. It is likely, however, that some minimization procedures will work their way into points A, C, or D and remain there unless provisions are made to test other regions of the surface. This is precisely what happened in two of the methods that were tried. In all likelihood, methods can be developed that will avoid or at least alleviate this difficulty somewhat but it will take time to do so. Therefore, it was felt that for the present it would be more profitable to go to a third method which, although more costly in terms of computer time, is not subject to the multiple minima difficulty and which could, in the time available, give some indication as to the feasibility of the entire scheme.

This method which we have called the GRID scheme requires the user to specify several values for each of the GAM parameters. The sum square function $F(\underline{P})$ is then calculated for each physically realizable and non-redundant combination of the specified parameter values. The $F(\underline{P})$ corresponding to each such combination is then inspected; the smallest $F(\underline{P})$ and its corresponding parameter set $\underline{P}_m$ being thus determined.

A physically realizable combination of parameters is one which satisfies the following conditions:

$$Z_2 \geq Z_1 \tag{8}$$

$$\Gamma_1 \ Z_1 \text{ or } \Gamma_2(Z_2-Z_1) \text{ or } \Gamma_1 \ Z_1 + \Gamma_2(Z_2-Z_1) \leq 20 \ . \tag{9}$$

The first condition simply states that the upper bound of the elevated layer lies above the lower bound. The second condition eliminates any combination of parameters which gives rise to inversion layers, ground or elevated, in which the temperature increase exceeds 20 C. A redundant set of parameters is a set subsequent to a first set in which $Z_1 = Z_2$, Γ_1 and Γ_3 are fixed, and only Γ_2 is varied.

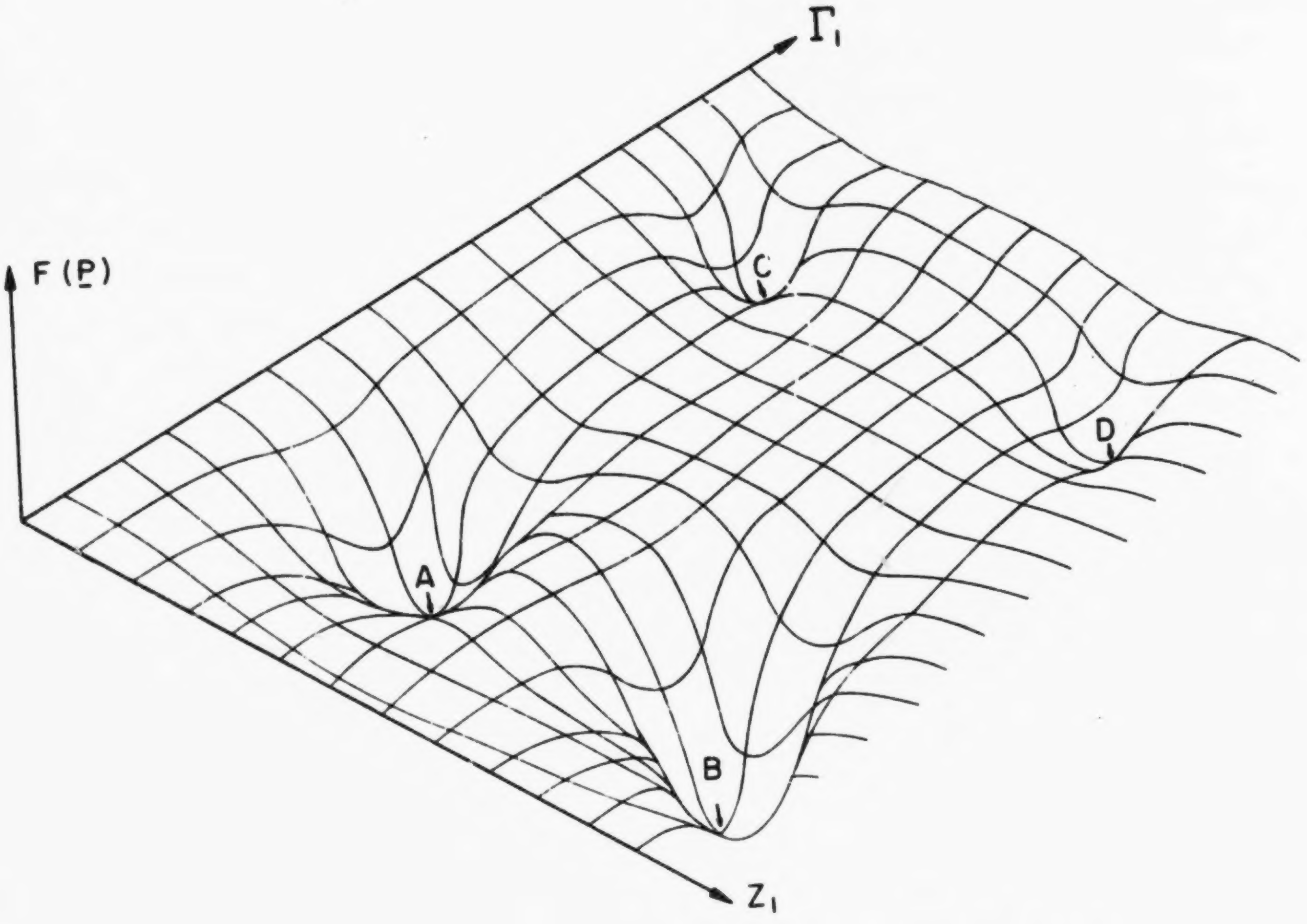

FIG. 3 Presumed nature of the F($\underline{P}$) surface illustrating the difficulty of finding the best fitting combination of parameters by certain analytical methods such as those employing gradients of F($\underline{P}$) .

Without any significant additional computational cost, we were able to include in the GRID scheme a calculation and ranking of $A(\underline{P})$, the sum of absolute values of the differences between measured and calculated brightness temperatures, i.e.,

$$A(\underline{P}) = \sum \left| T_{B_k} - \hat{T}_{B_k}(\underline{P}) \right| \tag{10}$$

It was suggested that a minimum sum of the absolute values of the differences might be a better criterion for determining the best fitting parameters than a minimum sum of the squares of the differences. The results, however, were inconclusive. The sum of absolute values criterion generally produced results similar to those obtained by the sum of squares criterion. In those instances where the results obtained by the two criteria differed, the sum of squares criterion tended to produce slightly better fitting parameters.

2.6 Test and Results Using the GRID Scheme to Determine the Best Fitting GAM Parameters from Radiometric Data

The first test was intended to establish the basic feasibility and practicality of the GAM inversion scheme. Specifically, the question posed was how well could the model and the inversion scheme, using a reasonable number of trial values for the GAM parameters and realistic radiometric records, distinguish between a lapse profile and elevated inversion-type profiles of average intensity? The test proceeded as follows: Exact brightness temperatures at 54.5 GHz and at elevation angles 0° to 40°, by 2° increments, and 40° to 90°, by 10° increments, were calculated for four GAM temperature profiles, the true parameters of which are given in Table IV. The termination altitude of each model profile was at 3 km; the residual profile for each was the U. S. Standard Atmosphere 1962. The atmospheres were assumed to be absolutely dry at all levels.

Gaussian noise with a standard deviation of 0.11 C was then added to the exact brightness temperatures to produce brightness temperature records which fairly accurately simulated the quality of data obtainable with our Mark O

TABLE IV

PARAMETERS OF THE MODEL PROFILES

Model Profile	Γ_1 Lapse Rate Surface to First Breakpoint (C/km)	Z_1 Altitude of First Breakpoint (km)	Γ_2 Lapse Rate First to Second Breakpoint (C/km)	Z_2 Altitude of Second Breakpoint (km)
Lapse	-6	None	-6	None
.5 km base Elev. Inv.	-6	.5	+20	.75
1. km base Elev. Inv.	-6	1.0	+20	1.25
1.5 km base Elev. Inv.	-6	1.5	+20	1.75

THERMASONDE™. Three "noisy" records were then produced from the exact or noiseless data of each model profile. The three simulated data records were then averaged and the resultant average data record for each of the model profiles was used as input to GRID.

The trial values used by GRID in the inversion of the simulated brightness temperature records are given in Table V. More values could have been used at the expense of increased computer time. In selecting these particular values, we were endeavoring to test a worst possible situation, namely, one in which none of the trial values would correspond to any of the actual or true parameter values listed in Table IV and, furthermore, that at best two trial values for each parameter would bracket the true values equally on both sides. Note that even with this limited number of trial values of Z_1 , the scheme (if it were successful) could, in theory, determine the altitude of the base of an elevated inversion laying between .2 and 2 km to within 20% of its actual value.

The computer program which implements the GRID scheme has an option for using either or both the exact and approximate brightness temperature cal-

TABLE V

TRIAL VALUES OF GAM PARAMETERS

Γ_1 (C/km)	Z_1 (km)	Γ_2 (C/km)	Z_2 (km)
-9.5, -8.5, -7.5, -6.5, -5.5, -4.5	.25, .35, .45, .55, .7, .9, 1.1, 1.35, 1.65	-10., -5., +7.5, +15., +25.	.83, 1.03, 1.28, 1.58, 1.93, 2.33* .65, .85, 1.1, 1.4, 1.75, 2.15**

* These trial values of Z_2 were used in the analysis of data from the lapse and .5 km base elevated inversions.

** These trial values of Z_2 were used in the analysis of data from the 1. and 1.5 km base elevated inversions.

culating routines. In this test we used only the FRBTM routine. The assumed humidity values in the GAM and residual profile regions were all zero, thus eliminating from the test any water vapor effects. The assumed termination altitude used in GRID was 5 km, whereas the data samples were calculated using a 3 km termination altitude. The residual profile assumed was the U. S. Standard Atmosphere 1962; again, the same was used to calculate the simulated radiometric data, thus eliminating the effects of this variable from the test.

The first and second choice best fitting parameters selected by GRID according to a minimum sum of squares of differences between measured and calculated brightness temperatures are given in Table VI and illustrated in Fig. 4. The designations "first choice" and "second choice" in Table VI and Fig. 4 indicate the first and second best parameter sets selected by GRID. The second choice for the lapse profile, when plotted, was indistinguishable from the first choice, hence it is not shown. The first and second choice best fitting parameters selected by GRID according to a minimum sum of absolute values of differences between measured and calculated brightness temperatures are given in Table VII. With the exceptions of the second choice Z_2 in the lapse case and both choices in the 1 km elevated inversion case, the parameters

TABLE VI

FIRST AND SECOND CHOICE BEST FITTING PARAMETERS

SELECTED BY GRID ACCORORDING TO A MINIMUM SUM OF SQUARES CRITERION

Model Profile	Choice	Γ_1 (C/km)	Z_1 (km)	Γ_2 (C/km)	Z_2 (km)	F(P)
Lapse	1st	-6.5	.45	-5.	.83	.325
	2nd	-6.5	.55	-5.	1.58	.330
.5 km base	1st	-5.5	.55	+15.	.85	.336
Elev. Inv.	2nd	-7.5	.35	+ 7.5	.85	.368
1. km base	1st	-6.5	.9	+25.	1.1	.448
Elev. Inv.	2nd	-5.5	1.35	+15.	1.75	.450
1.5 km base	1st	-6.5	1.35	+25.	1.58	.342
Elev. Inv.	2nd	-6.5	1.1	+ 7.5	1.58	.418

TABLE VII

FIRST AND SECOND CHOICE BEST FITTING PARAMETERS

SELECTED BY GRID ACCORDING TO A MINIMUM SUM OF ABSOLUTE VALUES CRITERION

Model Profile	Choice	Γ_1 (C/km)	Z_1 (km)	Γ_2 (C/km)	Z_2 (km)	A(P)
Lapse	1st	-6.5	.45	-5.	.83	2.285
	2nd	-6.5	.55	-5.	1.28	2.326
.5 km	1st	-5.5	.55	+15.	.85	2.338
Elev. Inv.	2nd	-7.5	.35	+ 7.5	.85	2.446
1. km	1st	-5.5	1.35	+15.	1.75	2.684
Elev. Inv.	2nd	-6.5	.9	+25.	1.1	2.732
1.5 km	1st	-6.5	1.35	+25.	1.58	2.421
Elev. Inv.	2nd	-6.5	1.1	+ 7.5	1.58	2.632

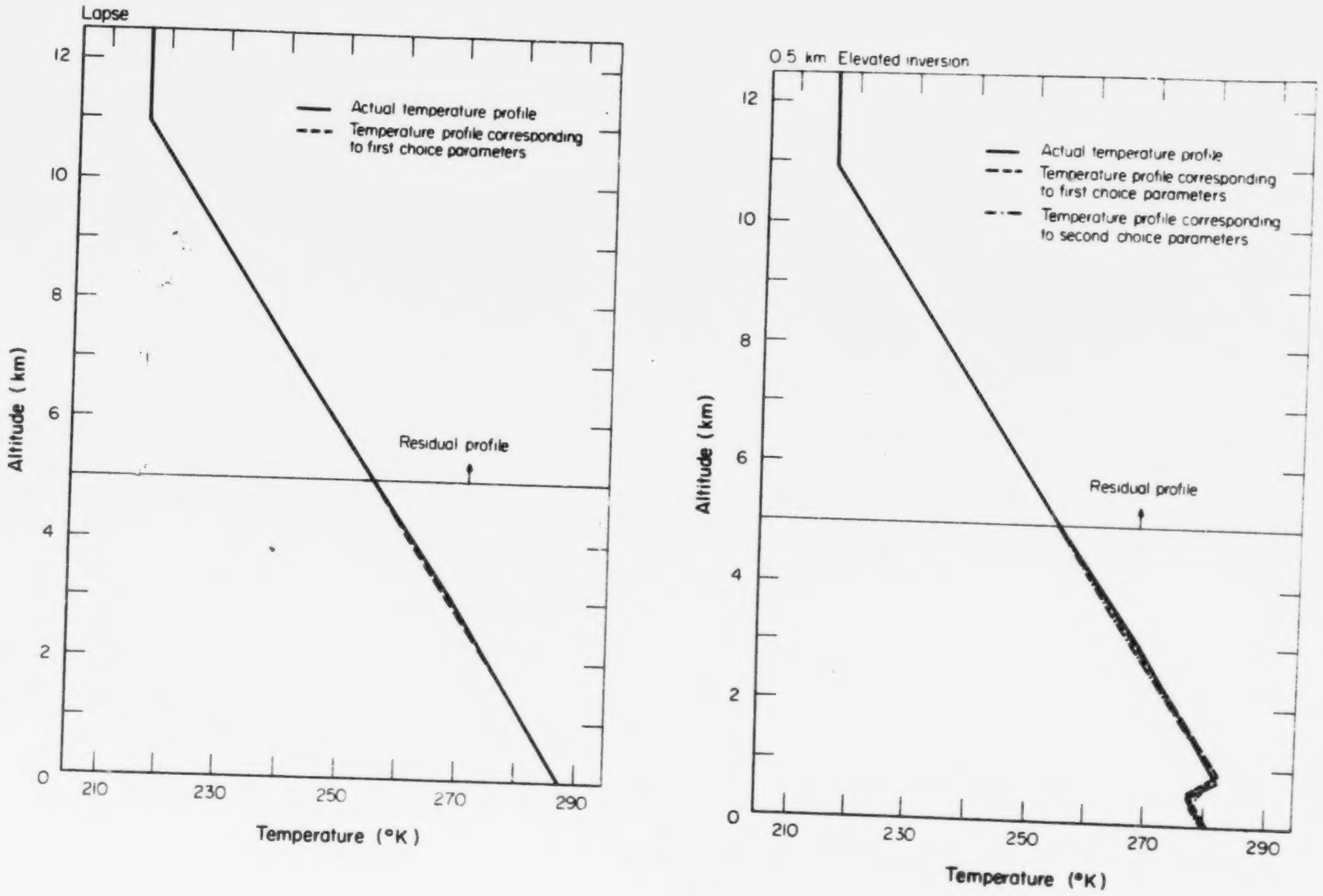

FIG. 4 Results of using GRID inversion scheme on simulated radiometric data from four model temperature profiles.

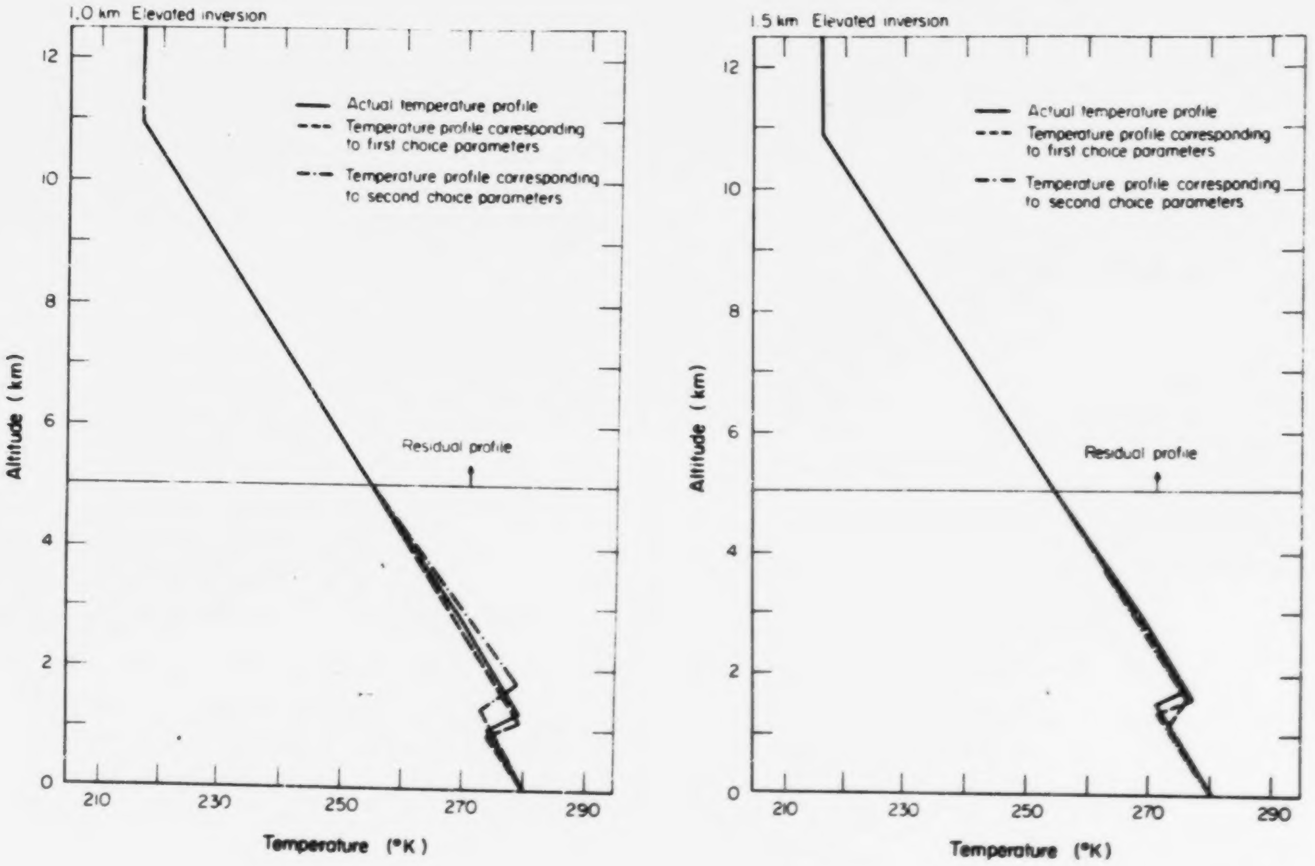

FIG. 4 (Continued) Results of using GRID inversion scheme on simulated radiometric data from four model temperature profiles.

selected by each of the criteria were the same. Equally apparent in the results was the closeness of the numerical values of F(P) of Table VI for the first and second choice parameters which represent noticeably different temperature profiles. The same was true for the absolute value criterion.

This first comprehensive test of the various aspects of the GAM inversion scheme working together was a significant success. In the case of each model profile the first choice best fitting parameters selected according to a minimum sum of squares criterion was a best possible choice. This was particularly gratifying in view of the fact that the trial parameters were as different from the actual parameters as they are ever likely to be in practice. Another promising aspect was that these results were obtained using noisy data similar in nature to that which is obtained from real radiometers.

The next step was to move from model profiles to a real profile as the source of simulated data. A search was made in our library of North America RAOB/RAWINSONDE records for temperature profiles exhibiting low-level (0 to 2 km base) elevated inversion. Several such profiles were found and from them the Bismarck, N.D. 00Z 2 April 1968 RAOB was chosen to be the source of data for a series of tests. This particular profile (see Fig. 5) was selected because it appeared to be typical of an elevated inversion-type profile that is decidedly difficult to model with three line segments. This profile provided a good test to determine whether the GRID scheme and GAM could define the mixing layer depth, which in this case would be defined as the base of the elevated isothermal layer.

The exact values of simulated brightness temperatures were calculated at 54.5 GHz for elevation angles 0° to 50°, in increments of 2° and for the angles 60°, 70°, 80° and 90°. The Bismarck RAOB, humidity profile included, was used as the input temperature and water vapor profile from the surface to 100 mb where the record terminated. Since 100 mb is not high enough for calculations of 54.5 GHz brightness termperature at high elevation angles, the RAOB sounding of Rapid City, S.D. 00Z 2 April 1968 from 70 mb to 13 mb was added. The particular questions which we were endeavoring to answer in the series of tests using the Bismarck, N.D. data sample required errorless data; accordingly, no random noise was added as in the previous test. The trial values of the

GAM parameters from which the solution was to be chosen are given in Table VIII.

TABLE VIII

TRIAL VALUES OF THE GAM PARAMETERS USED IN THE SERIES OF TESTS ON THE BISMARCK, N.D. SIMULATED DATA

Γ_1 (C/km)	Z_1 (km)	Γ_2 (C/km)	Z_2 (km)
-10.5, -9.5, -8.5,	.25, .35, .45,	-8, -4.5, 0,	.6, .75, .9, 1.1,
-7.5, -6.5, -5.5	.55, .7, .9, 1.1	+7.5, +15, +25	1.35, 1.65, 2.5

The primary purpose of the test using the Bismarck, N.D., data was to evaluate the ability of the GRID scheme and GAM on ideal data from real profiles. Even though the real profile cannot be fit by three straight lines, it was hoped that the best set of parameters determined by the method in the statistical sense would accurately define the mixing depth. Since the method can be applied under a variety of conditions, the test was also performed to appraise: 1) the effect of the approximate, rather than the exact, brightness temperature calculating routine; 2) the effect of a standard, rather than the actual, residual profile; and 3) the effect of varying termination altitudes. The various combinations of these test conditions are presented in Table IX, and are identified by indices of the form Ai or Ei where A and E indicate the use of approximate (A) and exact (E) computations of brightness temperature. The index i is an integer from 1 to 4, indicating the four combinations of termination altitude and residual profile. Table IX also contains the results (i.e., parameter sets chosen) under each of the combinations using both the sum of the squares (SSQ) criterion and the sum of the absolute values (SAV) criterion. The values of these criteria are also presented in Table IX. It is immediately noted that both criteria chose the same parameter set as optimum for the same test conditions. This indicates that no advantage is gained using one criterion rather than the other.

TABLE IX

BEST FITTING GAM PARAMETERS SELECTED BY GRID ACCORDING TO MINIMUM SUM OF SQUARES AND MINIMUM SUM OF ABSOLUTE VALUES CRITERIA

Test	Criteria	Termination Altitude (km)	Residual Profile	Brightness Temperatures	PARAMETERS				F (P) (SSQ)	A (P) (SAV)
					I_1 (C/km)	Z_1 (km)	Γ_2 (C/km)	Z_2 km		
A1	SSQ	5.0	Actual	Approximate	-10.5	1.1	+15.	1.35	.109	
	SAV	5.0	Actual	Approximate	-10.5	1.1	+15.	1.35		1.602
E1	SSQ	5.0	Actual	Exact	-10.5	1.1	+15.	1.35	.098	
	SAV	5.0	Actual	Exact	-10.5	1.1	+15.	1.35		1.469
A2	SSQ	5.0	Std. Atmos.	Approximate	-9.5	1.1	0.	1.35	.313	
	SAV	5.0	Std. Atmos.	Approximate	-9.5	1.1	0.	1.35		2.447
E2	SSQ	5.0	Std. Atmos.	Exact	-10.5	.9	0.	1.35	.120	
	SAV	5.0	Std. Atmos.	Exact	-10.5	.9	0.	1.35		1.677
A3	SSQ	10.0	Actual	Approximate	-10.5	.9	0.	1.65	.268	
	SAV	10.0	Actual	Approximate	-10.5	.9	0.	1.65		2.430
E3	SSQ	10.0	Actual	Exact	-10.5	.9	0.	1.65	.156	
	SAV	10.0	Actual	Exact	-10.5	.9	0.	1.65		1.564
A4	SSQ	10.0	Std. Atmos.	Approximate	-9.5	.9	-4.5	2.5	.724	
	SAV	10.0	Std. Atmos.	Approximate	-9.5	.9	-4.5	2.5		3.735
E4	SSQ	10.0	Std. Atmos.	Exact	-9.5	1.1	0.	1.65	.291	
	SAV	10.0	Std. Atmos.	Exact	-9.5	1.1	0.	1.65		2.391

Both the SSQ and SAV have their smallest values for the test case E1 which corresponds to a termination altitude of 5 km, the actual residual profile beyond 5 km, and exact calculations of brightness temperature. This result is expected, since these conditions are the most ideal presented in Table IX. Similarly, the case expected to provide the worst results (largest error) would be the conditions corresponding to a termination altitude of 10 km, the standard atmosphere profile as the residual beyond 10 km, and the approximate calculations of brightness temperature. These conditions correspond to test case A4, and indeed this case has the largest errors. It is difficult to make judgements beyond the best and worst cases, since many of the error values are nearly the same; in some cases they correspond to the same predicted parameters. For this reason, plots of the predicted profiles versus the true profile are presented in Figs. 5, 6, 7, and 8 for each of the test cases.

With the possible exception of the results of Test A4, the temperature profiles corresponding to the first choice best fitting parameters selected in all tests of this series clearly indicate the existence of an elevated inversion or isothermal layer. Furthermore, the base of this layer, and consequently the mixing layer depth, is determined in all cases by the chosen parameters to within 20% of its true value. The overall result of this test series is that the GRID scheme and GAM can (at least in the case of the ideal data) determine with fair accuracy the mixing layer depth of a real temperature profile exhibiting an elevated inversion. In those tests where the results were poorest, the functions $F(\underline{P})$ and $A(\underline{P})$ were large. This should be construed by the user as an indication that other trial parameter values might produce better results which correspond to lower values for $F(\underline{P})$ and $A(\underline{P})$.

A comparison of all the results show that the parameter choices appear to be affected less by the method of calculating brightness temperature than they are by the particular choice of residual profile. It is, nevertheless, evident that some improvement would be obtained if the exact or at least a more accurate brightness temperature calculating routine were used. This seems to be particularly true, as a comparison of the results of tests A4 and E4 indicates, when the true residual profile is not known.

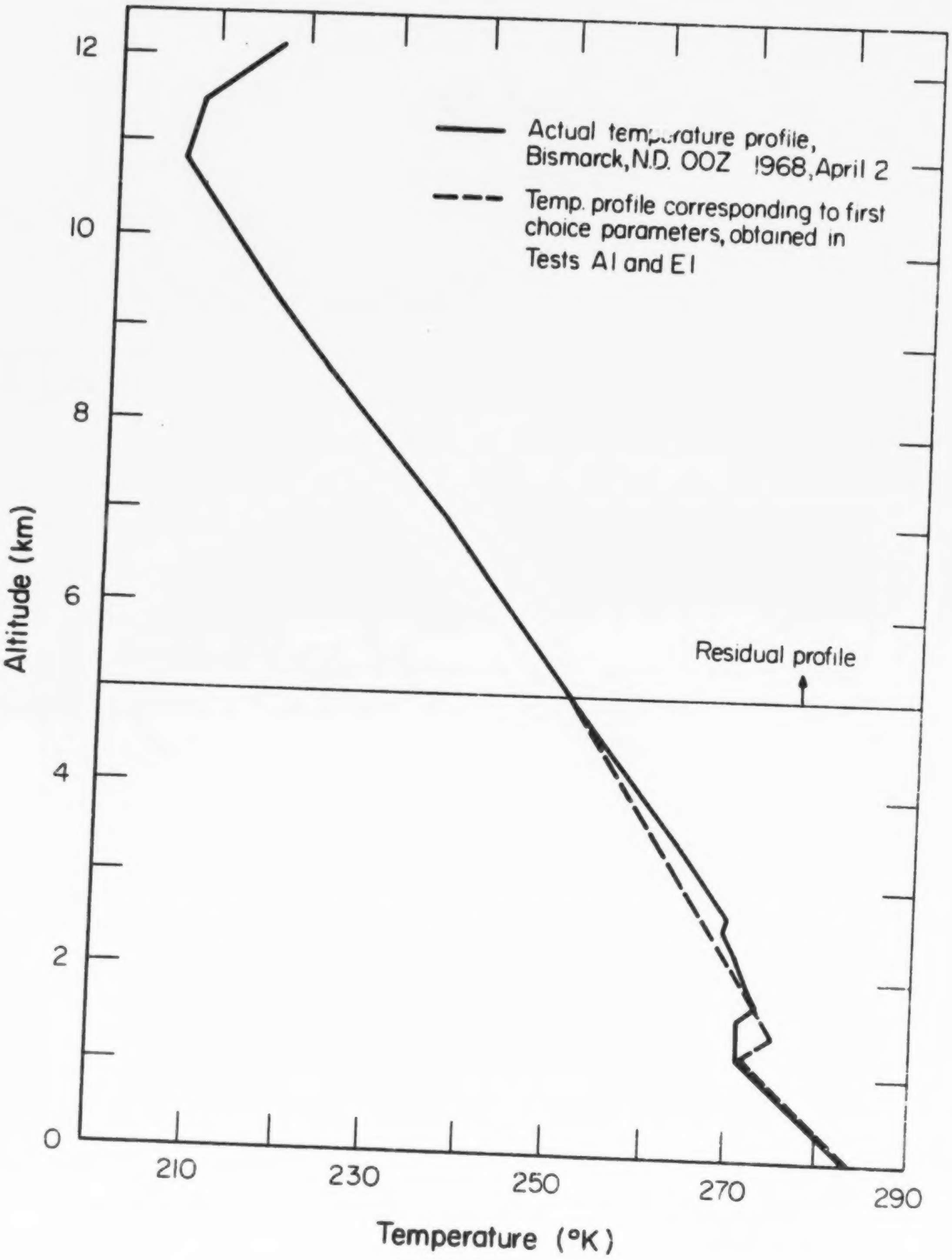

FIG. 5 Results of Tests A1 and E1.

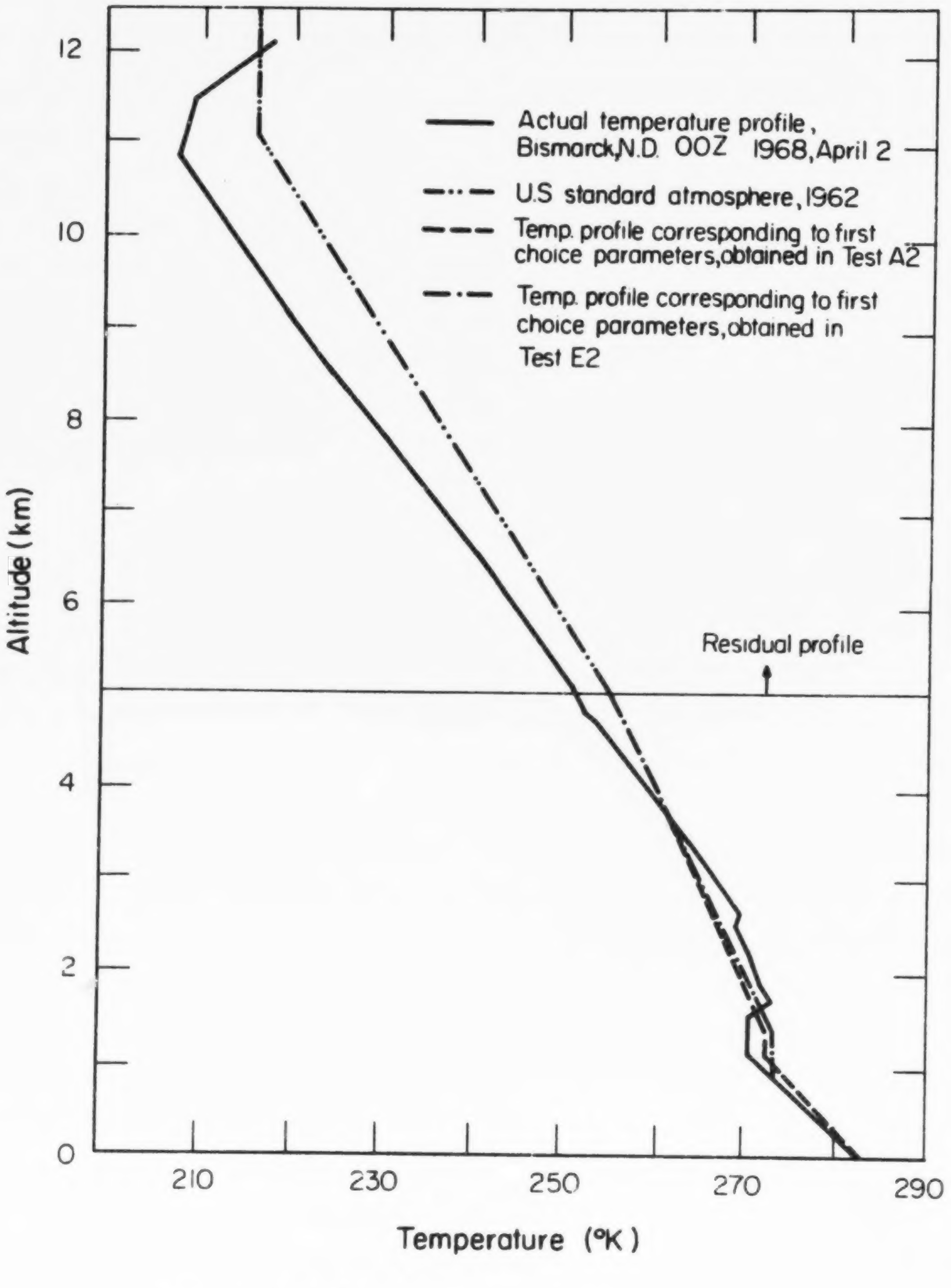

FIG. 6 Results of Tests A2 and E2.

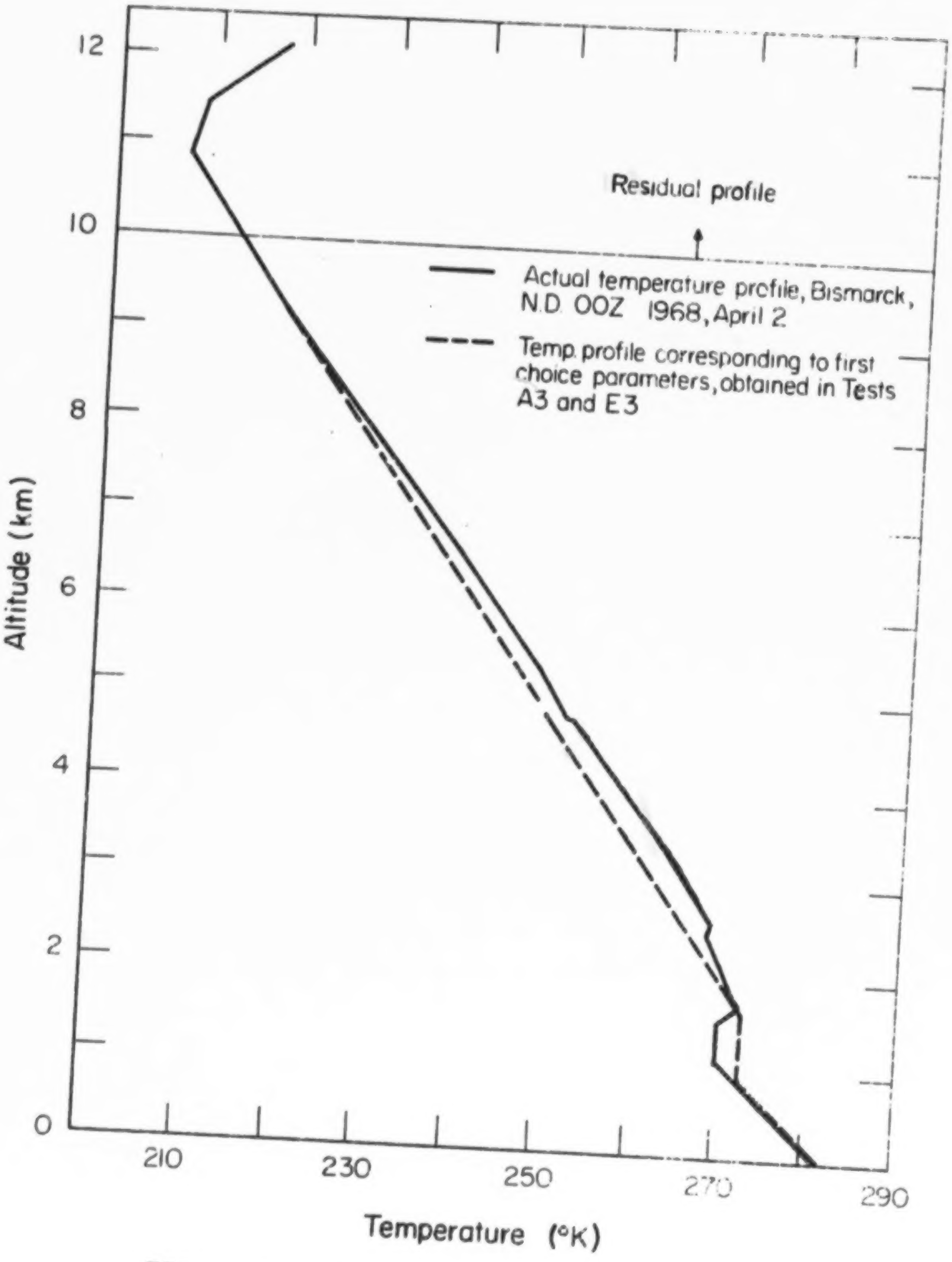

FIG. 7 Results of Tests A3 and E3.

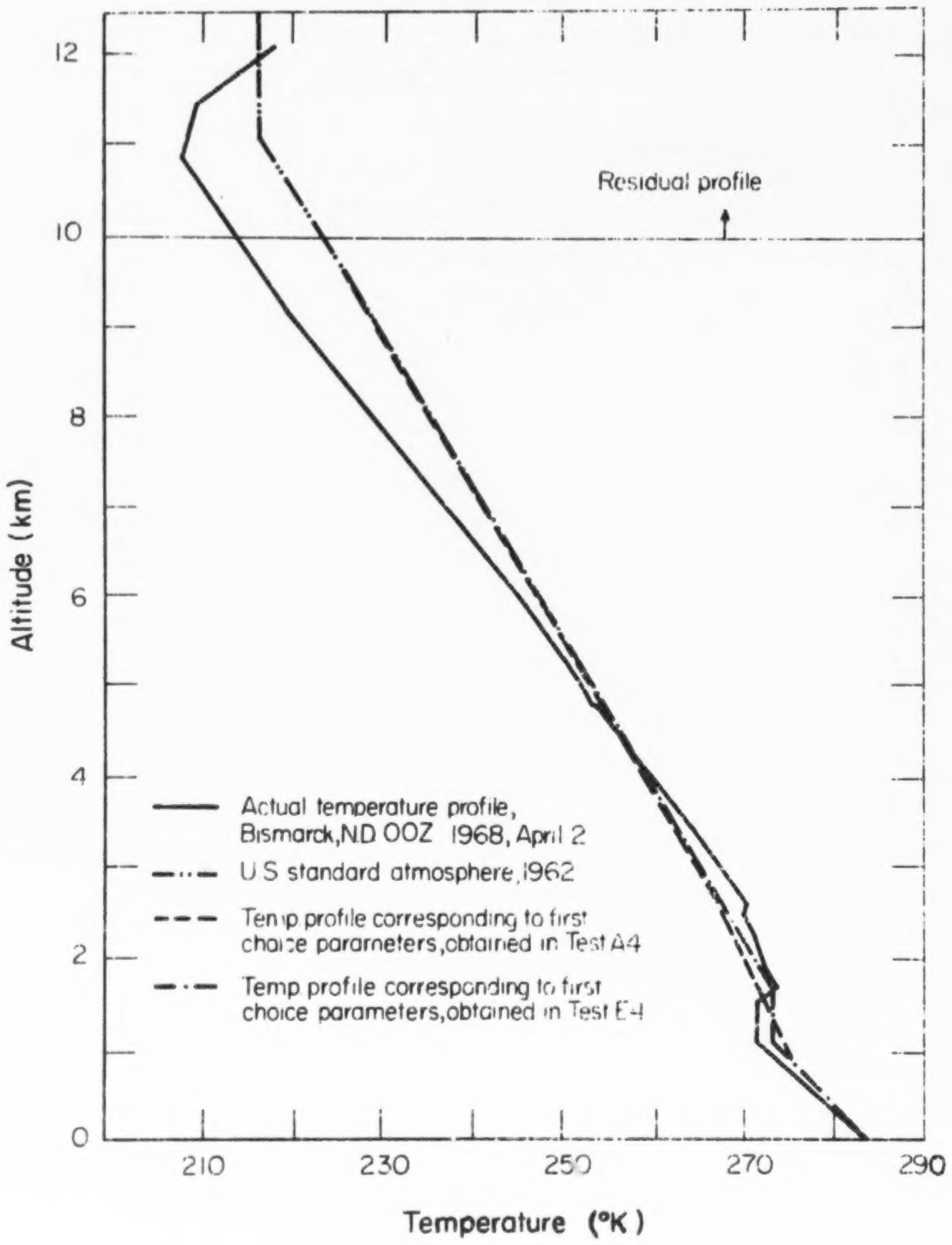

FIG. 8 Results of Tests A4 and E4.

It also appears from these results that the presumed benefits of higher termination altitudes versus lower altitudes, as discussed earlier, do not in fact exist. The higher termination altitude does result in smaller contributions of the residual profile to brightness temperature at the ground level, as shown in Sec. 2.4. However, the benefit of this, as far as the inversion scheme is concerned, is apparently offset by the increased depth over which an even slightly inaccurate Γ_3 exists. This effect is even present to a small extent in the results of tests A3 and E3. The residual profile and termination altitude, insofar as they effect Γ_3 , are the most serious problems. Lowering the termination altitude definitely seems to help in the case of the Γ_3 effect. The problem would probably be further alleviated if a climatological average temperature profile for the location, season, and general meteorological conditions under which the radiometric data were obtained were used as a residual profile rather than a standard atmosphere. Other approaches to the solution of this problem such as modifying the GAM, reducing the number of higher elevation angle measurements, or allowing Γ_3 to be determined more directly by the radiometric data should be investigated.

The models and the method as they have been described were tried next on a few cases where we had actual radiometric data. The first case chosen was that of Cincinnati, Ohio, Gest Street, 1969 February 26. For this case we inverted both the actual radiometric data and simulated ideal null balance radiometric data by using the actual temperature and humidity profiles to calculate the exact brightness temperatures. Figure 9 is a comparison of the actual scanning mode measured brightness temperatures and exact null balance calculated data. The measured data corresponds quite well to the calculated data and appears to contain the general character of the exact null balance calculated data.

The trial parameter values used in the inversions are given in Table X. The assumed relative humidities were zero at all levels. The assumed residual profile was the U. S. Standard Atmosphere 1962, and the termination altitude was 5 km. The elevation angles of the measured and calculated brightness temperature input data was 0° to 40°, by 2° increments, then 50°, 60°, 70°,

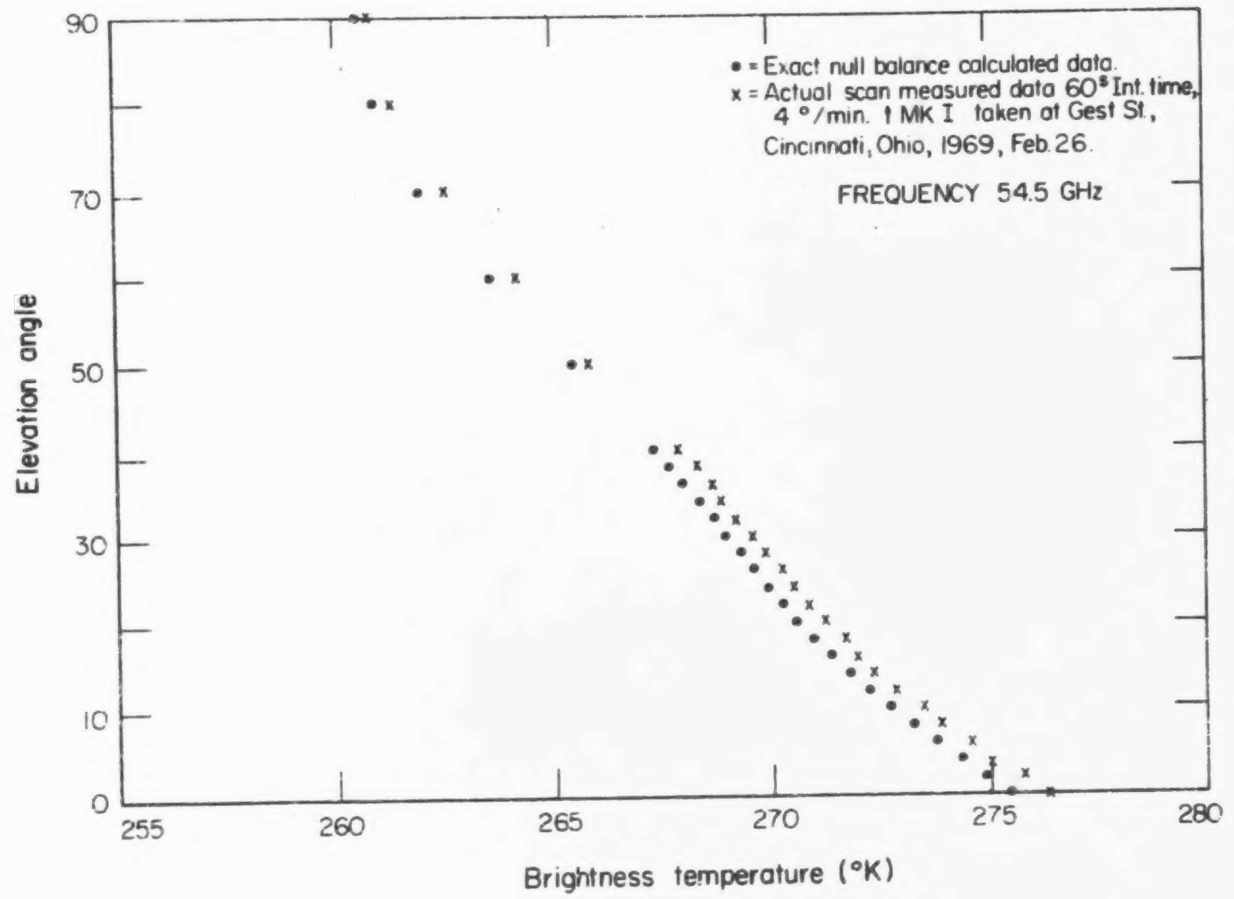

FIG. 9 Comparison of measured and calculated brightness temperatures.

80°, and 90°. The number of upper elevation angle measurements was reduced slightly from that used in the Bismarck, N. D., trials in an effort to reduce the overall influence of the residual profile. The FRBTM was used to calculate the comparison brightness temperatures in the inversion process.

TABLE X
TRIAL VALUES OF GAM PARAMETERS

Γ_1 (C/km)	Z_1 (km)	Γ_2 (C/km)	Z_2 (km)
-10., -9., -8., -7., -6.	.35, .45, .65, .80, .95, 1.15, 1.35, 1.5, 1.6	-10., -5., 0., +7.5, +15., +22.5	.95, 1.15, 1.35, 1.6, 1.85, 2.1

The temperature profiles resulting from the analyses of both the measured and calculated data in comparison with the actual profile are shown in Fig. 10. Both of the radiometrically determined temperature profiles clearly depict the base of an inversion, or at least an isothermal layer. The results obtained using the calculated data are very good; those obtained using the measured data are also good, especially in view of the fact that the actual data was obtained in the scan mode, whereas the FRBTM calculated comparison brightness temperatures are the equivalent of null balance observations. The inclusion of a scanning algorithm to convert the calculated equivalent null balance brightness temperature records to scan mode brightness temperatures might very well have improved the measured data results.

The next case was that of Raleigh, N. C., 1969 October 15. In this case, the profile was measured only to a height of 2 km by helicopter and no RAOB data were available; therefore, no exact brightness temperatures could be generated on which to perform a comparison inversion. The same trial parameters and other conditions were used on the inversion of this measured data as were used in the previous case. The temperature profile resulting from the analysis of this data is shown in Fig. 11 in comparison with the

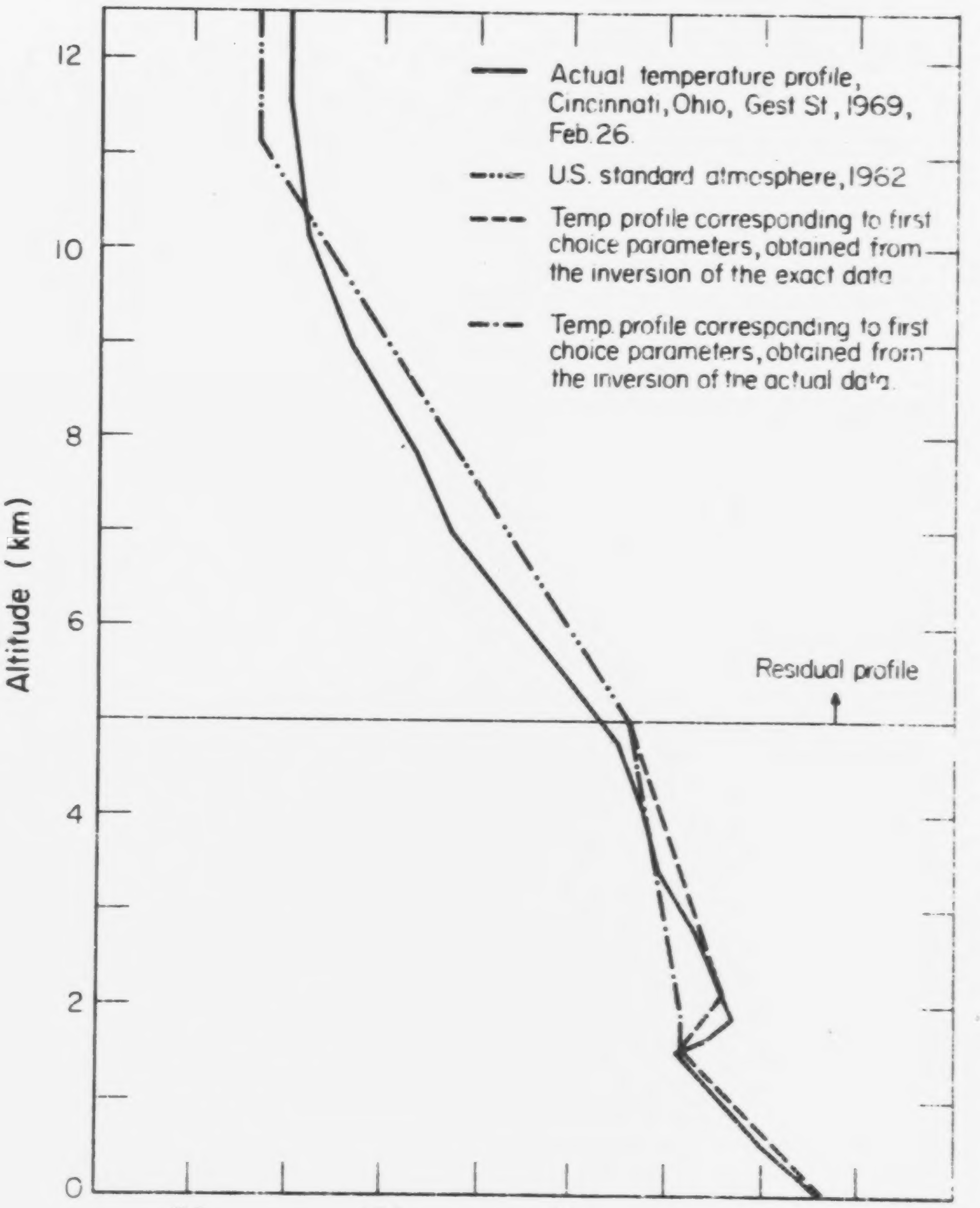

FIG. 10 Results of using GRID inversion scheme on actual and simulated radiometric data from Cinn., Ohio, Gest St., 1969 Feb. 26.

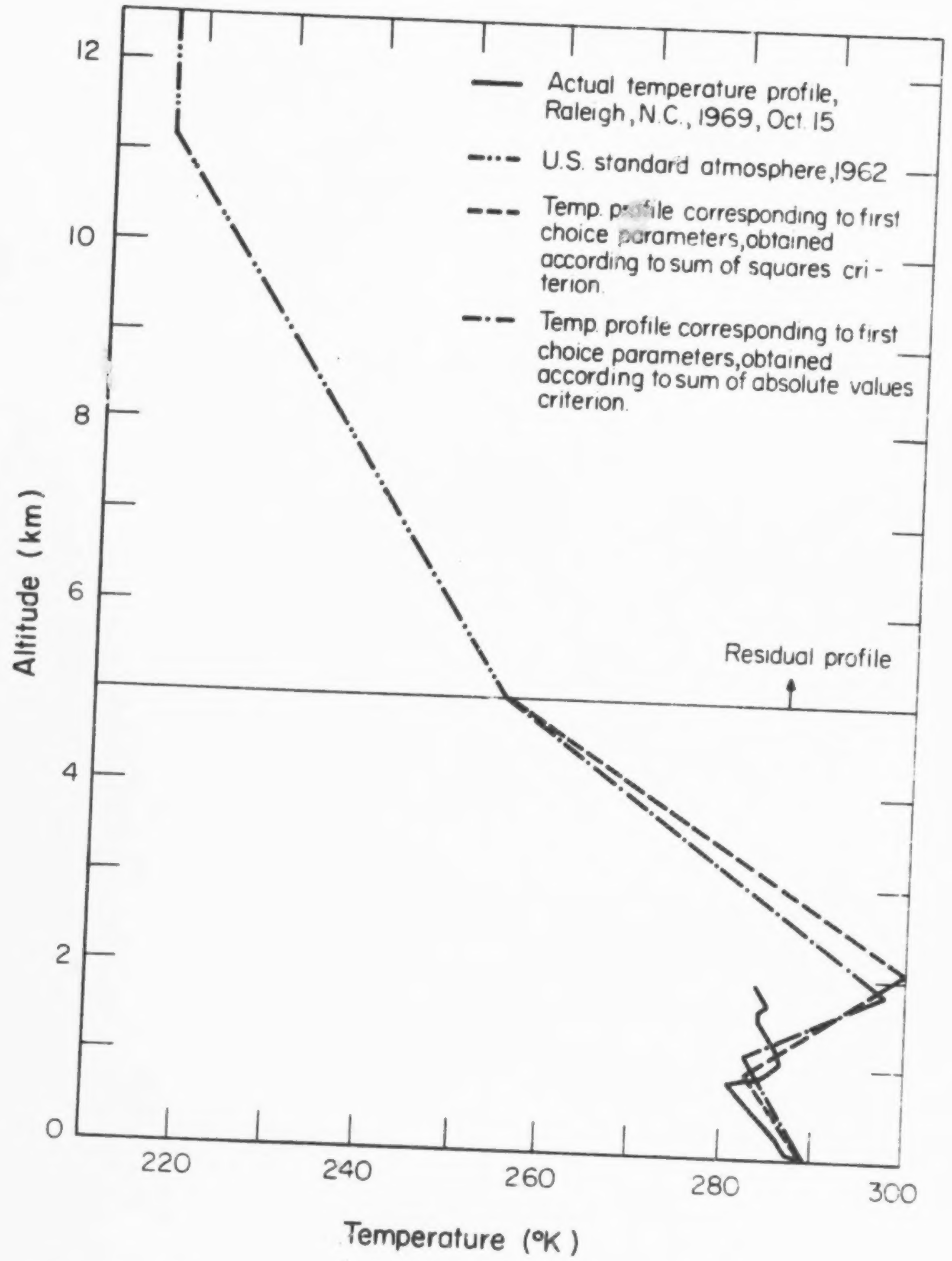

FIG. 11 Results of using GRID inversion scheme on actual radiometric data from Raleigh, N. C., 1969 Oct. 15.

actual helicopter sounding. Although the elevated inversion layer is dramatically exaggerated, the base of the layer is actually defined by the parameters of the GAM; again a very good result in view of the null balance character of the calculated brightness temperatures and scan mode nature of the measured data.

The final case on which the GRID scheme and GAM was tried was that of Vandenberg Air Force Base, 1969 December 5, 1547 to 1609 PST. As in the previous case, no RAOB data were available from which exact brightness temperature could be calculated for comparison with the measured. Consequently, the analysis was performed only on the measured data. The trial parameters used are given in Table XI.

TABLE XI

TRIAL VALUES OF GAM PARAMETERS

Γ_1 (C/km)	Z_1 (km)	Γ_2 (C/km)	Z_2 (km)
-9.5, -8.5, -7.5, -6.5, -5.5, -4.5	.25, .35, .45, .55, .7, .9, 1.1	-10., -5., +7.5 +15., +25.	.5, .6, .75, .9, 1.1, 1.35, 1.65, 2.05

The termination altitude, residual profile, assumed humidity profile and elevation angles of data used are the same as in the previous two cases. The results of the inversion process are shown in Fig. 12. In this case, although an elevated inversion was detected, the base of the inversion layer as determined from the radiometric data was over twice as high as that shown in the helicopter sounding. Unfortunately, without a RAOB sounding with which to compare the actual and assumed residual profiles, brightness temperatures cannot be calaculated for comparison with the measured data. It is therefore difficult to further analyze this result.

Two features in the last two cases that are worth noting as possible indications that there is some serious error in the results are: (1) the

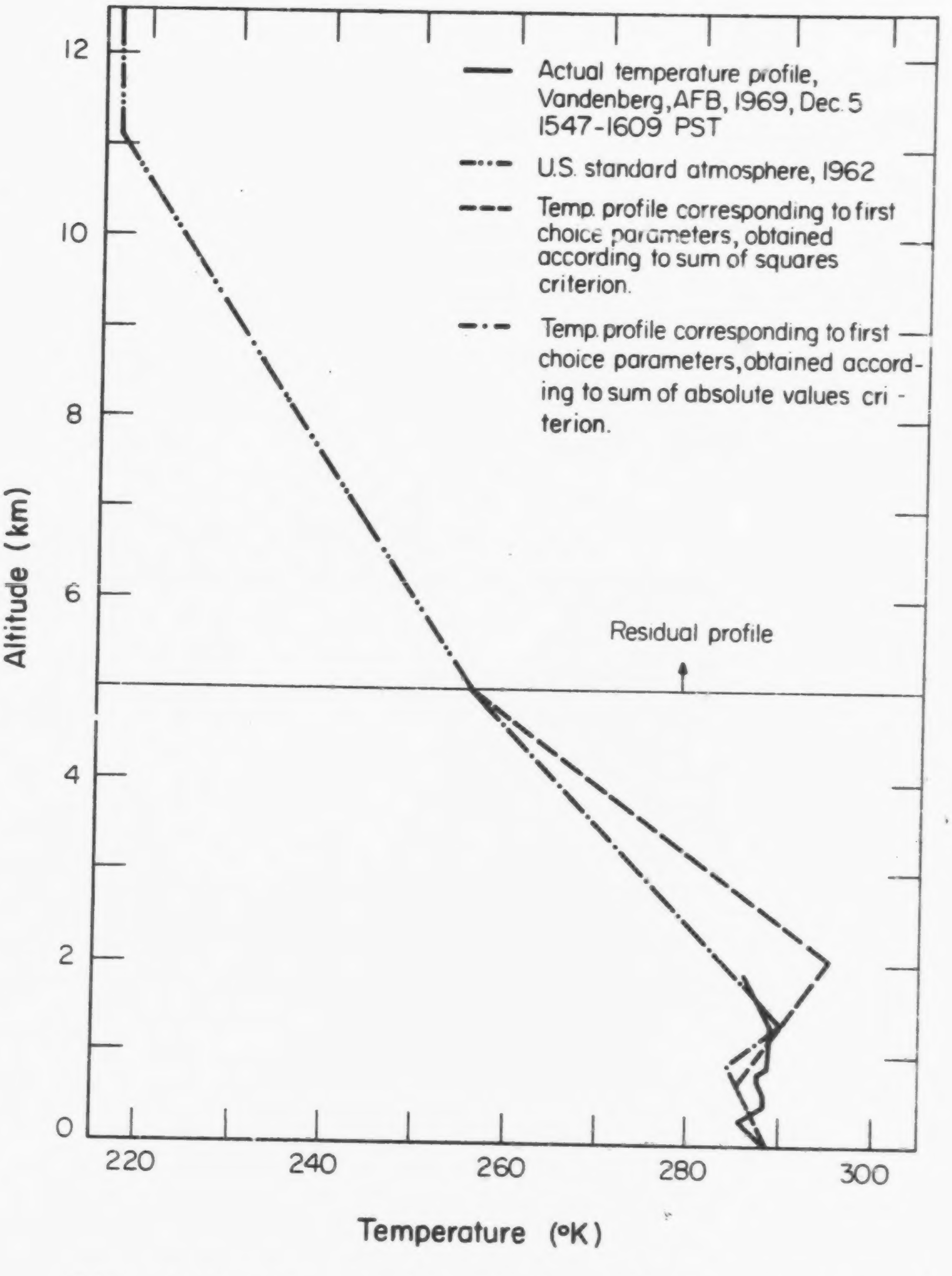

FIG. 12 Results of using GRID inversion scheme on actual radiometric data from Vandenberg AFB 1969 Dec. 5, 1547 - 1609 PST.

absence of an agreement between the first choice parameters as determined by the sum of squares criterion and sum of absolute values criterion, and (2) the magnitude of F(P̲) for the best fitting set. As to the first distinction, in most every case where a good result has been obtained, the first, second, and several subsequent parameter choices obtained by each criterion have agreed. In the second feature, another obvious indication of a poor fit, the problem of what the order of magnitude of F(P̲) should be for a best fit in practice is yet to be determined.

2.7 Conclusions

The results of the gradient altitude model as the basis of a technique for inverting radiometric data indicate the following:

1) The salient features of real temperature profiles in which an elevated inversion is present can be obtained.
2) With respect to the specific details of the method, a standard atmosphere can be used as the residual profile with the result that a good specification of the base of the inversion is obtained.
3) The termination altitude has a marked effect on the accuracy of the inversion. Lower, rather than higher, termination altitudes tend to produce better results, especially when the residual profile is seriously in error.
4) The use of an approximate brightness temperature calculating routine produces acceptable results at this time, but there is some noticeable deterioration of the results when the approximate brightness temperatures are used in combination with residual profiles that are seriously in error.
5) The main emphasis of future investigations of this method should focus mainly on methods for selecting the best fitting parameters faster, extending the model to more line segments, and improving the brightness temperature approximation scheme and incorporating a scanning mode converter in the brightness temperature calculations.

SECTION 3

LIMITED RANGE RELAXATION TECHNIQUE

A relaxation technique is an iterative numerical method for determining an unknown quantity. The technique associates a "residual", based upon an initial estimate of the unknown quantity, with each point of a predetermined grid and then updates the estimate via a relaxation equation. The relaxation equation is based upon the residuals and previous estimate of the unknown quantity. When the residuals vanish, it is assumed that the unknown has been determined and is equal to that estimate producing the zero or near-zero residuals. This section describes the initial development and implementation of a limited range relaxation technique for deriving the ambient temperature profile from the surface to a height of 2.54 km using radiometric data collected at 54.5 GHz. The technique can be considered in two parts: 1) the development of a predictor equation for observed brightness temperature that is dependent only upon the temperature profile up to 2.54 km, and 2) a relaxation equation for deriving the true temperature profile from $z_1 = 0.0$ to $z_{16} = 2.54$ km using an initially guessed profile.

The predictor equation for radiometric brightness temperatures was derived by considering the radiometric brightness temperature as the sum of two integrals, the first having the limits from $z_1 = 0.0$ to $z_{16} = 2.54$ km and the second having limits from z_{16} to z_f, where z_f is the height beyond which no significant contribution is received by the radiometer. By applying the mean value theorem to the second integral, the brightness temperature is given by

$$T_{B_\nu}(\theta) = \int_{z_1}^{z_{16}} T(z)\left(-\frac{d\tau_\nu(\theta,z)}{dz}\right)dz + \overline{T}_\theta[z_{16},z_f]\left\{\tau_\nu(\theta,z_{16}) - \tau_\nu(\theta,z_f)\right\} \qquad (11)$$

The ratio of the mean value temperatures over the interval $[z_{16}, z_f]$ at 0° and 90° can be expressed as the ratio of the mean value temperatures over the interval $[z_1, z_f]$ plus an error term, i.e.,

$$\frac{\overline{T}_\theta[z_{16}, z_f]}{\overline{T}_{90}[z_{16}, z_f]} = \frac{\overline{T}_\theta[z_1, z_f]}{\overline{T}_{90}[z_1, z_f]} + \frac{\delta(\theta)}{\overline{T}_{90}[z_{16}, z_f]} \qquad (12)$$

Solving Equation(12)for $\overline{T}_\theta[z_{16}, z_f]$

$$\overline{T}_\theta[z_{16}, z_f] = \overline{T}_{90}[z_{16}, z_f]\,\frac{\overline{T}_\theta[z_1, z_f]}{\overline{T}_{90}[z_1, z_f]} + \delta(\theta) \qquad (13)$$

Since the ratio of the mean value temperatures over the interval $[z_1, z_f]$ is the ratio of the observed brightness temperatures divided by the changes in transmissivity, Equation(13) reduces to

$$\overline{T}_\theta[z_{16}, z_f] = \overline{T}_{90}[z_{16}, z_f]\,\frac{T_{B_\nu}(\theta)}{T_{B_\nu}(90)} \cdot \frac{1-\tau_\nu(90, z_f)}{1-\tau_\nu(\theta, z_f)} + \delta(\theta) \qquad (14)$$

Letting

$$K(\theta) = \frac{T_{B_\nu}(\theta)}{T_{B_\nu}(90)} \cdot \frac{1-\tau_\nu(90, z_f)}{1-\tau_\nu(\theta, z_f)} \qquad (15)$$

and

$$\beta(\theta) = \delta(\theta)\{\tau_\nu(\theta, z_{16}) - \tau_\nu(\theta, z_f)\} \qquad (16)$$

Equation (11) reduces to

$$T_{B_\nu}(\theta) = \int_{z_1}^{z_{16}} T(z)\left(-\frac{d\tau_\nu(\theta, z)}{dz}\right)dz + \overline{T}_{90}[z_{16}, z_f]K(\theta)\{\tau_\nu(\theta, z_{16})$$

$$- \tau_\nu(\theta, z_f)\} + \beta(\theta) \qquad (17)$$

The purpose of this manipulation has been to express the observed brightness as a function of the temperature profile up to $z_{16} = 2.54$ km and the mean value temperature associated with 90° over the interval $[z_{16}, z_f]$. This will have been accomplished if $K(\theta)$ is known and $\beta(\theta)$ is sufficiently small, so that its value can be assumed to be zero. From Equation (15), it is seen that $K(\theta)$ depends upon the observed brightness temperatures and the final transmissivity values corresponding to θ and 90° elevation angle. The observed brightness temperatures are known so that the only question remaining concerns the final transmissivity values. It has been shown in a previous report^3 that transmissivity is only a weak functional of temperature and further that its value is nearly stable beyond the 10 mb pressure level. For these reasons, it is assumed that the final value of transmissivity is known and, therefore, it is assumed that $K(\theta)$ is known.

Evaluation of $\beta(\theta)$ has been done for four cases: 1) lapse profile, 2) 5 C elevated inversion from .5 - .75 km, 3) 5 C elevated inversion from 1.0 - 1.25 km, and 4) 5 C inversion from 1.5 - 1.75 km. The values of $\beta(\theta)$ for 16 elevation angles are presented in Table XII for each of the above cases. The evaluation of $\beta(\theta)$ was accomplished by calculating the brightness temperatures from the true temperature profiles specified to a height of 30 km for each of the four cases. These four sets of brightness temperatures correspond to four sets of observed measurements. Brightness temperatures were then calculated for each case from Equation (17) with the assumption that $\beta(\theta) = 0$. The first term was evaluated by integrating the true temperature profile to a height of 2.54 km and the second term by noting that

$$\overline{T}_{90}[z_{16}, z_f] = \frac{T_{B_\nu}(90) - TB1(90)}{\tau_\nu(90, z_1) - \tau_\nu(90, z_f)} \qquad (18)$$

where TB1(90) is the contribution to the observed brightness temperature at 90° from the surface to 2.54 km.

The result is four sets of predicted brightness temperatures. The difference between the observed and predicted brightness temperatures within each set gives the value of $\beta(\theta)$ in degrees Celsius.

TABLE XII

Values of $\beta(\theta)$ for the Four Model Profiles

θ	CASE 1 $\beta(\theta)$	CASE 2 $\beta(\theta)$	CASE 3 $\beta(\theta)$	CASE 4 $\beta(\theta)$
0	.0	.0	.0	.0
2.5	.001	.000	.002	.002
5.0	.009	-.002	.003	.004
7.5	.013	-.006	.006	.006
10.0	.018	-.003	.010	.010
15.0	.031	.017	.032	.031
20.0	.056	.063	.080	.073
25.0	.084	.113	.134	.122
30.0	.091	.141	.163	.152
35.0	.086	.147	.171	.161
40.0	.070	.134	.157	.149
50.0	.033	.086	.106	.102
60.0	.009	.044	.057	.056
70.0	.000	.017	.023	.023
80.0	.000	.004	.006	.006
90.0	.000	.000	.000	.000

The results show that $\beta(\theta)$ is small in all cases, thereby indicating the feasibility of developing a limited range inversion scheme for obtaining the temperature profile in the first 2.54 km. For the present investigation, $\beta(\theta)$ was assumed to be identically zero in all cases. This assumption has the effect of saying that the observed brightness temperature is represented by Eq. (17) without the $\beta(\theta)$ term, i.e.,

$$T_{B_\nu}(\theta) = \int_{z_1}^{z_{16}} T(z)\left(-\frac{d\tau_\nu(\theta,z)}{dz}\right)dz + \overline{T}_{90}[z_{16},z_f]K(\theta)\{\tau_\nu(\theta,z_{16}) - \tau_\nu(\theta,z_f)\} \quad (19)$$

By providing an initially guessed temperature profile $\hat{T}(z)_o$, a set of predicted brightness temperatures $\hat{T}_{B_\nu}(\theta)_o$ can be computed from Equation (19) for any elevation angle. The applicable height concept has been shown to provide some measure of the true temperature profile. For this reason, the applicable height profile is always used as the initially guessed temperature profile. By appropriately choosing the set of observing angles for observed brightness temperature, a representative height distribution (or height grid) is obtained. A set of sixteen angles has been selected to define the height grid. It is assumed that measurements of observed brightness temperatures are available at each of these angles. The set of angles and the height grid to which they correspond (via the applicable height concept) are presented in Table XIII. The angle θ_j is the elevation angle in degrees corresponding to the applicable height z_j in km.

TABLE XIII

Angle-Height Grid

j	θ_j	z_j	j	θ_j	z_j	j	θ_j	z_j	j	θ_j	z_j
1	0.0	.0	5	10.0	.26	9	30.0	.84	13	60.0	1.96
2	2.5	.07	6	15.0	.40	10	35.0	1.01	14	70.0	2.27
3	5.0	.13	7	20.0	.54	11	40.0	1.19	15	80.0	2.47
4.	7.5	.20	8	25.0	.69	12	50.0	1.59	16	90.0	2.54

Using the applicable height concept, the initially guessed profile is given by $\hat{T}(z_j)_o = T_{B_\nu}(\theta_j)$. Substituting $\hat{T}(z_j)_o$ into Equation (19), a set of predicted brightness temperatures can be computed at each angle corresponding to an observed brightness temperature measurement. For each angle, the difference between the predicted brightness temperature and the observed brightness temperature is a residual representing that portion of brightness temperature not explained by the guessed temperature profile. Computing these residuals and manipulating, we have the following:

$$\epsilon(\theta_j)_o = \hat{T}_{B_\nu}(\theta_j)_o - T_{B_\nu}(\theta_j)$$

$$= \int_{z_1}^{z_{16}} \hat{T}(z)_o \left(-\frac{d\hat{\tau}_\nu(\theta_j,z)}{dz}\right) dz - \int_{z_1}^{z_{16}} T(z) \left(\frac{d\tau_\nu(\theta_j,z)}{dz}\right) dz$$

$$+ \hat{\overline{T}}_{90}[z_{16},z_f]_o K(\theta_j)\{\hat{\tau}_\nu(\theta_j,z_{16})_o - \hat{\tau}_\nu(\theta_j,z_f)\}$$

$$- \overline{T}_{90}[z_{16},z_f] K(\theta_j)\{\tau_\nu(\theta_j,z_{16})_o - \tau_\nu(\theta_j,z_f)\}$$

As stated earlier, transmissivity is only a weak functional of temperature. It is reasonable to assume that the transmissivity values resulting from the predicted temperature profile are good estimates of the true transmissivity values. For this reason, no distinction is made between the predicted and observed transmissivity values, so that

$$\epsilon(\theta_j)_o = \int_{z_1}^{z_{16}} \{\hat{T}(z)_o - T(z)\} \left(-\frac{d\tau_\nu(\theta_j,z)}{dz}\right) dz$$

$$+ \{\hat{\overline{T}}_{90}[z_{16},z_f]_o - \overline{T}_{90}[z_{16},z_f]\} K(\theta_j)\{\tau_\nu(\theta_j,z_{16}) - \tau_\nu(\theta_j,z_f)\} \quad (20)$$

Noting that

$$\overline{T}_{90}[z_{16},z_f] = \frac{T_{B_\nu}(90) - \int_{z_1}^{z_{16}} T(z)\left(-\frac{d\tau_\nu(90,z)}{dz}\right) dz}{\tau_\nu(90,z_{16}) - \tau_\nu(90,z_f)} \quad (21)$$

we let

$$\hat{T}_{90}[z_{16}, z_f]_0 = \frac{T_{B_\nu}(90) - \int_{z_{16}}^{z_f} \hat{T}(z)_0 \left(- \frac{d\tau_\nu(90,z)}{dz} \right) dz}{\tau_\nu(90,z_{16}) - \tau_\nu(90,z_f)} \tag{22}$$

Letting

$$C(\theta_j) = K(\theta_j) \left\{ \frac{\tau_\nu(\theta_j, z_{16}) - \tau_\nu(\theta_j, z_f)}{\tau_\nu(90, z_{16}) - \tau_\nu(90, z_f)} \right\}$$

and substituting Eq. (21) and Eq. (22) into Eq. (20), we have the following

$$\begin{aligned}
\epsilon(\theta_j)_0 &= \int_{z_1}^{z_{16}} \{\hat{T}(z)_0 - T(z)\} \left(- \frac{d\tau_\nu(\theta_j,z)}{dz} + C(\theta_j) \frac{d\tau_\nu(90,z)}{dz} \right) dz \\
&= \sum_{i=1}^{15} \int_{z_i}^{z_{i+1}} \{\hat{T}(z)_0 - T(z)\} \left(- \frac{d\tau_\nu(\theta_j,z)}{dz} + C(\theta_j) \frac{d\tau_\nu(90,z)}{dz} \right) dz \\
&= \int_{z_{j-1}}^{z_{j+1}} \{\hat{T}(z)_0 - T(z)\} \left(- \frac{d\tau_\nu(\theta_j,z)}{dz} + C(\theta_j) \frac{d\tau_\nu(90,z)}{dz} \right) dz \\
&\quad + \left(\sum_{i=1}^{j-2} + \sum_{i=j+1}^{15} \right) \int_{z_i}^{z_{i+1}} \{\hat{T}(z)_0 - T(z)\} \left(- \frac{d\tau_\nu(\theta_j,z)}{dz} + C(\theta_j) \frac{d\tau_\nu(90,z)}{dz} \right) dz
\end{aligned} \tag{23}$$

It should be noted that mathematical convention dictates that the summation is ignored if the index is indicated in a negative direction.

The first integral is defined for all values of j such that $2 \le j \le 15$; letting the mean value of the integrand in this interval $[z_{j-1}, z_{j+1}]$ be $T(z_j)_0 - T(z_j)$, we can solve for $T(z_j)$, which is a new estimate for the ambient temperature at height z_j and is therefore denoted in the solution by $T(z_j)_1$.

$$\hat{T}(z_j)_1 = \hat{T}(z_j)_o - \frac{1}{\Delta\tau_\nu(\theta_j,[z_{j-1},z_{j+1}]) - C(\theta_j)\Delta\tau_\nu(90,[z_{j-1},z_{j+1}])}$$

$$\times \left\{ \epsilon(\theta_j)_o - \left(\sum_{i=1}^{j-2} + \sum_{i=j+1}^{15} \right) \int_{z_i}^{z_{i+1}} [\hat{T}(z)_o - T(z)] \left(\frac{d\tau_\nu(\theta_j,z)}{dz} + C(\theta_j) \frac{d\tau_\nu(90,z)}{dz} \right) dz \right\}$$

The formulation of the above equation has been such that the quantity

$$\Delta\tau_\nu\left(\theta_j,[z_{j-1},z_{j+1}]\right) - C(\theta_j)\Delta\tau_\nu\left(90,[z_{j-1},z_{j+1}]\right) \to 0$$

as $\theta_j \to 90^\circ$.

Its role in the above equation is that of an amplification factor of the correction to $\hat{T}(z)_o$; decreasing its value makes the corrections to $\hat{T}(z)_o$ smaller, but at the same time provides more stability for the higher angles. The above equation has therefore been simplified to the following,

$$\hat{T}(z_j)_1 = \hat{T}(z_j)_o - \frac{1}{\Delta\tau_\nu(\theta_j,[z_{j-1},z_{j+1}])} \times \left\{ \epsilon(\theta_j)_o \right.$$

$$\left. - \left(\sum_{i=1}^{j-2} + \sum_{i=j+1}^{15} \right) \int_{z_i}^{z_{i+1}} \{\hat{T}(z)_o - T(z)\} \left(-\frac{d\tau_\nu(\theta_j,z)}{dz} + C(\theta_j) \frac{d\tau_\nu(90,z)}{dz} \right) dz \right\} \quad (24)$$

The evaluation of Equation (24) would be a nearly exact solution of the ambient temperature at height z_j if the values of the integrals were known. The only available information about their value is provided by the residuals at the angles associated with the limits of the integrals. The relaxation equation results by letting the mean value of each integrand be given by the average of the residuals corresponding to the limits of each integral, i.e.,

$$\overline{\hat{T}(z)_o - T(z)} = \frac{\epsilon(\theta_i) + \epsilon(\theta_{i+1})}{z} = \bar{\epsilon}_i \tag{25}$$

Using this estimate and substituting Equation (24) reduces to

$$T(z_j)_1 = T(z_j)_o - \frac{1}{\Delta\tau_\nu(\theta_j,[z_{j-1},z_{j+1}])} \times \left\{ \epsilon(\theta_j)_o - \left(\sum_{i=1}^{j-2} + \sum_{i=j+1}^{15} \right) \bar{\epsilon}_i D_i \right\} \tag{26}$$

where

$$D_i = \Delta\tau_\nu(\theta_j,[z_i,z_{i+1}]) - C(\theta_j)\Delta\tau_\nu(90,[z_i,z_{i+1}]) \tag{27}$$

The above equation is valid only for $2 \le j \le 15$, so that it cannot be used to make corrections to the initial estimates of ambient temperature at heights z_1 and z_{16}. The new estimate of the ambient temperature at z_1 is provided by letting the residual in brightness temperature at $\theta_1 = 0^\circ$ correspond to the ambient temperature error at height z_1; this implies that the new estimate of temperature at z_1 is given by

$$T(z_1)_1 = T(z_1)_o - \epsilon(\theta_1)_o \tag{28}$$

The new estimate of the ambient temperature at height z_{16} is obtained by assuming that the temperature correction that results from Equation (26) for height z_{15} also applies at height z_{16}, therefore,

$$T(z_{16})_1 = T(z_{16})_o - [T(z_{15})_1 - T(z_{15})_o] \tag{29}$$

The above Equations (26), (28) and (29) constitute the relaxation equation for generating a new predicted temperature profile from the previous estimate of the temperature profile and from the corresponding residuals in brightness temperature. The new predicted temperature profile $\hat{T}(z_j)_1$ is used to compute a set of new predicted brightness temperatures $\hat{T}_{B_\nu}(\theta_j)_1$, and residuals $\epsilon(\theta_j)_1$. The relaxation equation is applied again, and a new predicted temperature profile $\hat{T}(z_j)_2$ results. The process is repeated until the residuals $\epsilon(\theta_j)_n$ resulting from $\hat{T}(z_j)_n$ are sufficiently small. That the residuals are sufficiently small depends upon the choice of an error criterion. Three error criterions are used in evaluating the convergence of the residuals to zero: 1) the sum of the residuals $\Sigma\epsilon_i$, 2) the sum of the squares of the residuals $\Sigma\epsilon_i^2$, and 3) the sum of the absolute values of the residuals $\Sigma|\epsilon_i|$. As to which error criterion best indicates the convergence of the predicted temperature profile to the observed (or true) temperature profile, the final choice has not been made.

To date, the limited range relaxation technique (LRRT) has been applied to three cases which are of particular interest for air pollution purposes. All three cases are 5 C elevated inversions of .25 km depth where the bases are at .5 km, 1.0 km, and 1.5 km. The results of these cases serve to indicate the feasibility of LRRT in inverting radiometric data and simultaneously point out particular problems associated with the technique.

If LRRT is to be successful, the first requirement is that at successive iterations the residuals are smaller, indicating a convergence toward zero. This indicates that the successive predicted temperature profiles are improvements to the initially guessed temperature profile in the sense of satisfying the observed brightness temperatures. It is important to note that since the residuals are measured between the predicted and observed brightness temperatures, they do not necessarily reflect a convergence of the predicted temperature profile to the observed temperature profile. A comparison of the magnitudes of the three error criteria ($\Sigma\epsilon_i$, $\Sigma\epsilon_i^2$, $\Sigma|\epsilon_i|$) as a function of iteration index for the three elevated inversion cases previously described is shown in Fig. 13. Two observations are immediately apparent from the figure: 1) regardless of the error criterion, the residuals for all three cases are getting smaller with successive iterations, and 2) the residuals in brightness temperature resulting from the initially guessed profile (i.e. applicable height profile) are smaller the higher the elevated inversion. The implication

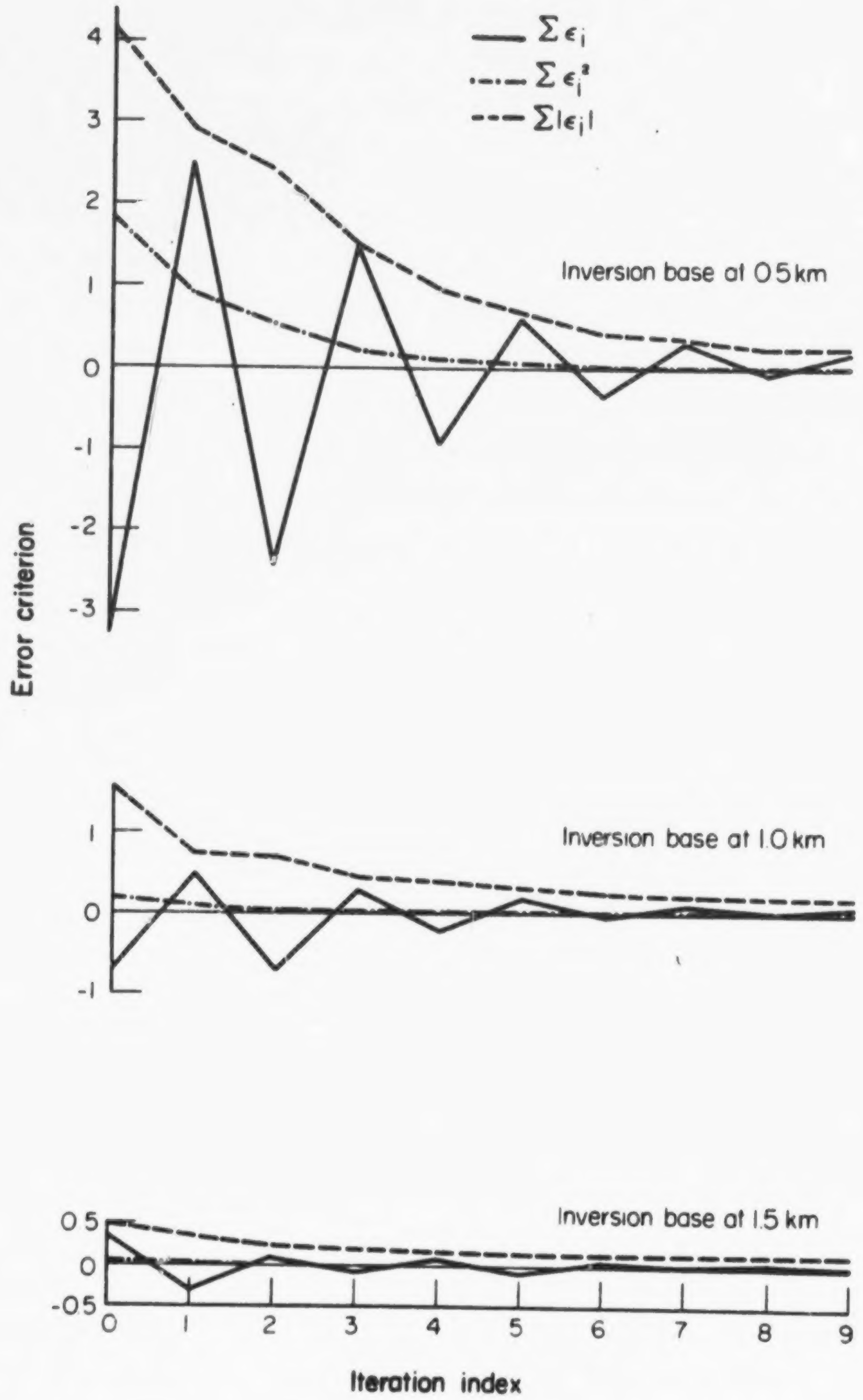

FIG. 13 Sum of the residuals, the sum of the squares of the residuals, and the sum of the absolute values of the residuals due to the relaxation of three 5 C elevated inversions of .25 km thickness where the bases of the inversions are at .5 km, 1.0 km, and 1.5 km, respectively.

of the first observation is the relaxation technique is successful in that the residuals are vanishing. The implication of the second observation is that discontinuities in the temperature profile at higher heights will be more difficult to derive via the relaxation technique, since their contribution is less pronounced.

The predicted temperature profiles corresponding to the initially guessed profile $\hat{T}(z)_0$, the first correction to the initially guessed temperature profile $\hat{T}(z)_1$, and the predicted temperature profile after the ninth iteration $\hat{T}(z)_9$ are superimposed upon the true temperature profile $T(z)$ and are presented in Fig. 14. The true temperature profile in this case is a 5 C elevated inversion from .5 to .75 km. The initially guessed profile $\hat{T}(z)_0$ is a nearly lapse profile showing no sign of the relatively intense, low-level inversion that is present in the true temperature profile. After only one iteration, the predicted temperature profile reflects the elevated inversion but at a height of .2 km with a 3.5 C intensity. By the ninth iteration the base of the inversion has been raised such that a nearly isothermal layer is depicted from .26 km to .4 km and a 5.5 C inversion occurs from .4 km to .84 km. The change from the initially guessed profile has been significant and reflects the dominant characteristics of the unknown profile.

It should be noted that the grid z_j is such that the relaxation scheme could never converge to the exact temperature profile since no grid point corresponds to .5 km or .75 km--the beginning and ending points of the true elevated inversion. It is significant then that the last grid point below the true base of the inversion is .4 km, where the predicted 5.5 C inversion begins; and that the first grid point after the top of the elevated inversion is .84 km, where the predicted 5.5 C inversion ends. It is also to be noted that the relaxation technique produced a small elevated inversion on the order of .5 C from .07 to .13 km, and a super-adiabatic lapse rate from .13 km to .26 km. These conditions are indicative of some instability in the technique. This instability is present in all three cases and, as yet, its source cannot be isolated. If its source cannot be isolated and subsequently eliminated through some modification of the technique, then realistic physical constraints may be used so that profiles with characteristics that are

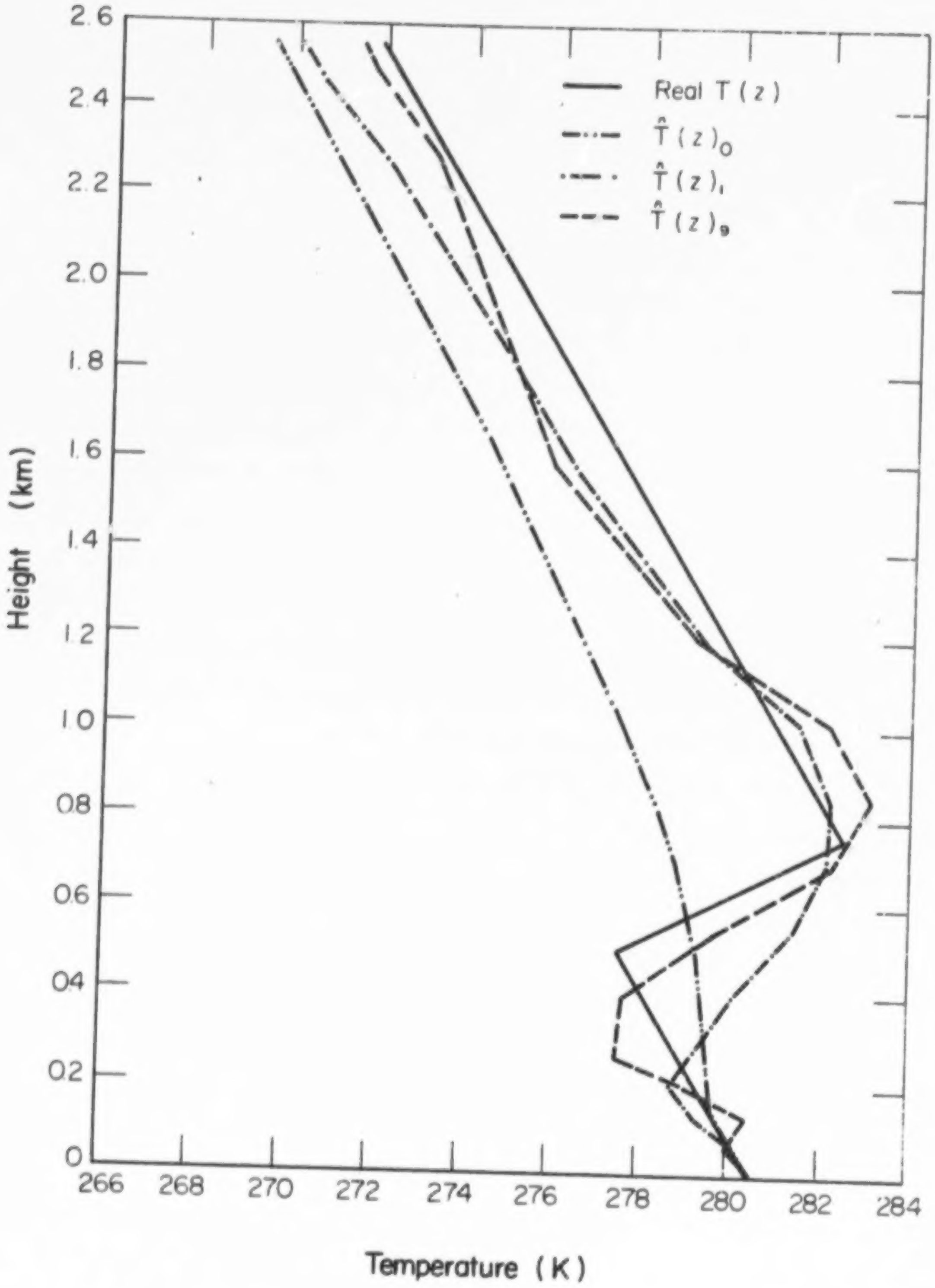

FIG. 14 Comparison of the initially guessed profile $\hat{T}(z)_0$ and the resulting predicted profiles after the 1st and 9th iterations with the true temperature profile T(z) having a 0.5 km elevated inversion.

physically improbable (e.g., elevated super-adiabatic conditions) will not be considered. At present, the relaxation technique is free to converge to any configuration of temperature profile, so that if an uncommon temperature characteristic does occur, the technique is potentially capable of detecting it.

Figure 15 presents the result of the relaxation technique for the 5 C elevated inversion from 1.0 km to 1.25 km. The same predicted profiles, namely, $\hat{T}(z)_0$, $\hat{T}(z)_1$, $\hat{T}(z)_9$, that were presented for the .5 km case are again presented for comparison with the true temperature profile. The initially guessed profile is essentially a lapse profile indicating no elevated inversion is present. The predicted temperature profile after the ninth iteration shows a nearly isothermal layer from .4 km to .54 km, a 3.2 C elevated inversion from .54 km to .84 km, and a nearly isothermal layer above from .84 km to 1.01 km. The same instabilities noted in the .5 km elevated inversion are present in this case but are more severe. The fictitious low-level inversion persists over a greater depth (.07 km to .2 km) and the super-adiabatic conditions are predicted from .2 km to .4 km. Further, the dominant predicted elevated inversion does not correspond as well in intensity, base or top, to the true elevated inversion as did the results of the .5 km inversion. This case serves to point out a particular problem area associated with the relaxation technique. The relaxation technique corrects the predicted temperatures at each of the sixteen heights z_j with each iteration. The problem is that the dominant correcting influence at each z_j is $\epsilon(\theta_j)$ which is not entirely due to the temperature error at z_j , but rather is a weighted average of the temperature errors at all the grid points. For most of the heights the sign of $\epsilon(\theta_j)$ causes a correction to be made which is closer to the true profile so that the predicted temperature profile as judged by the error criterion indicates an improvement. Since the residuals are now smaller, the subsequent iteration cannot produce as significant a correction in the next predicted profile as was encountered in the previous predicted profile. The effect continues with subsequent iterations. The result is that the technique is locked in or biased toward the predicted profile resulting from the first or second iteration.

Figure 16, which presents the results for the 5 C elevated inversion at 1.5 to 1.75 km, shows another consideration which must be observed when the

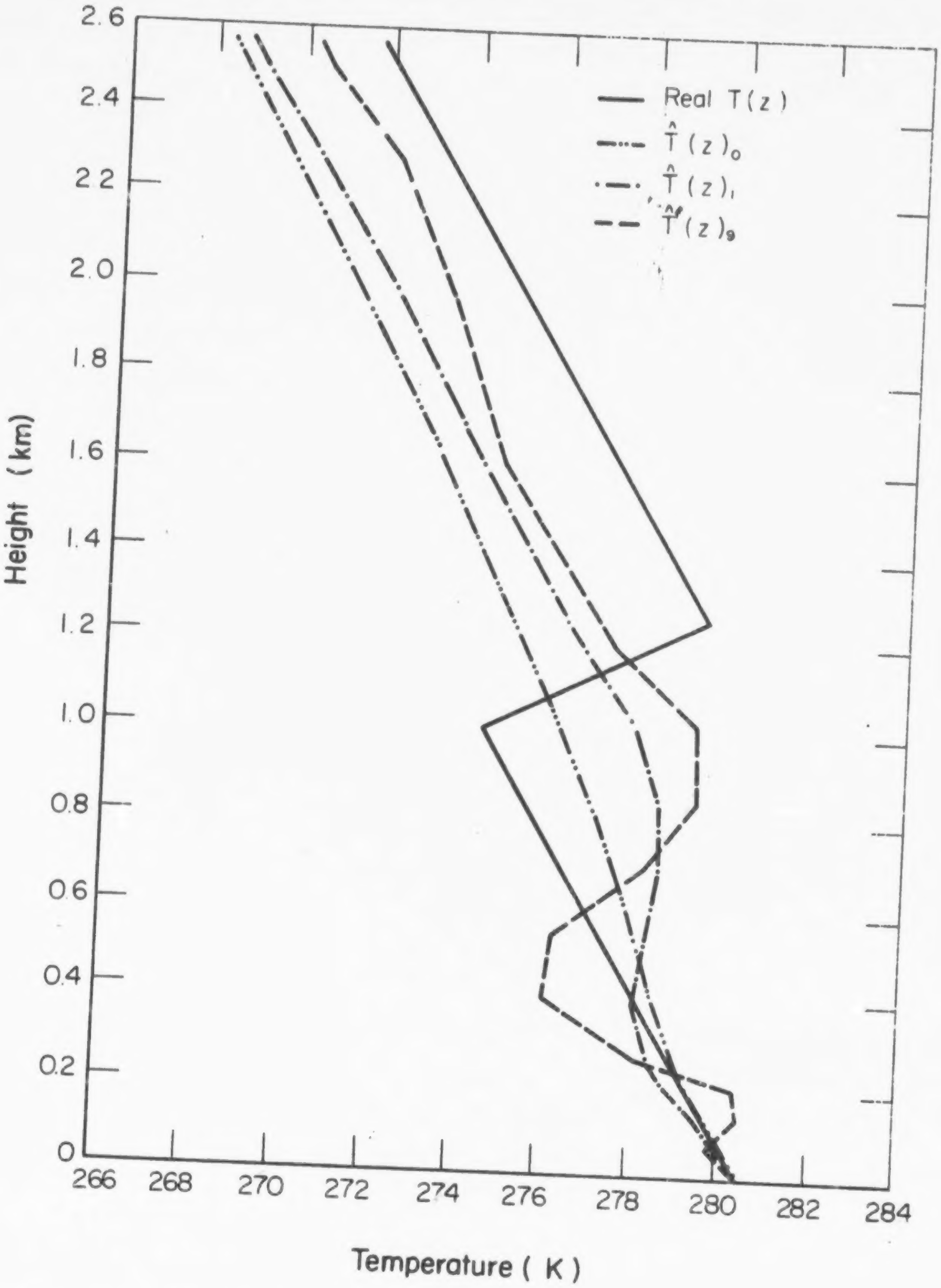

FIG. 15 Comparison of the initially guessed profile $\hat{T}(z)_0$ and the resulting predicted profiles after the 1st and 9th iterations with the true temperature profile T(z) having a 1.0 km elevated inversion.

relaxation technique is employed. The intially guessed profile $\hat{T}(z)_o$ produces brightness temperatures which are extremely close to the observed brightness temperatures corresponding to the true temperature profile. The result of the first iteration $\hat{T}(z)_1$ is a temperature profile only slightly different from $\hat{T}(z)_o$. The residuals are decreased further and, effectively, have no real meaning relative to making corrections to temperature. They are smaller than the combination of errors introduced by the predictor equation and by the fact that no finite height grid can be selected such that the predicted temperature profile can describe all (true) temperature profiles perfectly. In effect, the relaxation technique is being applied to noise after the first or second iteration for the elevated inversion at 1.5 km. The iteration at which this effect becomes dominant varies from profile to profile.

The following strategy has been implemented in the use of the relaxation technique in the hope of reducing the problem of the predicted profile being biased toward an incorrect profile. After the initially guessed profile $\hat{T}(z)_o$ is used to compute predicted temperatures $T_{B_\nu}(\theta_j)_o$ the values of the residuals $\varepsilon(\theta_j)_o$ are computed and the maximum residual in absolute value is found. The relaxation equation is then applied to correct the predicted temperatures at height z_i corresponding to max $\{\varepsilon(\theta_j)_o\}$ and at all heights z_k above this height. The values of temperature that were previously used for heights below z_i are again used. The combination of previous temperatures plus new predictions of temperature beyond and including z_i comprise the next predicted profile $\hat{T}(z)_1$. Brightness temperatures are calculated using this new set of predicted temperatures, the corresponding residuals are computed and the maximum absolute value is found. The above process is then repeated to find the next predicted temperature profile. If the corrections at the higher heights are closer to the true profile, then some portion of the residuals for the lower heights (that had been due to the temperature errors at the higher heights) will have been eliminated. In this manner the corrections that are made at the lower heights (i.e. when their corresponding residuals become maximum) will not be as severely influenced by the errors that existed at the higher heights. The result should be less bias in the predicted profiles and more rapid convergence of the residuals.

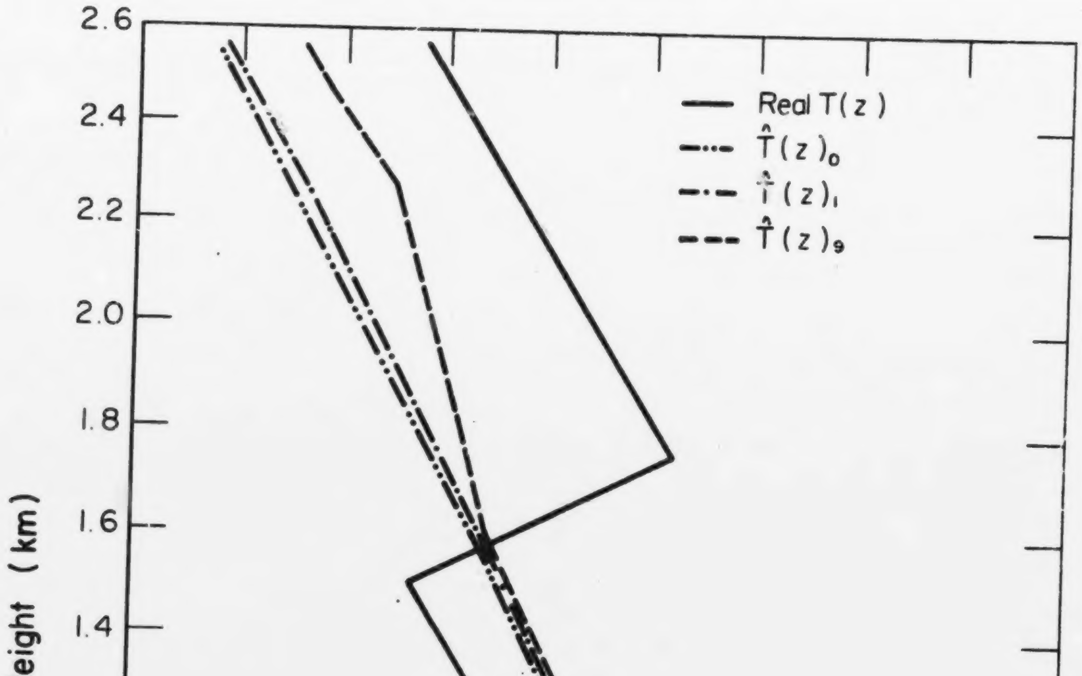

FIG. 16 Comparison of the initially guessed profile $\hat{T}(z)_0$ and the resulting predicted profiles after the 1st and 9th iterations with the true temperature profile T(z) having a 1.5 km elevated inversion.

A comparison of the magnitudes of the three-error criteria versus iteration index resulting from the relaxation technique implemented on the basis of the maximum residual is shown in Fig. 17. The figure gives the results for all three elevated inversions previously described. Comparison of Fig. 13 and Fig. 17 shows that the convergence rate of the residuals for the elevated inversions at .5 km and 1.0 km is far superior when the maximum residual consideration is employed. Very little change is noted for the inversion at 1.5 km, substantiating the previous conclusion that the residuals are on the order of the noise level of the technique.

The result of the relaxation technique used with the maximum residual consideration for the elevated inversion at .5 km is presented in Fig. 18. Of the nine iterations performed, the predicted temperature profile corresponding to the seventh iteration $\hat{T}(z)_7$ has the smallest error as measured by the sum of the absolute values of the residuals. For this reason $\hat{T}(z)_7$ is presented for comparison with the true profile. The results are a significant improvement to those obtained previously (Fig. 14) for the same case: the instabilities that were presented in the lower layers are greatly reduced; the predicted base (.4 km) and the predicted top (.84 km) are the best possible choices from the sixteen-point height grid; the predicted intensity (5.5 C) is in error only .5 C; and the profile is more accurately described above and below the inversion.

The other case showing improvement in the convergence of the residuals with the use of the maximum residual consideration was the 1.0 km based elevated inversion. The results for this case are presented in Fig. 19. The predicted profile corresponding to the eighth iteration $\hat{T}(z)_8$ showed the smallest error as measured by the sum of the absolute values of the residuals and is therefore presented for comparison with the true profile. There is improvement in the results in that the low-level instabilities have been reduced and the lapse rate is more accurately predicted above the inversion. In this case, the maximum residual strategy did not eliminate the bias toward an incorrect profile. The maximum residual for the initially guessed profile occurred for an elevation angle of 35°, which corresponds to the 1.01 km height. The sign of the residual indicated that a positive correction was necessary, when in fact a negative correction was warranted. The result was that the

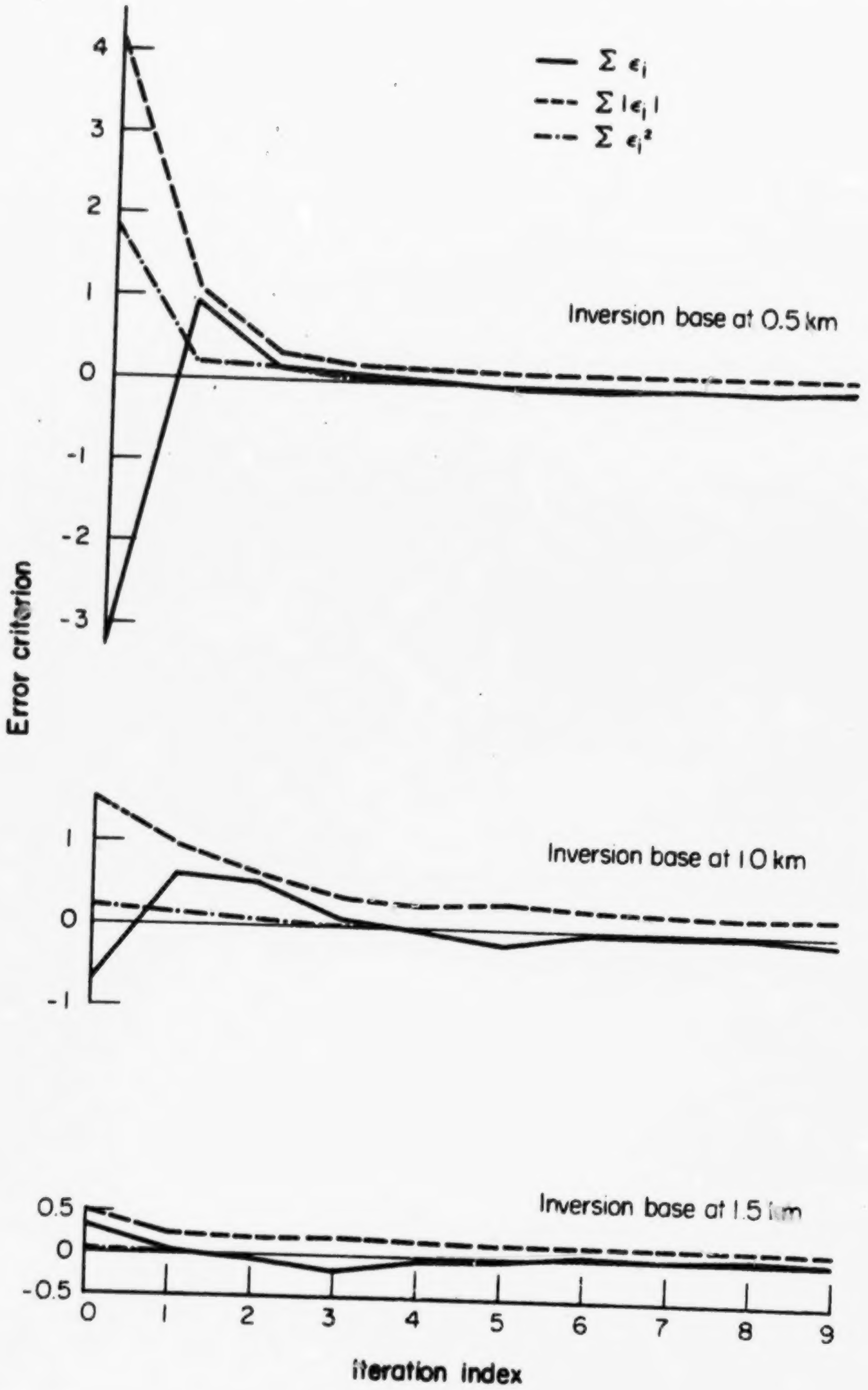

FIG. 17 Sum of the residuals, the sum of the squares of the residuals, and the sum of the absolute values of the residuals due to the relaxation of three 5 C elevated inversions of .25 km thickness where the bases of the inversions are at .5 km, 1.0 km, and 1.5 km, respectively.

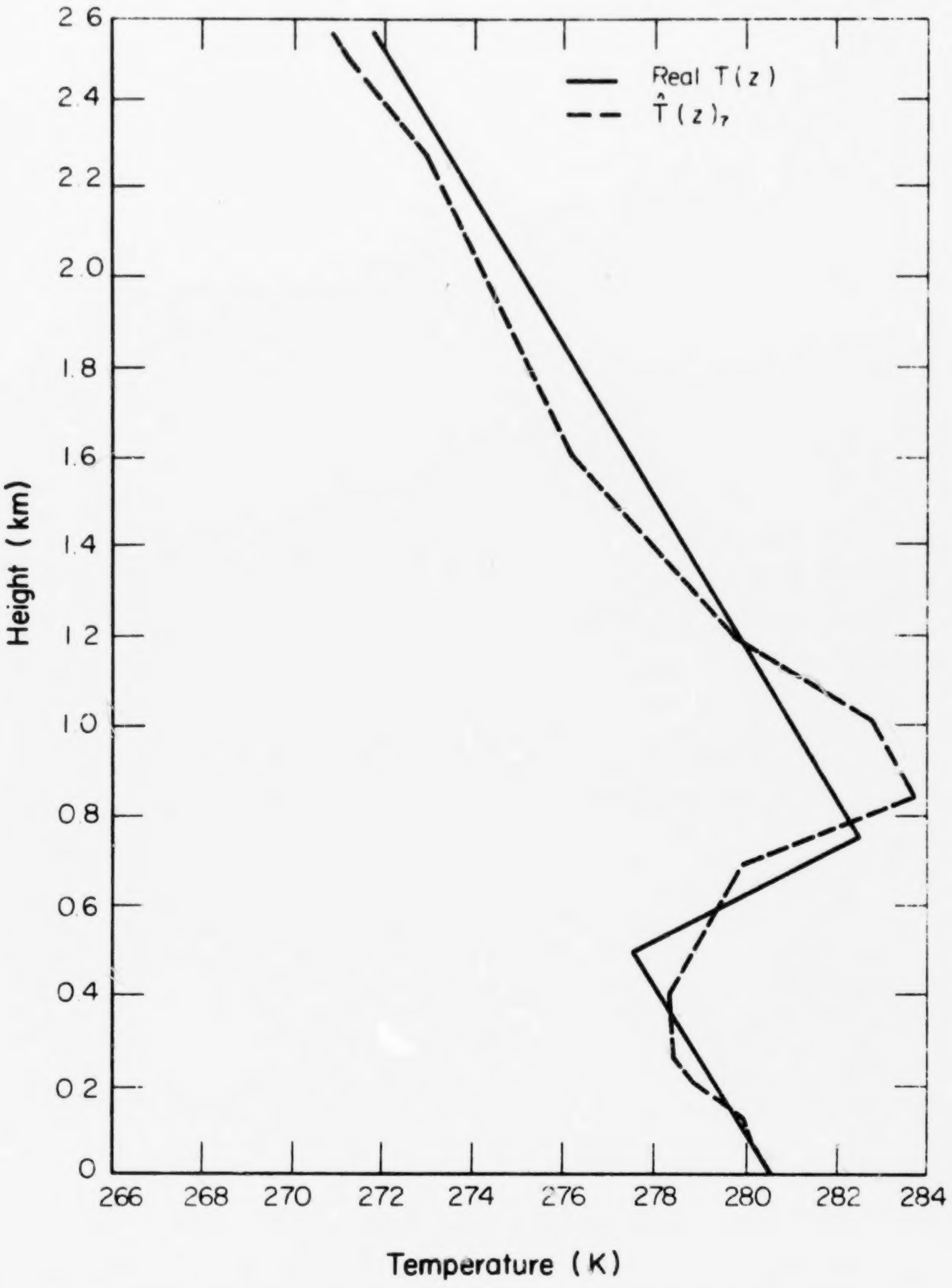

FIG. 18 Comparison of the predicted profile resulting after the 7th iteration with the true temperature profile having a 0.5 km elevated inversion.

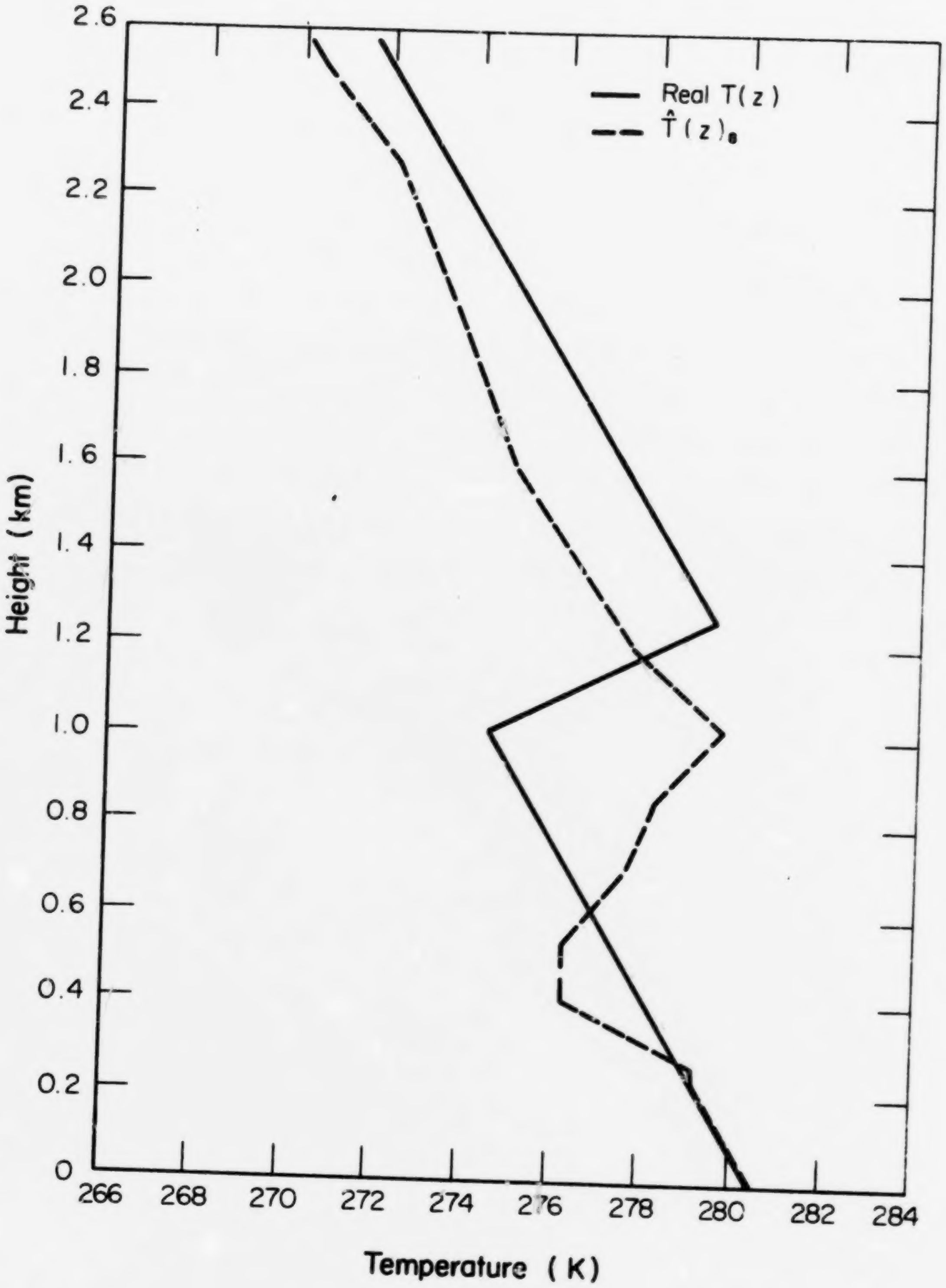

FIG. 19 Comparison of the predicted profile resulting after the 8th iteration with the true temperature profile having a 1.5 km elevated inversion.

relaxation technique was biased toward a profile having the top of its elevated inversion at 1.01 km rather than the base, as is the case for the true temperature profile.

This completes the discussion of the initial development and implementation of the limited range relaxation equation. There remain many areas in both the development and implementation that have yet to be investigated and evaluated. Some of the obvious areas are: the possibility of improving the predictor equation by providing estimates of the error term $\beta(\theta)$; the effect of different initially guessed profiles $\hat{T}(z)_0$ upon the solution; and the development of an optimum strategy in the implementing of the relaxation equation. The initial results, however, do suggest that the relaxation technique will indicate the existence of elevated temperature inversions within the first kilometer of the atmosphere and provide an accurate measure of those temperature inversions within the first half kilometer of the atmosphere.

SECTION 4

ANALOG AND EMPIRICAL TECHNIQUES

4.1 Introduction

In addition to the studies of the relaxation and the gradient altitude model inversion techniques, concurrent studies of analog and empirical methods were made for obtaining information about atmospheric temperature structure. All these techniques, because of their vastly different approaches, provide a broad base from which to attack the elevated inversion problem. Analog and empirical methods differ from the other techniques mentioned because they are strictly mathematical in nature and are not, therefore, vulnerable to some of the problems inherent in those approaches. Also, the empirical and analog techniques do not require access to a computer for operational use. On the other hand, the degree of success that is attainable by using an empirical or analog approach depends upon the extent and the variety of temperature profiles used to select or to generate the information these techniques employ for deriving atmospheric temperature structure. Before proceeding, to avoid confusion it is necessary to point out which of the several techniques mentioned in this section of this report are referred to as "empirical" and which are called "analog." The techniques that involve breakpoint, intersections or crossovers, angles of upper and lower inflection, and brightness temperature differential in their sub-section titles are regarded as empirical. Only the analog library technique is regarded as an analog approach. To prevent misunderstanding, "analog" as used in this report does not have the same meaning it has to many employed in various types of engineering pursuits, but instead refers to the pattern-matching of simulated model and observed curves.

4.2 Breakpoint Technique

The first part of the study was empirical, and involved selecting radiometric scan data taken in the field under elevated inversion conditions. Elevated inversions cause a region in a brightness temperature vs. elevation angle curve to be convex upward. Thus the elevation angle at which this convexity begins can be considered to be a significant point. For this reason, these angles (breakpoints) were picked off the radiometric data in an attempt to establish a correlation with elevated inversions. The data used for this study were 54.5 GHz, 4 deg/min upward scans for 64- and 128-second integration times (Mk. 0) and 60-second integration time (Mk. I). The scans used in the study were made in 1969 November at Clearwater, Florida, and in 1969 December at Vandenberg Air Force Base, California. The results are shown in Fig. 20 for Mark 0 and Mark I at 64- and 60-second integration times, respectively. Whereas the breakpoint generally increases with increasing height of inversion base, there is very poor correlation between the two. The results for Mark 0 data obtained at a 128-second integration time showed the same type of distribution. The scatter about any imaginary line through the data points of Fig. 20 can be explained on the basis of instrumental noise, ground effects, short-term or small-scale atmospheric fluctuations, and the inability of the data analyst to select the breakpoint with the certainty required. The first three items have the effect of causing the analyst to interpret any breakpoint that may or may not be produced by an elevated inversion as being due to that particular atmospheric phenomenon. On the other hand, breakpoint selection is hindered by the fact that no well-defined breakpoint exists under most elevated inversion conditions. These points are, in most cases, second-order discontinuities and not discontinuities in the mathematical sense. Any number of this type of discontinuity occurs in a given scan with slopes changing in the same direction so as to make selection of the correct breakpoint virtually impossible. For these reasons, breakpoints alone cannot be used to obtain heights of elevated inversions.

4.3 Generation of Model Temperature Profiles and Model Brightness Temperature Curves

In order to increase our catalog of elevated inversions and to be able to vary inversion height, intensity, and thickness systematically and separately, 163 model temperature profiles were specified for use in computer simulation of radiometric data. These profiles contained elevated inversion, elevated isothermal, and elevated dry-adiabatic lapse layers with each profile limited to one type of layer. Above these layers, the U. S. Standard Atmosphere (1962) temperature profile was used. Below the layers, the temperature profiles had the Standard Atmosphere lapse rate (-6.5 C/km). The inversion heights, intensities, and thicknesses were 0.1, 0.3, 0.5, 1.0, 1.5,

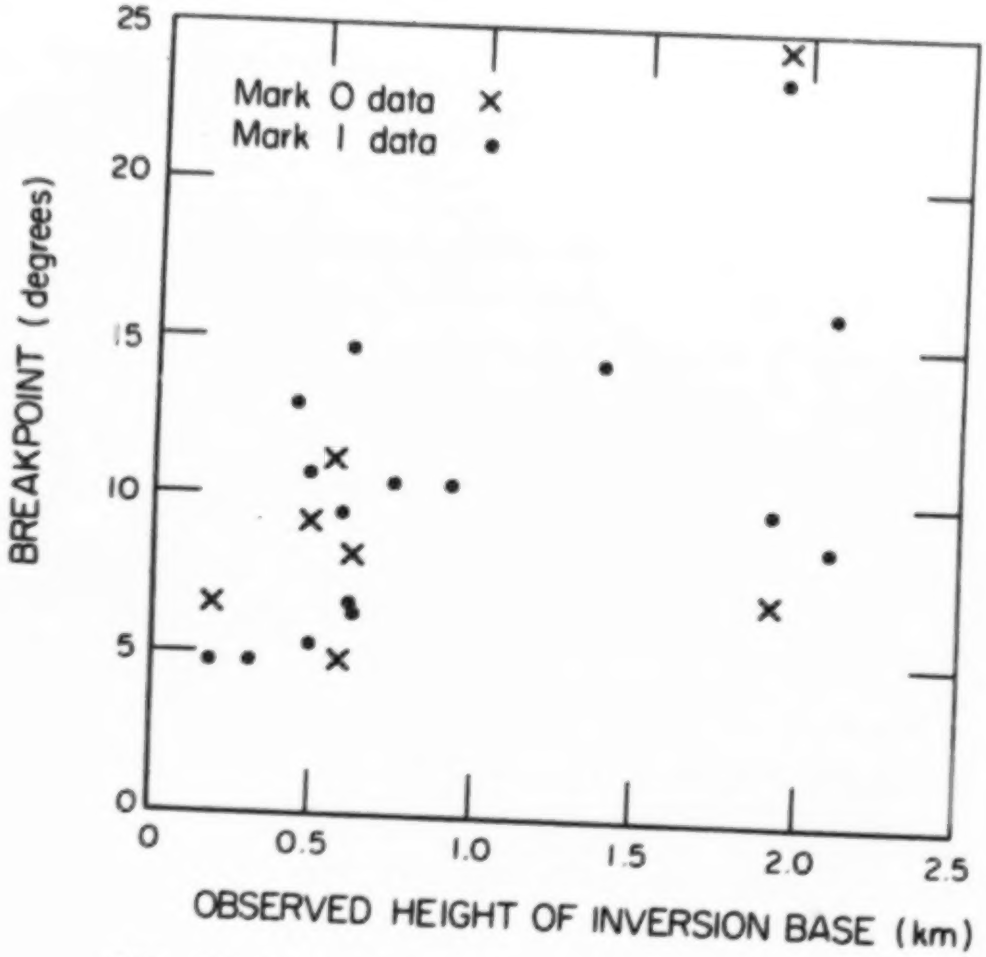

FIG. 20 Lack of correlation between breakpoint and inversion height.

and 4.0 km; 0.5, 1.0, 2.5, 5.0, and 10.0 C; 0.1, 0.3, 0.5, 1.0, and 1.5 km, respectively. The elevated isothermal layers had the same heights and thicknesses as the elevated inversions, except no isothermal layers based at 4.0 km were included. This yielded 127 elevated inversion profiles and 25 elevated isothermal profiles. The remainder was made up of 10 elevated dry-adiabatic lapse profiles and the lapse U. S. Standard Atmosphere profile. The lapse profiles were included to find out whether significantly different results from the simulation would be obtained between the lapse and the inversion and isothermal cases.

Figure 21 shows 15 of these model elevated inversion profiles with each set containing inversions having the same heights and thicknesses, but different intensities. No set of 5 profiles should be interpreted as being warmer or colder than another set. Only the profiles within each set have the correct temperatures relative to one another. The temperature at the top of each inversion layer is the U. S. Standard Atmosphere temperature at that height.

The 163 model profiles were used to calculate simulated brightness temperature records for a ground-based radiometer. The calculations were made at a frequency of 54.5 GHz for null-balance and scanning modes of operation. Null-balance brightness temperatures were calculated for each 2 degrees of elevation within the range 0 through 20 degrees, each 5 degrees from 25 through 40 degrees, and each 10 degrees from 50 through 90 degrees. The null-balance brightness temperatures were then converted to simulated scan data by our scanning mode algorithm. A scan rate of 4 deg/min in both the up and down directions at integration times of 60 and 128 seconds was used. The surface pressure was 1013.25 mb for the 163 model profiles used in the simulation.

The scanning mode simulated brightness temperature records were plotted in the form of brightness temperature versus elevation angle. These simulated brightness temperature records were employed in all the empirical studies described in the remainder of this section. A sampling of these curves is shown in Figs. 22, 23, and 24, but the significant features in these figures are discussed later in the section.

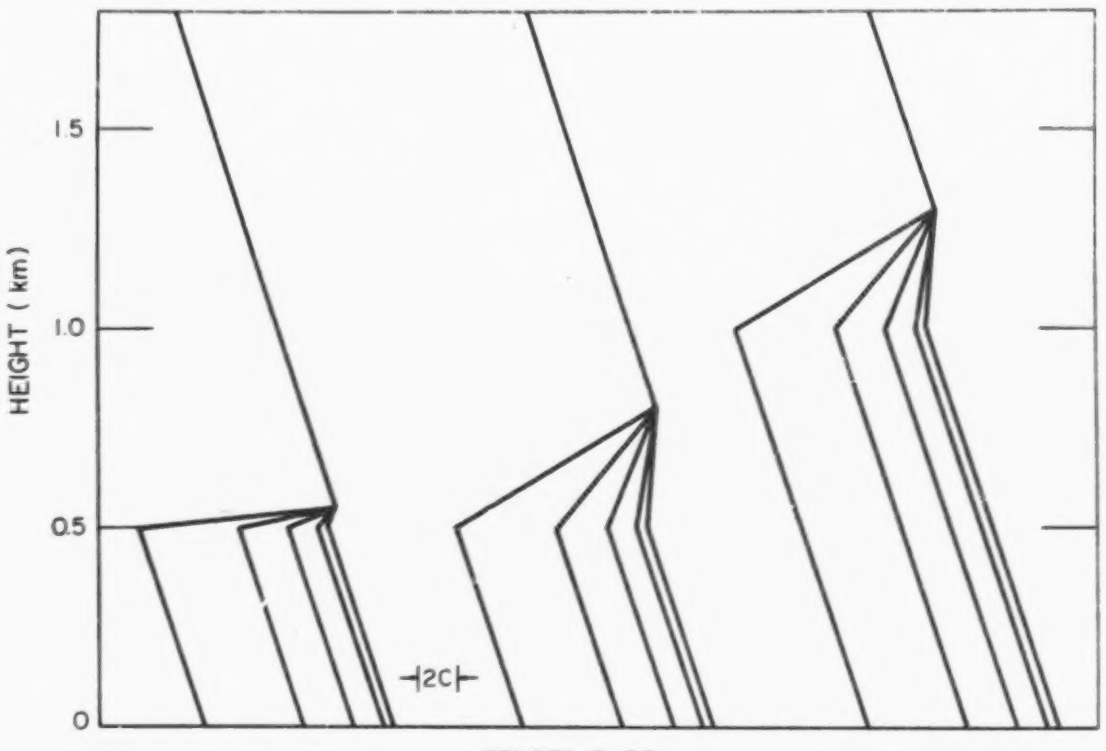

FIG. 21 Model elevated inversion temperature profiles. In all three sets the profile above the inversion is the U. S. Standard Atmosphere.

4.4 Crossover Technique

The simulated brightness temperature curves were analyzed to obtain the intersections or crossovers of the 60-second integration time up and down scan curves. The crossover analysis was performed in two manners. In the first case, the indicated absolute brightness temperatures (no translation along brightness axis) were compared to determine if one scan crossed over another. This method of analysis is termed crossover without superposition. In the second case, one of the curves was translated along the brightness temperature axis so as to make the curves cross or contact at a specified elevation angle. This method of analysis is termed crossover with superposition at the specified elevation angle, which in this case was 70 degrees. Of specific interest in both of the crossover analyses were the highest elevation angles at which scans crossed, called the upper crossover, and the lowest elevation angles at which they crossed, called the lower crossover.

For all the profiles used in the simulation, none of the scans exhibited more than one upper and one lower crossover; some of the scans had only an upper crossover, and some had no crossover. The basis for selecting crossovers as a possible means of determining the salient features of an elevated inversion is the hypothesis that during a down scan, the relatively warm brightness temperatures (due to a warmer inversion layer) incident on the radiometer at the higher elevation angles are outputted at lower elevation angles due to the radiometer's integrator circuit. If the inversion is very intense, the contribution of the inversion layer to the brightness temperature is considerable, so that the down scan crosses over the upward scan and remains warmer down to zero degrees elevation without crossing at a lower angle. For a sufficiently less intense inversion, the contribution from the inversion layer is not great enough to cause the down scan to remain warmer. In the latter case, in addition to an upper crossover, a lower crossover occurs resulting in the down scan being colder below some elevation angle. An inversion that is weaker than the preceding ones may cause convergence of the scans, but no crossing.

The height of inversion base was plotted against angle of lower crossover, against angle of upper crossover, and against both together. Only the scans for a 60-second integration time were used. When no superpositioning of the scans was done, 27 of the 127 cases exhibited upper crossovers. Of these 27, 22 cases had lower crossovers or converged. (The number of lower crossovers is always less than or equal to the number of upper crossovers, since an upper crossover must occur in order for a lower one to occur.) These crossover cases occurred when the inversions were intense or based at a low height. The plot of inversion height vs. the different crossovers showed a great deal of overlap of crossover angles for the different heights.

For superposition of scans at 70 degrees elevation, a greater number of crossovers occurred, especially for the profiles with elevated inversions at 0.5, 1.0, and 1.5 km. When either the upper or the lower crossover was used to predict inversion height, very ambiguous results were obtained. However, when both crossovers were used simultaneously, a good separation (very little overlap of crossover angles) was noted between those cases with inversions at 0.5 km and the cases with 1.0 or 1.5 km inversions. Poor separation was obtained between the 1.0 km inversions and the 1.5 km inversions. Lower crossovers for 70-degree superposition were not present for the model profiles with inversions at 0.1 km and 0.3 km. Without both upper and lower crossovers, the ambiguity could not be eliminated. Thus the crossover technique exhibited a low degree of success in its ability to specify all possible heights of elevated inversions.

4.5 Breakpoint with Crossover Technique

Neither the breakpoint nor crossover techniques when used by themselves indicated much ability as a predictor of inversion height. Another study was made to determine whether these two techniques could be used simultaneously in order to obtain a better measure of the height of the inversion base. Very little was gained from the combination of these two schemes. Only the angle of lower crossover for 70 degrees superposition when used in conjunction with the breakpoint showed an improvement over the results for the crossover technique. This improvement was manifest by the fact that the scans corresponding to the profile models with inversions at 1.5 km had breakpoints and lower crossovers that separated these cases from all other inversion cases. However, only a small fraction of the 1.5 km inversion cases showed any crossover, which indicates that the breakpoint and lower crossover parameters have a very limited ability in specifying inversions at this height.

4.6 Upper and Lower Inflection and Brightness Temperature Differential Technique

A fourth set of parameters was employed in an attempt to extract elevated inversion information from the scan data for the model profiles. This set, however, is pertinent to only those scans that showed an increase in brightness temperature over some range of elevation angle. The names assigned to this set were angle of lower inflection, angle of upper inflection, and brightness temperature differential. The angle of lower inflection is the point at which the brightness temperature vs. elevation angle curve changes sign and becomes positive, whereas the angle of upper inflection is the point at which the slope of the curve changes sign and becomes negative. Thus, these points are the lower and upper bounds of increasing brightness temperature associated with an elevated inversion. The brightness temperature differential is merely that difference between these bounds.

These parameters were tested on the up scans for a 60-second integration time. The scans for inversions at 1.0 and 1.5 km showed no region over which brightness temperature increases; hence the study was limited to the scans for inversions at 0.1, 0.3, and 0.5 km. For inversions at 0.1 km, an intensity of 2.5 C was sufficient to cause a brightness temperature increase. At 0.3 km and 0.5 km, inversion intensities of 5.0 C and 10.0 C, respectively, were required to produce this increase. Bearing in mind that only a few discrete values of inversion intensity were included in the model profiles, it is likely that somewhat less intense inversions at each of these heights would have produced a brightness temperature increase had they been included in the model profiles. The results of this study indicate that inversion height can be predicted with very little ambiguity using these parameters, and that inversion thickness and intensity can be predicted--but with less resolution than for height. One drawback of this method is that it can be used only when elevated inversions exist at low heights and are sufficiently intense to cause a brightness temperature increase.

4.7 Analog Library Technique

All aforementioned techniques in Section 4 were either unsuccessful or displayed limited success in their ability to specify the characteristics of elevated inversions. At least part of this lack of ability is attributed to the ambiguity involved in selecting the proper point of application for a given predictor and to the limited number of predictors used in any one combination. In order to maximize the profile information available from scan data and to minimize dependence on a single predictor or a few predictors, one can use all the information in a scan. This can be accomplished by comparing an observed brightness temperature scan with an analog library of scan data generated either in the field under known profile conditions or by computer simulation of radiometric scans from models of different air temperature profiles. The technique is as follows: The search through the library of analogs continues until the scan is found that is most analogous to the observed scan from which profile information is to be extracted. The most analogous scan is deemed to be the one which best matches the measured scan. Once the search is completed and the best analog chosen, one concludes that the profile corresponding to the scan under consideration is the same as or similar to the known profile used to generate the analog model scan. The result is a specification of the ambient air temperature profile.

It should be mentioned that the 163 computer-simulated scans and corresponding model temperature profiles used in the aforementioned breakpoint, crossover and inflection studies were adopted for use as an analog library. This library is the source of all the analog model scans and model profiles discussed in the remainder of this report. There are many types of frequently occurring temperature profiles that are not contained within this library, but at this stage it is large enough to establish whether the analog library technique is worth pursuing further.

Figures 22, 23, and 24 are a few of the analog model scans for elevated inversion profiles. All the models shown in these three figures are upward scans for an integration time of 60 seconds. The models in Fig. 22 were generated from the profile models containing elevated inversions at the different heights 0.1, 0.3, 0.5, 1.0, and 1.5 km, but for the same intensity

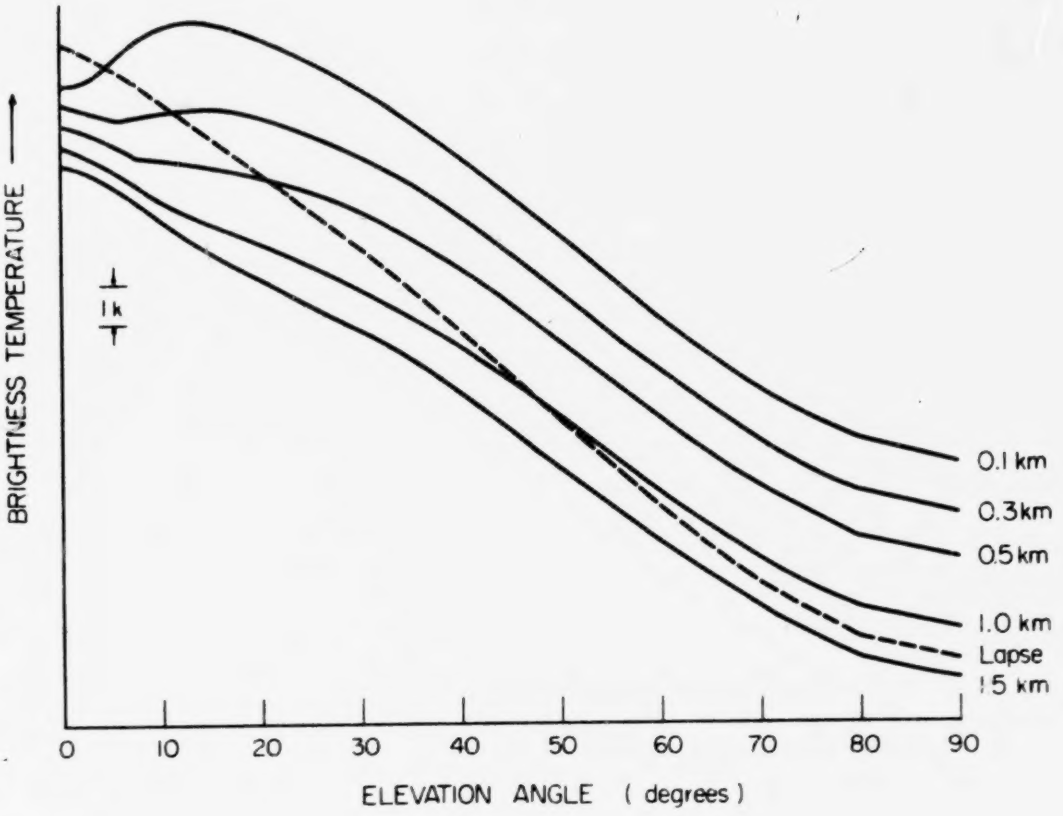

FIG. 22 Model scan curves for profiles having elevated inversions of different heights. The curves are displaced an arbitrary 0.5 K at 0 degrees elevation.

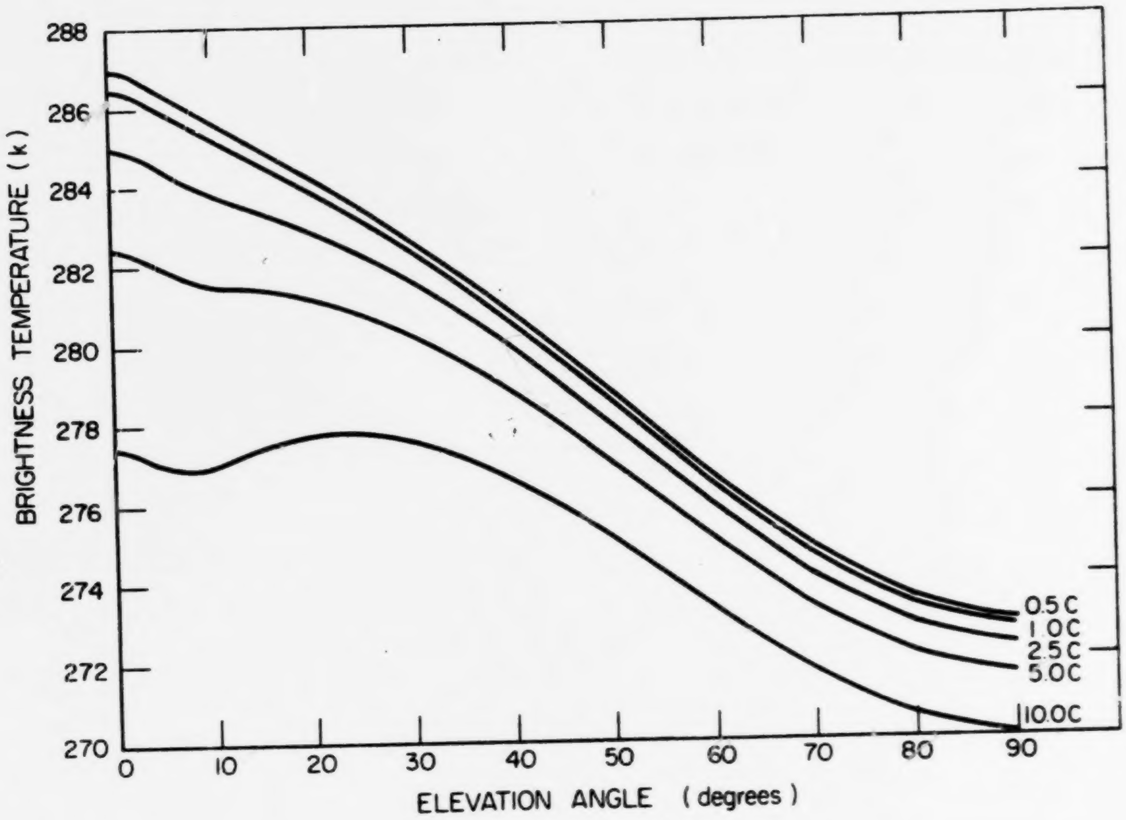

FIG. 23 Model scan curves for profiles having elevated inversions of different intensities.

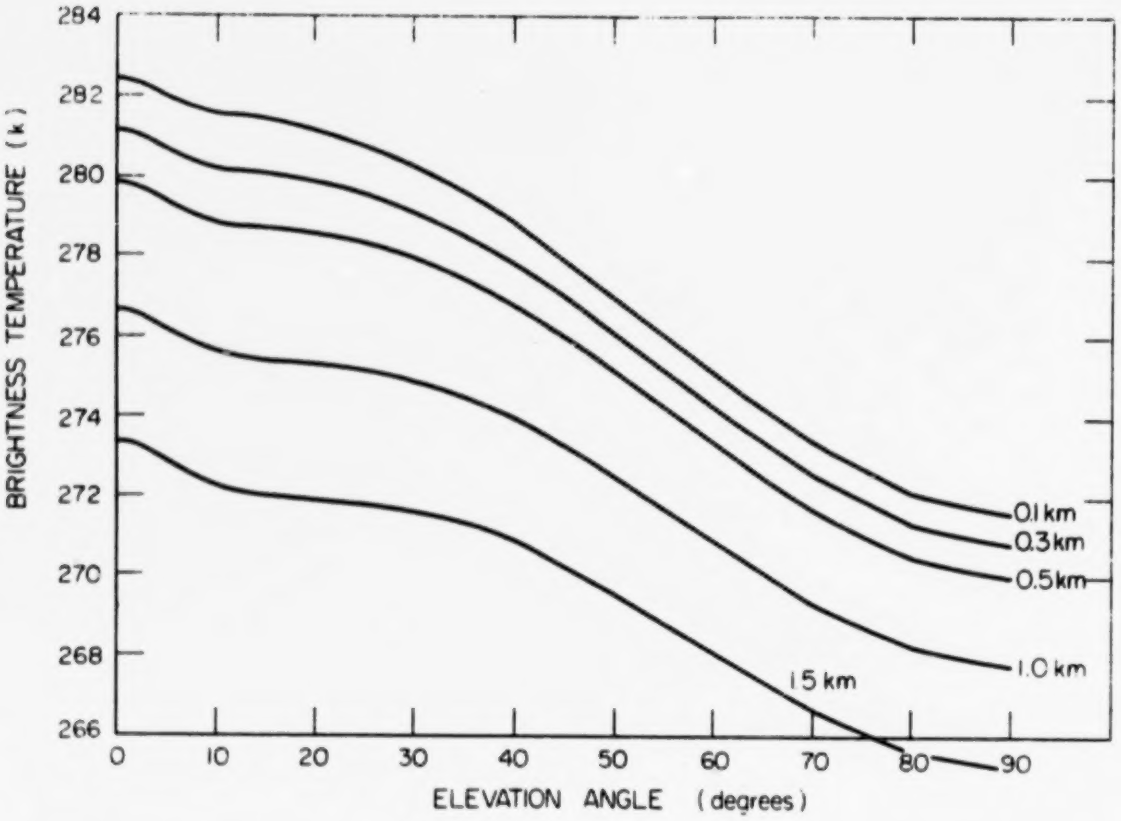

FIG. 24 Model scan curves for profiles having elevated inversions of different thicknesses.

(5 C) and thickness (0.1 km). The dashed curve is the model scan corresponding to the lapse U. S. Standard Atmosphere profile. Displacement of the scans by an arbitrary 0.5 K in brightness temperature at 0 degrees elevation was done for clarity. It is easily seen that the curves corresponding to the elevated inversion profiles differ considerably from the lapse curve, with the difference in shape being greatest for the lower inversion cases. As one expects, there is greater contribution to the brightness temperature from the lower inversions than from the higher inversions. This accounts for the more pronounced region of upward convexity for the cases corresponding to low inversion heights and the less pronounced difference between the lapse and the high inversion cases. Also, the region of convexity is displaced upward as the inversion height increases, and the greatest difference from curve to curve occurs below 40 or 50 degrees elevation. The latter fact suggests that the region below the middle elevation angles is the most important one for differentiating between inversions at different heights.

The brightness temperature curves in Fig. 23 were generated from the model profiles having the same inversion base at 0.5 km and the same thickness of 0.1 km, but different intensities. This is indicated just to the right of the curves. The 5 model elevated inversion profiles on the left hand side of Fig. 21 were used to produce the brightness temperature vs. elevation angle curves in Fig. 23. The outstanding feature, however, is the difference in the shapes of the curves for different intensities, with the greatest convexity occurring for the most intense inversion profiles. For the weakest inversion cases, 0.5 C and 1.0 C, the curves have shapes similar to the lapse curve shown in Fig. 22. In practice it may be difficult to distinguish between very weak inversions and lapse conditions unless these inversions are at low heights or have at least a moderate thickness.

Brightness temperature curves are presented in Fig. 24 for inversions of different thicknesses but of the same height (0.5 km) and intensity (5.0 C). The thicknesses are indicated to the right of the curves. Again the curves have very nearly identical shapes above the middle elevation angles, with the greatest difference occurring below these angles. The effect of increasing thickness, as shown in the figure, is a longer region of near-isothermal brightness temperature. Had the curves presented in this figure been for sufficiently low or intense inversions, an increase in brightness temperature over a range of elevation angles would have been indicated.

In Figs. 25 and 26 are shown comparisons between actual radiometric scan data (observed in the field) and analog model scan data. For clarity purposes, brightness temperatures of the actual and model scans are displaced in these figures. Both the models and the actual data are for a 60-second integration time, a frequency of 54.5 GHz, and a scan rate of 4 deg/min in the upward direction. The actual scans were made by the Mark I radiometer at the locations indicated at the top of each plot. The models were selected from the analog library consisting of the scans for the 163 model profiles. Selection of the models was achieved by the analyst without a priori knowledge of the temperature profile that existed during the time of the actual data observation. The model selection was complete when, in the opinion of the analyst, the closest agreement was obtained between the actual and one of the 163 model scans. Emphasis was placed on obtaining the best correspondence of the convex region in both the brightness temperature and elevation angle axes. The purpose here was to derive the temperature profile that existed during the actual data observation using this analog method. It should be mentioned that selection was based on establishing a correspondence in shape rather than on minimizing absolute brightness temperature differences between the actual and the models.

It can be seen that there are differences in shape between the actual and the model curves at the low and high elevation angles. These differences are explainable on the basis that the lapse rates under the field conditions were different than the lapse rates of the model profiles used to generate the corresponding scan data. The model profiles had only three temperature slopes below the tropopause: one slope above the elevated inversion layer (-6.5 C/km), one slope in the inversion layer, and one slope below the inversion layer (also -6.5 C/km). Another factor contributing to the differences in slope at low elevation angles is ground and vegetation effects, which remain in the integrator circuitry for a short time after the start of an upward scan due to the finite integration time. The differences between the actual and

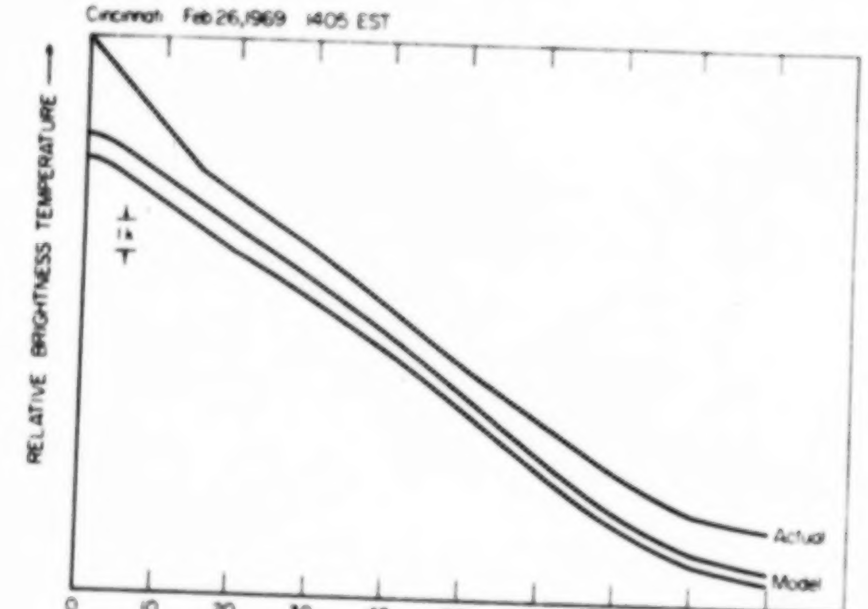

FIG. 25 Actual radiometric scan curve vs. analog model scan curve for Cincinnati and Raleigh.

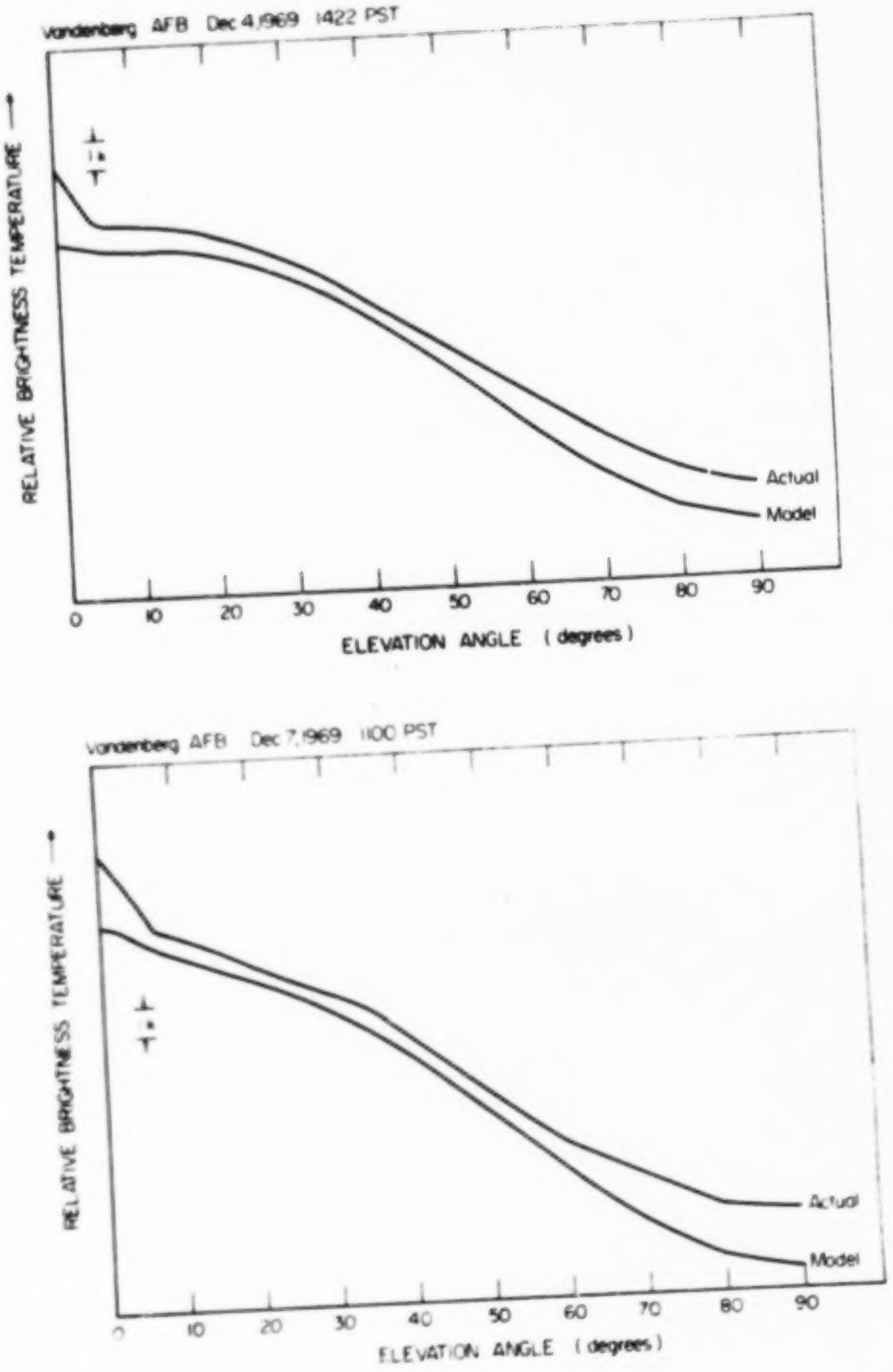

FIG. 26 Actual radiometric scan curve vs. analog model scan curve for Vandenberg AFB.

model scans caused by the fact that the model profiles contained only three temperature slopes can be reduced by the introduction of a greater number of slopes. This requires only the generation of a greater number of model profiles and computer radiometric simulation to obtain the corresponding model scans. On the other hand, the problem of ground and vegetation effects cannot be solved simply by any method, empirical or analytical. These effects are a complex function of the nature of the soil and vegetation, of their temperature, and of their frequency-dependent emissivities which may vary with their temperature and moisture content. The problem can, nevertheless, be eliminated or its effects reduced by selecting a site with a reasonably clear horizontal radiometric field of view, or by eliminating the very lowest elevation angle from the scan. However, the greatest difficulty in matching the observed with the analog scan was that most of the observed radiometric data were gathered during dry adiabatic lapse conditions in the lowest layers, and no such conditions were contained within this initial analog library.

A total of eleven scans made in the field was compared with the model scan library in order to obtain the temperature profiles that existed during the field observations. In the Cincinnati, Ohio, case for 1969 February 26, the analyst chose two model scans to be equally similar to the actual, resulting in two possible model profiles as representing the actual temperature profile. The corresponding analog model profiles for the eleven scans are presented in Figs. 27 through 37. The directly observed temperature profiles that existed during the time of the radiometric observations are also shown. The observed and model profiles are arbitrarily displaced along the temperature axis. At the top of each figure the location and date of observation is indicated along with the starting time of the radiometric scan. All the radiometric scan data presented in these figures were obtained at 54.5 GHz and an integration time of 60 seconds by the Mark I radiometer, except for the 1969 February 20 case at Cincinnati, which was obtained at a 30-second integration time. Scan rate was 4 deg/min in the upward direction. The observed profiles for the two Cincinnati cases are on-site radiosonde soundings, whereas the remaining observed profiles are on-site helicopter soundings.

In all cases there is a very good correlation between the analog model

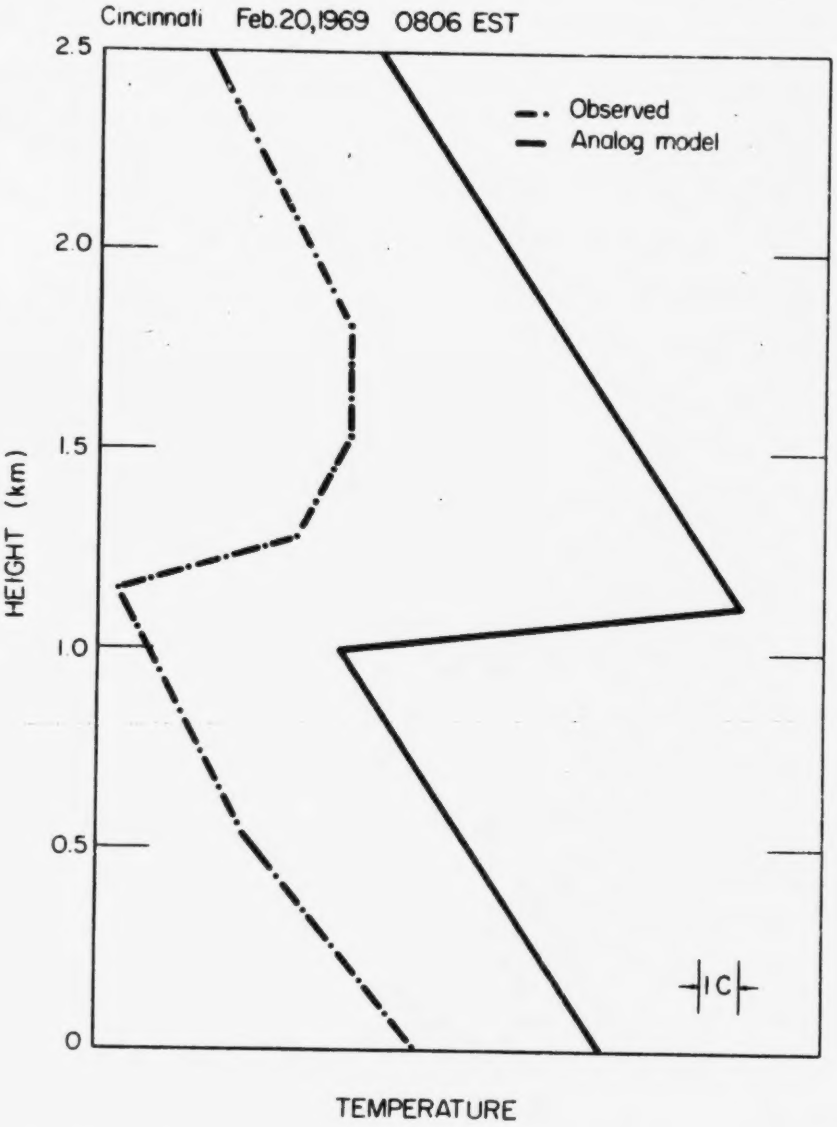

FIG. 27 Predicted analog model vs. observed temperature profile for Cincinnati 1969 Feb. 20, 0806 EST.

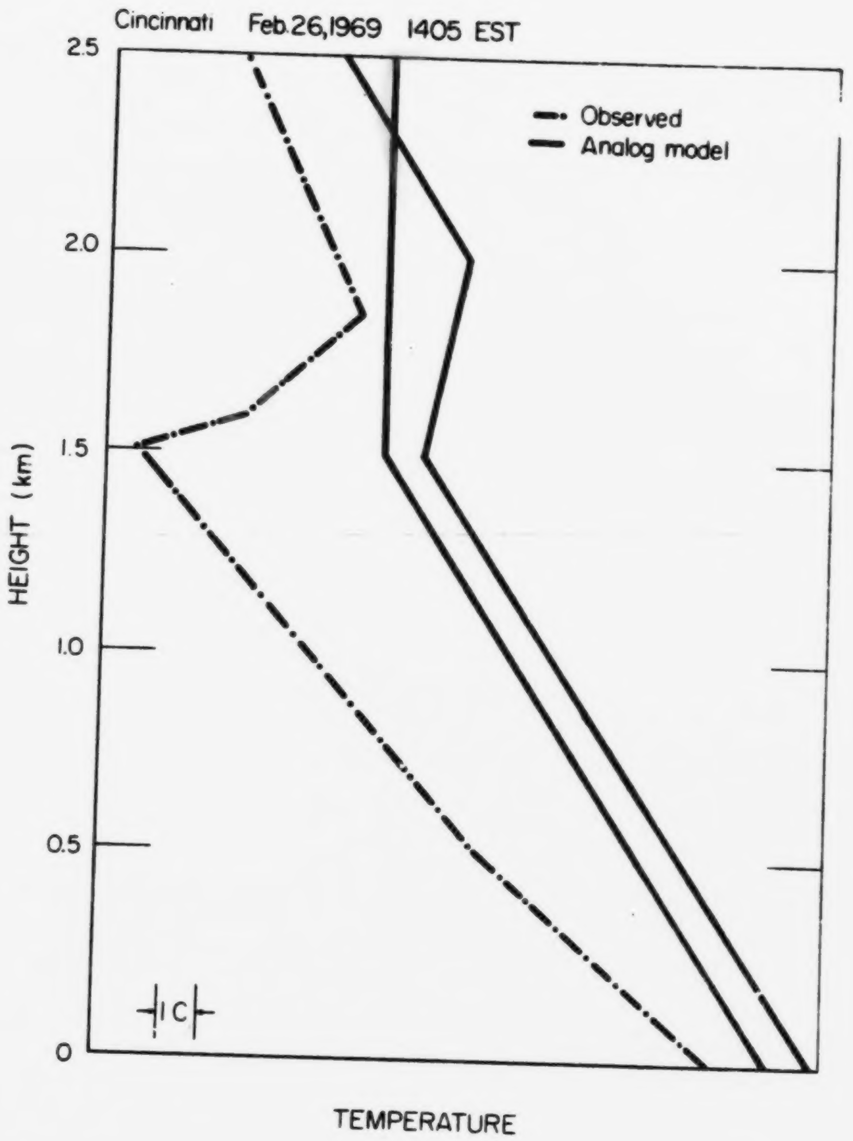

FIG. 28 Predicted analog model vs. observed temperature profile for Cincinnati 1969 Feb. 26, 1405 EST.

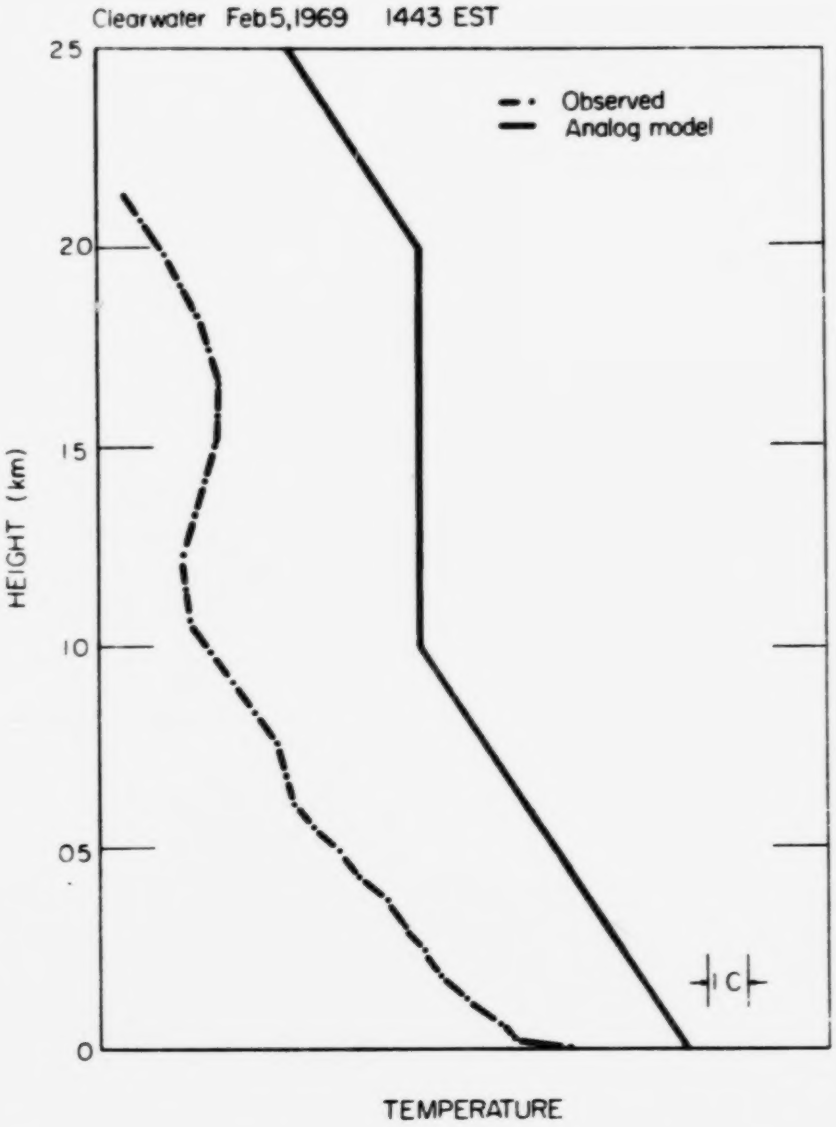

FIG. 29 Predicted analog model vs. observed temperature profile for Clearwater 1969 Feb. 5, 1443 EST.

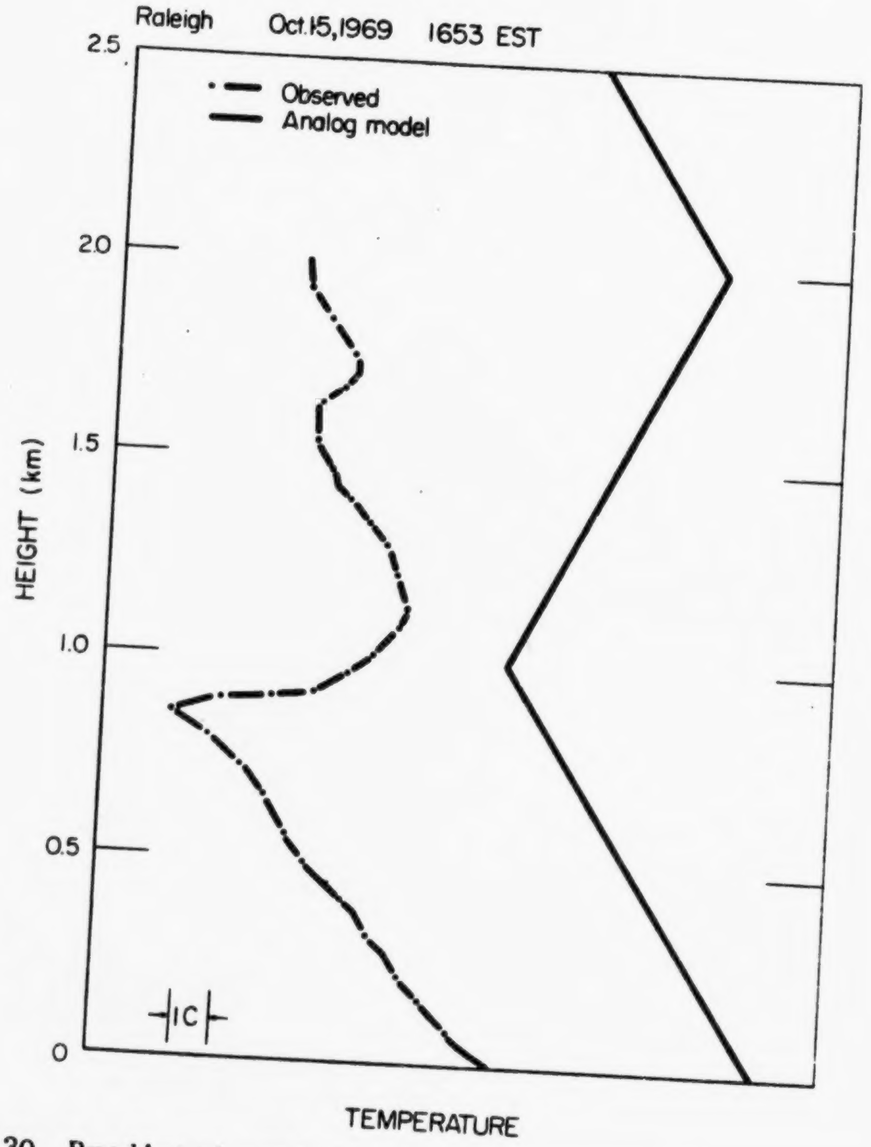

FIG. 30 Predicted analog model vs. observed temperature profile for Raleigh 1969 Oct. 15, 1653 EST.

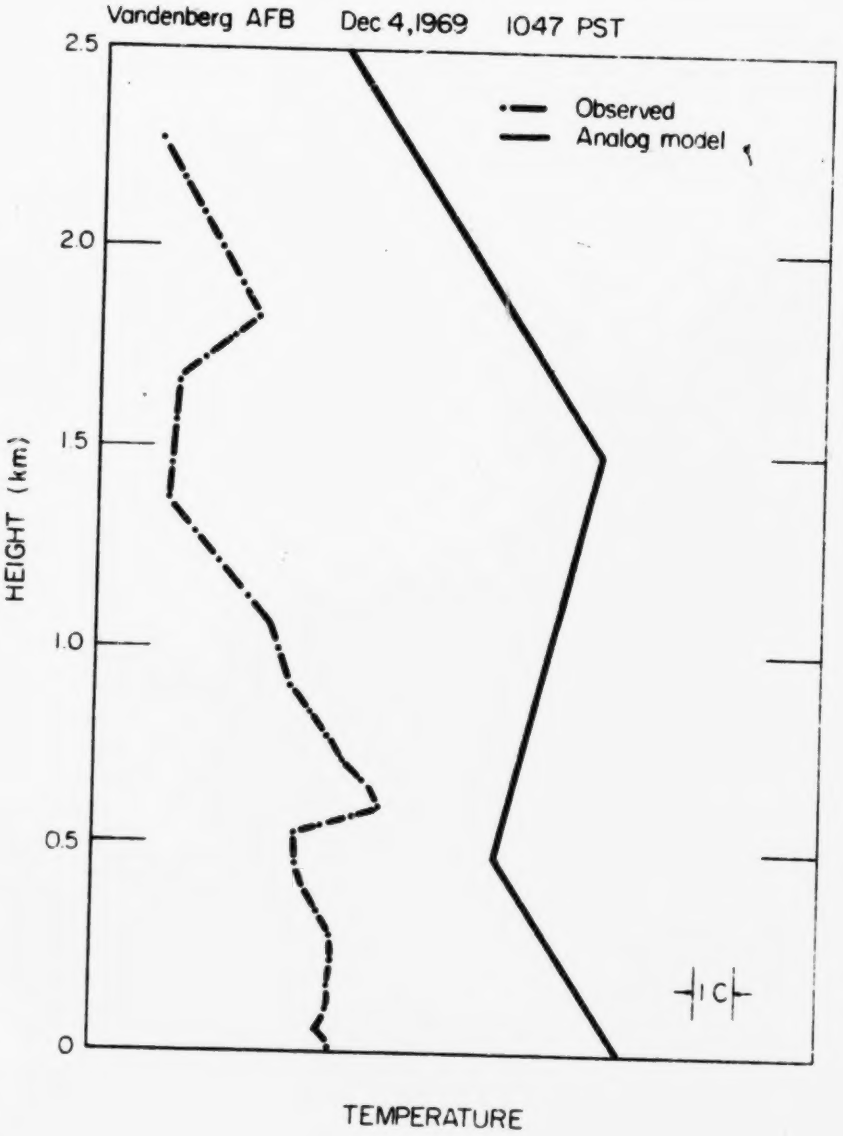

FIG. 31 Predicted analog model vs. observed temperature profile for Vandenberg AFB 1969 Dec. 4, 1047 PST.

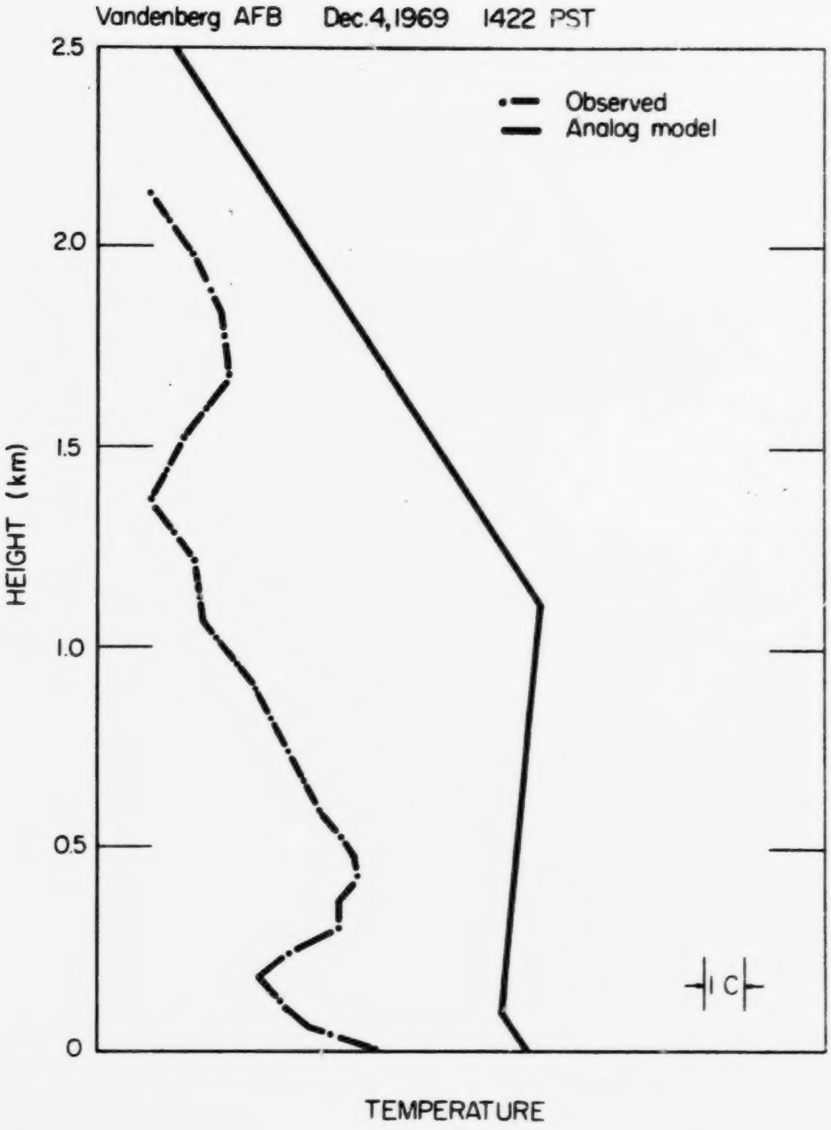

FIG. 32 Predicted analog model vs. observed temperature profile for Vandenberg AFB 1969 Dec. 4, 1422 PST.

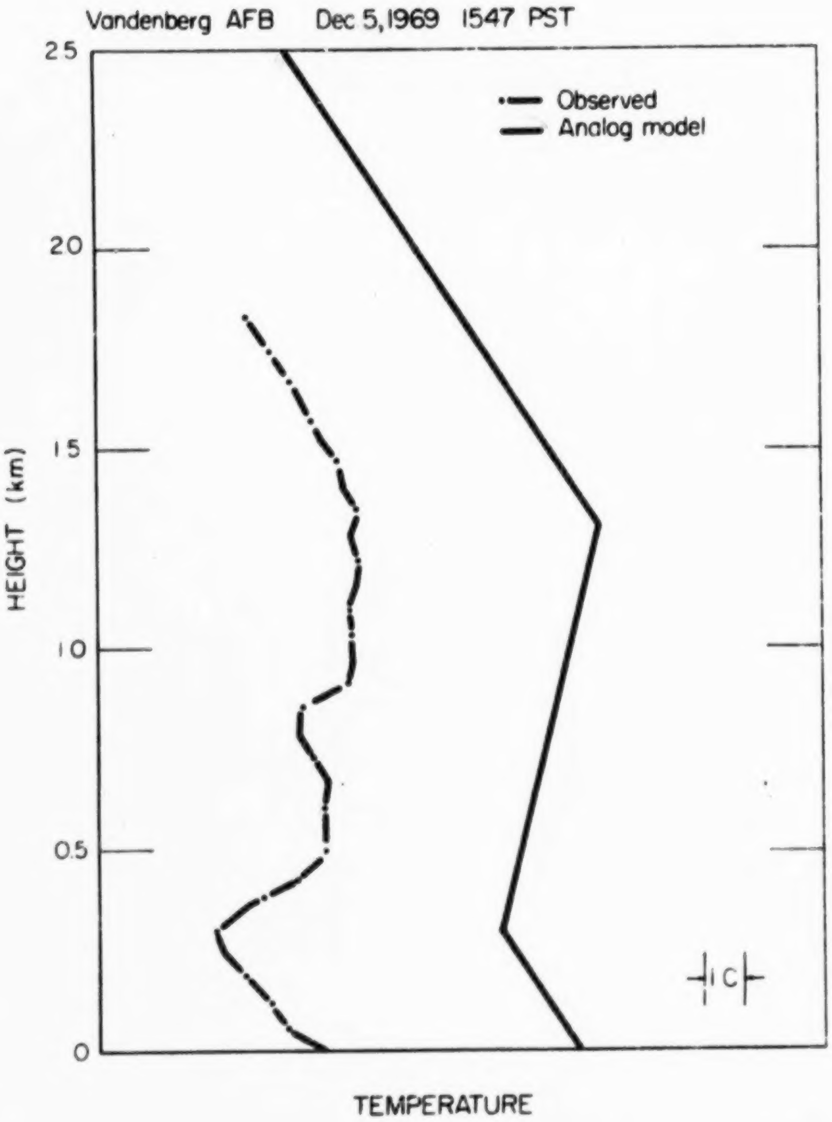

FIG. 33 Predicted analog model vs. observed temperature profile for Vandenberg AFB 1969 Dec. 5, 1547 PST.

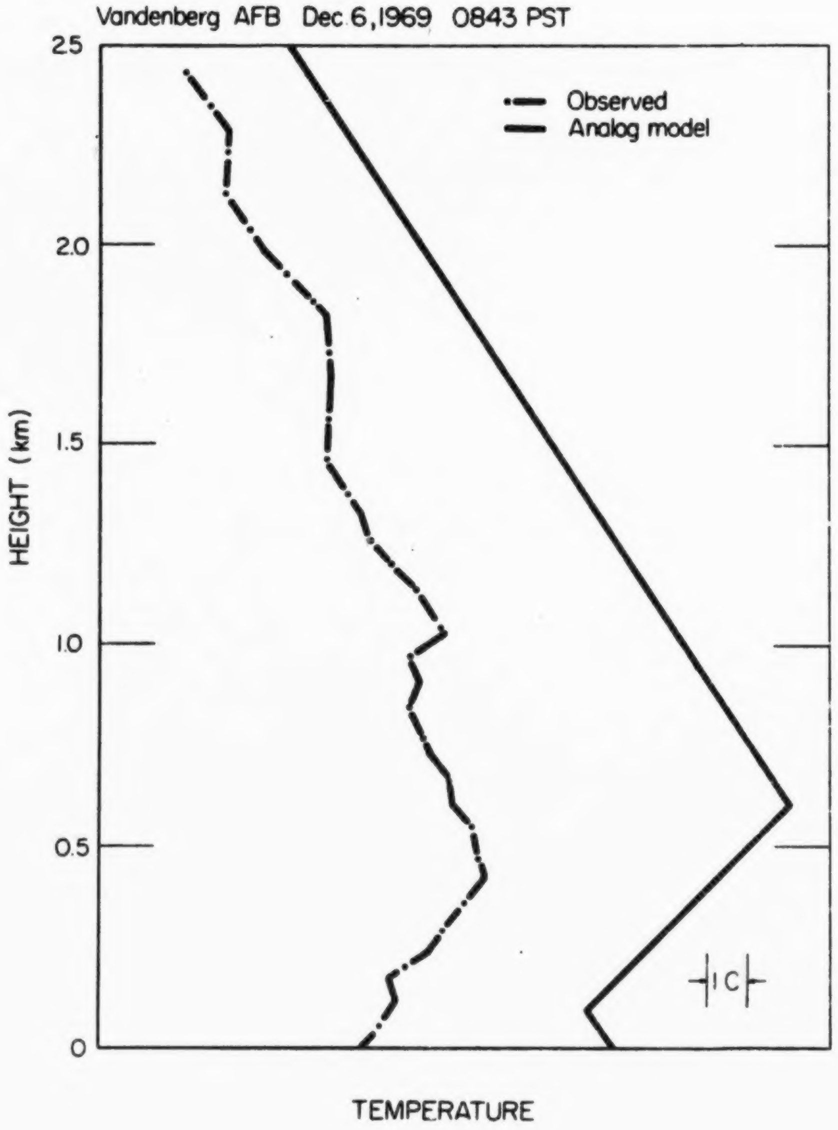

FIG. 34 Predicted analog model vs. observed temperature profile for Vandenberg AFB 1969 Dec. 6, 0843 PST.

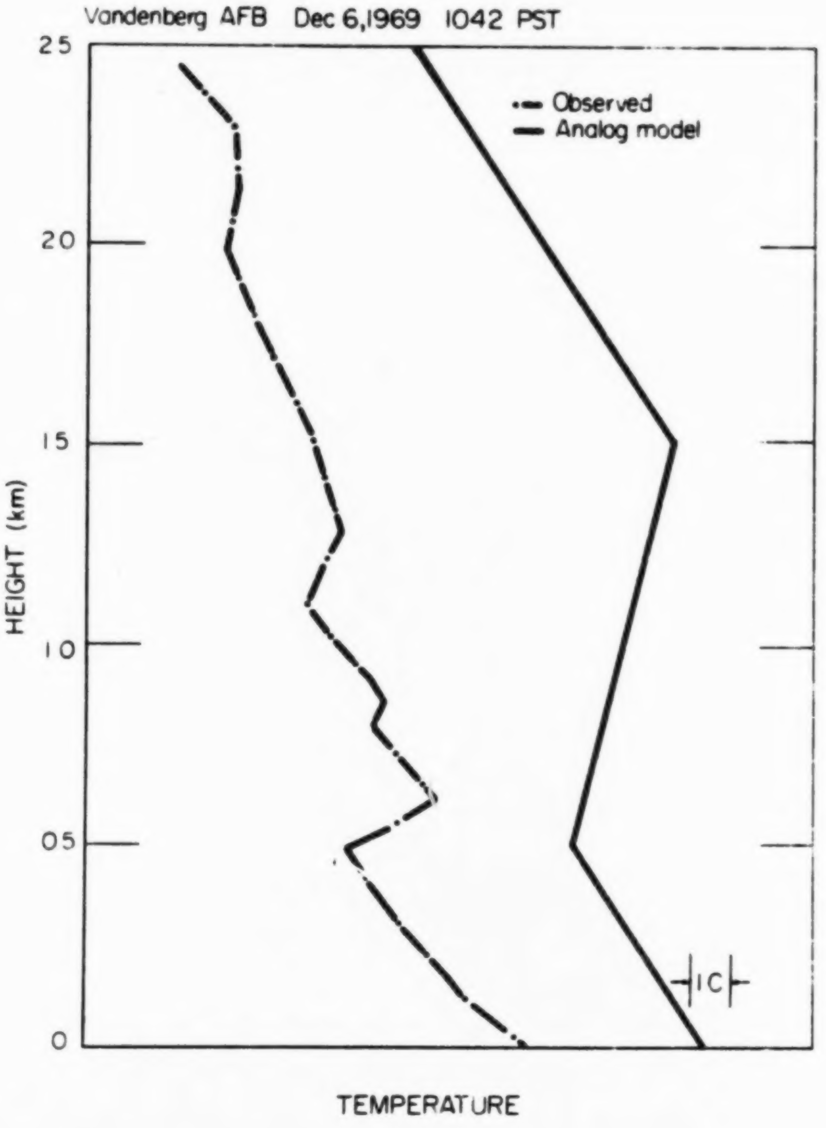

FIG. 35 Predicted analog model vs. observed temperature profile for Vandenberg AFB 1969 Dec. 6, 1042 PST.

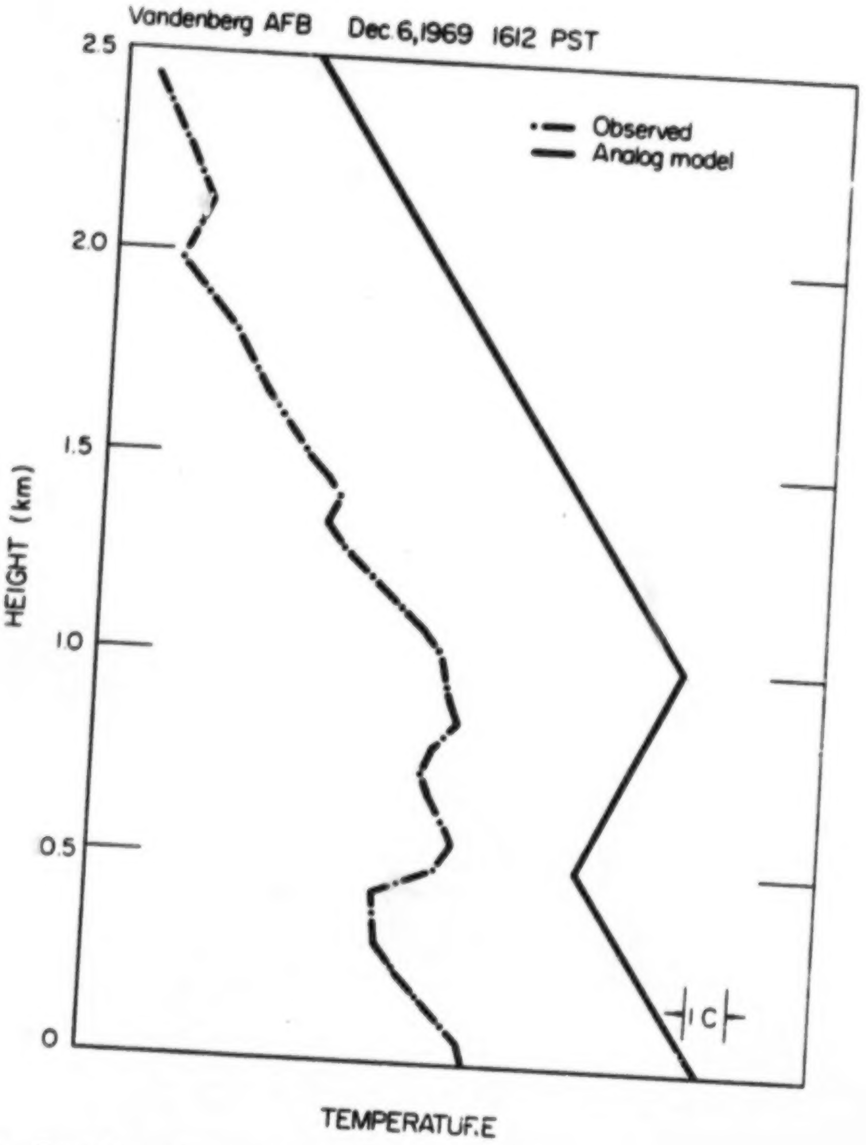

FIG. 36 Predicted analog model vs. observed temperature profile for Vandenberg AFB 1969 Dec. 6, 1612 PST.

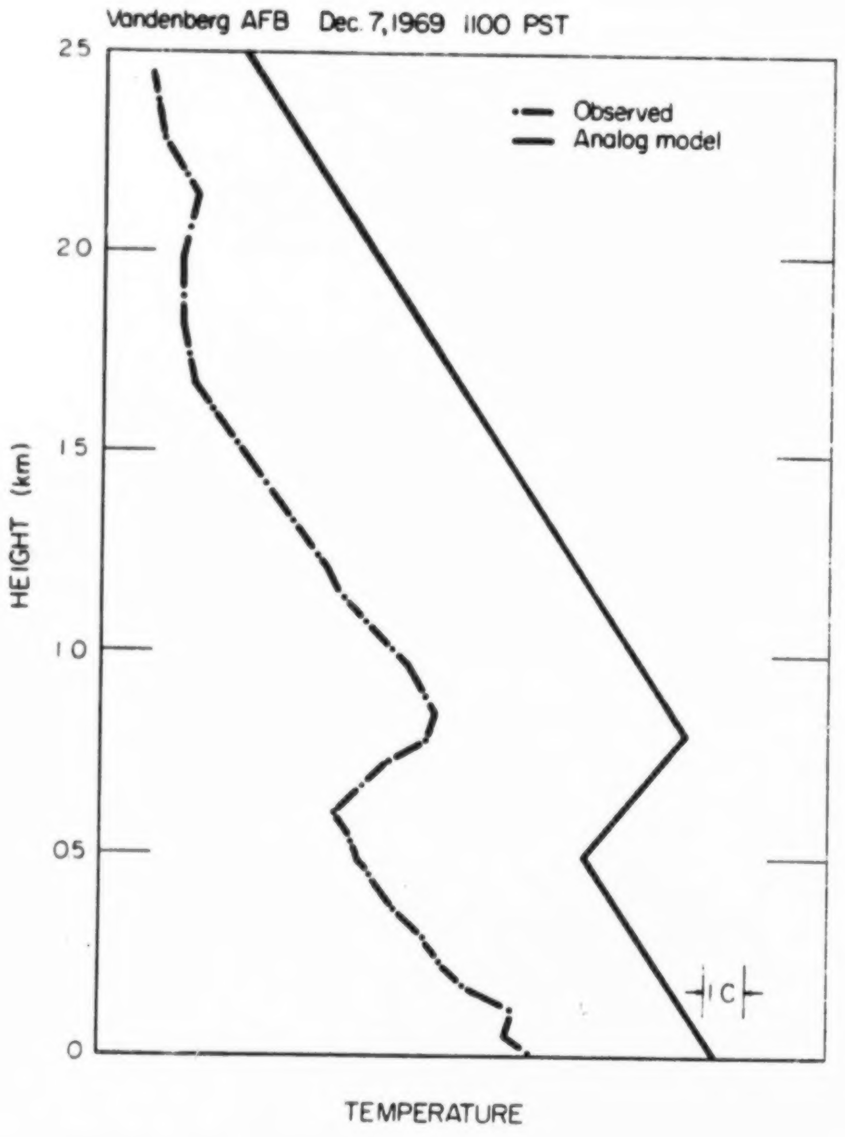

FIG. 37 Predicted analog model vs. observed temperature profile for Vandenberg AFB 1969 Dec. 7, 1100 PST.

and the observed inversion base height which ranges from 0 to 1.51 km. Recall that the analog model profile library included only the few inversion base heights previously mentioned. In every instance, however, the analog model selection (made with no a priori temperature profile knowledge) yielded the closest possible height of inversion base. Figure 34 indicates that a ground-based inversion existed at observation time, whereas the analog model indicates an elevated inversion at 0.1 km. In fact, the observed radiometric trace also showed a ground-based inversion, but no ground-based inversions were included in the model library so the selection yielded the lowest inversion height available in the library.

In some of the cases the analog model inversion intensity and thickness do not match well with those observed. In other cases there is a good match of these parameters, occurring when the observed slopes above and below the inversion approach those of the analog model. The implication is that when an analog model in the library is very similar to the observed profile, the analog technique predicts the profile well. Conversely, when no similar analog model exists, the prediction is poor. The two cases for December 4 at Vandenberg Air Force Base, shown in Figs. 31 and 32, are prime examples in which the observed profiles do not approach similarity with any library model. Thus a poor correspondence exists. For the instances in which the observed inversion is at a low height and the profile is similar to a library model, an excellent fit of height, intensity, and thickness is obtained. These profiles are displayed in Figs. 33, 36, and 37. The profiles which were observed to have high elevated inversions, shown in Figs. 27, 28, 29, and 30 were matched as closely as possible in height by the analog models, but not as well in intensity and thickness. Perhaps the reason for this result is the more subtle difference between the analog model scans and the actual scan data for inversions at higher heights, where a small difference in the inversion characteristics produces only a very small difference in the brightness temperature scan shape. If this hypothesis is correct, then the ability to resolve intensity and thickness is diminished for the higher inversions as indicated by the figures.

Let us consider quantitatively the performance of the first try of the limited analog approach in specifying the depth of the mixing layer. For the 11 cases previously discussed, the height of the inversion base (depth of the mixing layer) was determined from the best fit analog profile and compared with that observed with an instrumented helicopter. These results are tabulated as follows:

TABLE XIV

Helicopter Vs. Radiometrically Measured Depth of Mixing Layer

Helicopter (km)	Radiometer (km)	Error (km)	Error (%)
0.55	0.5	0.05	10
0.18	0.1	0.08	45
0.30	0.3	0.00	0
ground inversion			
0.49	0.5	0.01	2
0.43	0.5	0.07	16
0.61	0.5	0.11	18
1.21*	1.0	0.21	17
1.15	1.0	0.15	13
1.51*	1.5, 1.5	0.01	2
0.86	1.0	0.14	16
		average 0.08 km	average 13.9%

*Measured by Radiosonde

Recall that at this stage it was only possible for the analog scheme to specify 5 heights of the mixing layer, namely, 0.1, 0.3, 0.5, 1.0, and 1.5 km, and in all the above cases the nearest height available was selected. The percent error in measuring the mixing layer depth ranged from 0 to 45% with a 13.9% average, but a more meaningful parameter is the magnitude of the error is specifying the mixing depth.

Having an average absolute error of 80 meters in specifying the mixing layer depth may sound reasonable to some but not to others. In an effort to place this figure in proper perspective, the natural time variability of this parameter was investigated. A total sample of 103 cases of helicopter soundings was obtained from APCO for analysis of the time variations in the depth of the mixing layer. These data were gathered at four geographical locations (Cincinnati, Ohio; Salt Lake City, Utah; Vandenberg AFB, California; and Clearwater, Florida) for three seasons (summer, fall, and winter). These data were taken during daylight hours and were evenly distributed between morning and afternoon hours. Of the total sample there were 55 soundings taken equal to or less than one hour apart and 48 soundings greater than one hour but equal to or less than two hours apart. The respective average absolute time variabilities in the depth of the mixing layer for these two time intervals were 0.07 and 0.19 km. Hence the average error between the radiometer and the helicopter measurements is equal to the average variability in the depth of the mixing layer over a period less than or equal to one hour. Or expressed another way: Helicopter soundings on less than an hourly basis are required if the height of the mixing depth must be known to an accuracy equal to that obtained radiometrically. Considering ascent and descent time, helicopter soundings would have to be continuous to do better than radiometric soundings in specifying the mixing layer depth.

When viewing the figures of analog model vs. observed temperature profiles in an overall manner, the models yield an excellent measure of the height of the inversion base, even when the observed profiles were vastly different from any in the analog library. This suggests that it is not necessary to have analog profiles similar to the existing temperature profile in order to predict height of inversion bases. The measures of intensity and thickness are not as good as the height measure. It is apparent that an analog profile similar to the existing profile is required for prediction of intensity and thickness.

The analog library method has yielded vastly better results than any of the empirical techniques investigated for measurement of elevated inversions. It is anticipated that much improvement of this method can be realized by increasing the analog library to include a greater number of inversion heights and profile slopes both above and below the inversion. In addition, surface pressure effects not taken into consideration in the analog studies thus far can be taken into account when required. The inclusion of these features will make the analog technique more flexible, not only for prediction of the inversion portion of temperature profiles, but also for the prediction of slopes above and below inversions.

Not all the problems are solved, and we know that the adverse effects due to thick clouds will have to be considered. It does appear, however, that a key parameter to air pollution, namely the mixing layer, can be measured nearly continuously with the THERMASONDE™ operating in an operational environment.

SECTION 5

CONCLUSIONS

The overall results of this work on the analysis of ground-based radiometric data indicates that the salient features of the temperature profiles in the lowest few kilometers of the atmosphere, particularly the depth of the mixing layer in the presence of an elevated inversion, can be determined to within acceptable error limits by the radiometric THERMASONDE™. The relative accuracy with which the base height of the elevated inversion can be determined was found to be markedly dependent upon its absolute value as well as the thickness and intensity of the associated elevated inversion. The lower the base, the thicker the inversion layer; and the greater the intensity, the more accurately the height of the base can be specified. An average relative accuracy of 14 percent in the measurement of base heights as high as 1.5 km seems to be attainable using the analog or gradient altitude model techniques.

The determination of the thicknesses and intensities of elevated inversions to the same degree of accuracy as the base heights appears to be more difficult.

A comparative evaluation of the three techniques indicates that the analog method was the most successful, the gradient altitude model a close second, and the limited range relaxation technique least successful in determining the mixing layer depths. The latter technique, unlike the other two, is not constrained to a preselected finite number of solutions of a fixed form. It would therefore appear to have the most potential for obtaining the best representation of the true temperature profile from the measured data. However, solutions to the brightness temperature integral equation are not unique. Consequently, convergence to a solution as defined by the relaxation algorithm does not guarantee a resultant temperature profile which corresponds with the desired degree of accuracy to the true temperature profile. The incorporation of constraints similar to those implictly contained in the analog and gradient altitude model technique may improve the performance of the relaxation technique.

Verifying the radiometrically measured depth of the mixing layer against nearly simultaneous helicopter soundings of 11 elevated inversion cases gave an average difference of 0.08 km. Also, it is shown that the natural variability in the depth of the mixing layer averages 0.07 and 0.19 km for periods less than or equal to one hour and greater than one hour but less than or equal to two hours, respectively. This indicates that to maintain a better measure of the mixing depth than that provided by the THERMASONDE™, helicopter soundings would have to be made at least once an hour.

REFERENCES

(1) Twomey, S., "Information Content and Indirect Sensing Measurements." J. Atmos. Sci., Vol. 27, No. 3. pp 515-518, May 1970.

(2) Mount, W. D., et al, "Capabilities of Millimeter Wave Radiometers for Remotely Measuring Temperature Profiles Pertinent to Air Pollution," Final Report, NCAPC, PH86-67-76, Feb., 1968.

(3) Mount, W. D., et al, "Development of Mark I Radiometric THERMASONDE^{TM} and Simulation and Experimented Studies for Passively Probing Temperature Structure within the First Mile of the Atmosphere," Final Report, NAPCA PH22-68-22, Sept., 1969, Appendix II, p II-6.